eXPRESS Polymer Letters Vol.3, No.1 (2009) 1
Available online at www.expresspolymlett.com
DOI: 10.3144/expresspolymlett.2009.1

Preface

T. Czigány[1*], *J. Karger-Kocsis*[2], *L. Macskási*[3]

[1]Department of Polymer Engineering, Budapest University of Technology and Economics, Műegyetem rkp. 3., H-1111 Budapest, Hungary
[2]Institute for Composite Materials, University of Kaiserslautern, Erwin Schrödinger Str. 58, D-67663 Kaiserslautern, Germany
[3]Scientific Society of Mechanical Engineering (GTE), Fő u. 68., H-1027 Budapest, Hungary

Nowadays the global worldwide economic crisis is in every mouth, the news is pessimistic, the views of economic experts are also negative. However, one of the solutions - and likely the right one - is the strengthening and acceleration of research and development. This has already been recognized by the decision-makers, hence the state and industrial funds for research have been multiplied in several countries. This is especially true for the plastics industry partly due to the dramatic price decrease of crude oil at present. This had an impact on our journal ***eXPRESS Polymer Letters*** as well. More and more original research and technical papers are submitted by authors, and most of them involve industrial relevance. All these factors enhanced the international standard of the journal. Thomson Reuters also acknowledged this fact as all the papers published in ***eXPRESS Polymer Letters*** – from the very first one – have been uploaded to the Web of Science retroactively. This is a milestone in the two-year long history of the journal, which is now indexed not only by SCOPUS but also by Science Citation Index-Expanded (SCIE) including the Web of Science, the ISI Alerting Service, the Chemistry Citation Index (CCI), the Materials Science Citation Index (MSCI) and the Current Contents/Physical, Chemical & Earth Sciences (CC/ PC&ES). This means that the increasing impact factor of our journal expresses a real impact on the science!

The development of ***eXPRESS Polymer Letters*** is going on. From this year the DOI numbers of the references will be also available, hence all of them will be accessible just by a click. So, the background information in a given field will be available for the researchers in a much faster and more comfortable way than before.

This is the right place to express our thanks to the reviewers of the journal. The strict but still very fast reviewing process will continue in 2009. At least two but often three or more independent international experts will qualify a paper. In the first two years 2/3 of the papers have been rejected and this ratio is likely to increase with the rising impact factor of the journal.

In the name of the Editorial Board we wish all readers, authors and referees a lot of success in year 2009.

Prof. Dr.-Ing. Dr.hc. József Karger-Kocsis
Dr. Levente Macskási Prof. Dr. Tibor Czigány
editors

*Corresponding author, e-mail: czigany@eik.bme.hu

eXPRESS Polymer Letters Vol.3, No.1 (2009) 2–12
Available online at www.expresspolymlett.com
DOI: 10.3144/expresspolymlett.2009.2

Modelling of polypropylene fibre-matrix composites using finite element analysis

S. Houshyar, R. A. Shanks, A. Hodzic*

Applied Sciences, RMIT University, GPO Box 2476V, Melbourne, 3001, Australia

Received 1 September 2008; accepted in revised form 13 November 2008

Abstract. Polypropylene (PP) fibre-matrix composites previously prepared and studied experimentally were modelled using finite element analysis (FEA) in this work. FEA confirmed that fibre content and composition controlled stress distribution in all-PP composites. The stress concentration at the fibre-matrix interface became greater with less fibre content. Variations in fibre composition were more significant in higher stress regions of the composites. When fibre modulus increased, the stress concentration at the fibres decreased and the shear stress at the fibre-matrix interface became more intense. The ratio between matrix modulus and fibre modulus was important, as was the interfacial stress in reducing premature interfacial failure and increasing mechanical properties. The model demonstrated that with low fibre concentration, there were insufficient fibres to distribute the applied stress. Under these conditions the matrix yielded when the applied stress reached the matrix yield stress, resulting in increased fibre axial stress. When the fibre content was high, there was matrix depletion and stress transfer was inefficient. The predictions of the FEA model were consistent with experimental and published data.

Keywords: *polymer composites, poly(propylene), finite element analysis, mechanical properties, modelling*

1. Introduction

Polymer composites consist of two chemically distinct and physically separable constituents and they are widely used in many major engineering applications. Dispersed phase or reinforcement consists of fibres where the most common are glass, carbon, aramid, cellulose and metal oxide whiskers, used to improve the structural characteristics of the matrix-phase. The matrix serves two very important functions: it bonds the fibrous phase, and under an applied force, it deforms and distributes the stress to the high-modulus fibrous constituent. The ultimate properties of composites depend on the distinct properties of the constituents, shape and size of the individual reinforcing fibres or particles, their structural arrangement and distribution, the relative amount of each constituent, and the interface between reinforcement and matrix.

Thermoplastic-fibre composites of flexible polymers, such as polypropylene (PP), with natural cellulose fibres or polypropylene fibres provide environmentally friendly materials for application in construction and automotive industries [1, 2]. The melting temperature difference between PP fibre and random poly(propylene-co-ethylene) (PPE) have been exploited to prepare an all-PP composite [3–5]. The matrix must be liquid to ensure good wetting and impregnation of fibres during formation, though temperatures must be low enough to avoid melting and degradation of fibres. The high chemical compatibility of the two components allowed creation of strong physico-chemical interactions, favouring strong interfacial adhesion

*Corresponding author, e-mail: Robert.shanks@rmit.edu.au

[6, 7]. PP composites are of increasing importance because they increase the utility of PP from commodity polymer to engineering polymer applications. All-PP composites offer a new approach since they are thermoformable and recyclable as a mixture of PP grades. They avoid the abrasion to processing equipment that may occur with PP-glass fibre and other mineral filled composites. All-PP composites have been commercialized as PURE®, a technology from Lankhorst Indutech bv of the Netherlands [8], Milliken and Company, Spartanburg, S.C., introduced Moldable Fabric Technology (MFT), and Curv, produced commercially in Gronau, Germany, by Amoco Fabrics and Fibers Co., a unit of BP Amoco. All-PP composites require a difference between the matrix-PP and the PP fibres that will allow the matrix to consolidate by fusion without changing the fibres, this difference maybe a PP copolymer or even differing orientation [9]. All-PP composites combine by a process analogous to welding [10] and eliminate typical interfacial weakness problems or need for compatabilisers when non-polar PP is used with inorganic fillers [11, 12]. PP grafted with maleic anhydride is often used as a compatabiliser [13] though additional modification of fillers may be used [14]. PP fibres have lower modulus than glass fibres but can provide suitable reinforcement for many applications, and they do not suffer from exposure to variable humidity as do natural fibres such as flax [15]. Composite microstructures are determined by the physical and mechanical properties of the individual materials. Some analytical and numerical techniques have been used for prediction and characterization of composite behaviour. Analytical methods provide reasonable prediction for relatively simple configurations of the phases. Complicated geometries, loading conditions and material properties often do not yield analytical solutions, due to complexity and the number of equations. In this case, numerical methods are used for approximate solutions, but they still make some simplifying assumptions about the inherent microstructures of heterogeneous multiphase materials, one such method is finite element analysis (FEA) [8, 9]. The finite element method is an alternative approach to solving the prevailing equations of a structural problem. In the FEA method the equations are formulated for each finite element and combined to obtain a solution for the whole body instead of solving a uniform mathematical problem for the entire body. This method involves modelling the structure, using interconnected elements called finite elements, consisting of interconnected nodes and/or boundary lines and/or surfaces that are directly or indirectly linked with other elements via interfaces [16, 17]. Each finite element has an assumed displacement field. FEA requires selection of appropriate elements of suitable size and distribution (the FEA mesh). A displacement function and material property are associated with each finite element. Boundary conditions and loading define behaviour of each node and these are expressed in matrix notations [18, 19].

FEA combines a model in the form of microstructures with fundamental material properties such as elastic modulus or coefficient of thermal expansion of the constitutive phases as a basis for understanding material behaviour. Solutions are stress and strain data for each node in the system and they are summarized according to the usual criteria [16–19]. The aim of this analysis was prediction of the level of stress and stress distribution in fibre, matrix and fibre-matrix interface in composite with polypropylene fibres in a poly(propylene-co-ethylene) matrix. The experimental mechanical properties of the composites were determined by the fibre composition and interfacial bonding. For composites made with a constant mass fraction of fibre but smaller fibre diameter, more fibres are necessarily present, thus increasing the total amount of interface in the material for stress transfer (the principle mechanism for achieving a stiffened composite with the same mean fibre length but smaller fibre diameter). This acts to increase the total inter-fibre interaction, reducing the fibre stress concentration about the fibre ends, thus suppressing the onset of de-bonding/shear yielding. However, for the composite with very small fibre diameter, the number of the fibres was very high and resulted in a reduction of the composite stiffness, as shown in Figure 1a. At low fibre concentration, enough fibres did not restrain the matrix and localized strains occurred in the matrix at low stresses, as shown in Figure 1b. As the fibre concentration increased to 50% w/w, the stress was more evenly distributed and the composite stiffness increased. The deviation at high fibre concentration may be due to the (i) fibre packing, fibre-fibre contact which results in fibre damage and (ii) insufficiently rich polymer regions.

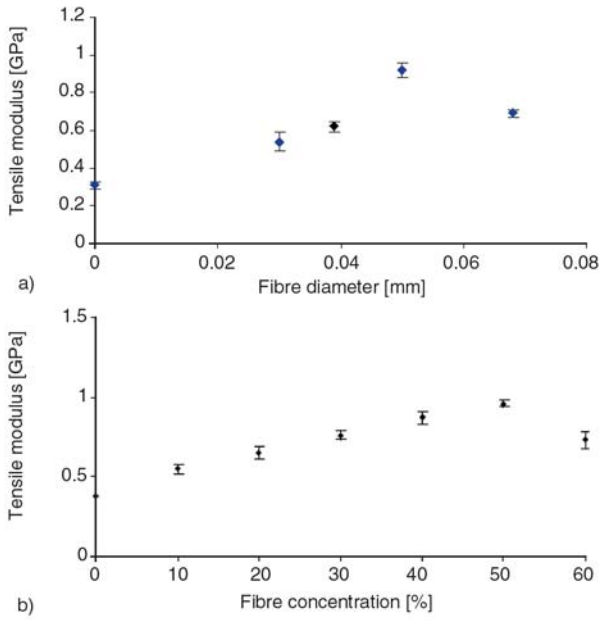

Figure 1. Tensile modulus for the composites of polypropylene fibre matrix as a function of (a) fibre diameter and (b) fibre concentration

This led to FEA investigation of the influence of fibre composition on the level of stress and stress distribution along the fibre-matrix interface, and within the fibre and matrix phases. A second objective dealt with variation of fibre content with constant material properties. The effect of fibre content on tensile properties and stress distribution in the composite are investigated in 3-dimensional (3D) mode. A third objective was to compare the all-PP composites with glass-PP and PE-PP fibre composites where the interface consists of unlike materials.

2. The composite model

The FEA method is used to model the behaviour of a material on the micro-mechanical level. Typically, a small section of a plate is considered, such as a square in plan view, where the side lengths are equal to the plate thickness and a complete depth of lay-up. This section is then modelled in detail using volume elements to represent the composite. Each element will have an isotropic property and be positioned corresponding to the centre line of the fibres. The model is small so a fine mesh of elements was used. This model could be used for various purposes but one factor that was important in this work, was to load it as if it were in a mechanical test instrument. All through-thickness edges could be held fixed and then boundary displacements applied to give unit strains to the model.

2.1. FEA modelling

A regular three-dimensional arrangement of long fibre in a matrix was adequate to describe the overall behaviour of the composite. The composite containing aligned long fibres was modelled as a regular uniform arrangement, as shown in Figure 2. This model assumed that the fibre was a perfect cylinder of length l, and diameter (d = 50 μm) in a cube of matrix. NE-Nastran FEA software version 8 and FEMAP graphics software version 7 was used for FEA in tensile mode. The model is treated as a linear axial-symmetric problem.

The FEA model in Figures 2a, 2b constituted 54 600 and 104 500 noded brick elements, used for a single fibre and a multiple fibre-matrix structure, respectively. The model included the fibre, the matrix and the fibre-matrix interface. Nine fibres in the matrix, Figure 2b, were modelled to eliminate the effect of edges on the level of stress and stress distribution in the central fibre and the surrounding matrix. The central fibre, surrounding matrix and interface were selected for stress analysis in this model. These regions were modelled using the fine mesh shown in Figure 3. Unit strain boundary conditions were applied as an imposed displacement on all boundary nodes to obtain the equivalent in-plane stiffness properties. Such models give detailed stress distributions around and within the fibre once the actual strains have been determined.

Equivalent properties were used in a global model, the problem was solved and the strains at any point were computed. The size of model was determined using Equation (1) [16, 17]:

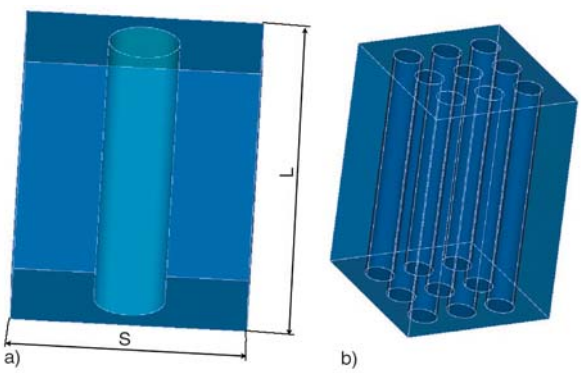

Figure 2. Unit cell of square array fibre packing geometry in 3D (a) for one-fibre and (b) multiple fibres

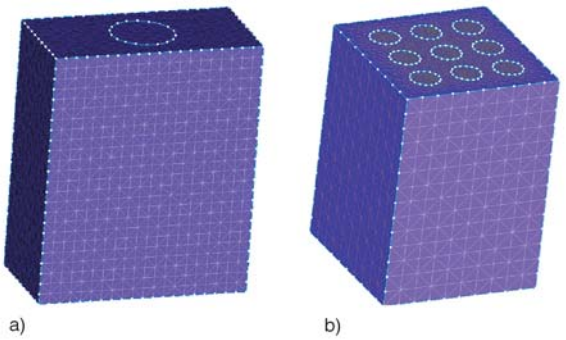

Figure 3. The FEA mesh used in the present analysis shown in 3D

$$V_f = \frac{\pi l d^2}{4LS^2} \tag{1}$$

where V_f is fibre content, d is fibre diameter, l is fibre length, L is longitudinal fibre spacing and S is fibre spacing, as shown in Figure 2.

According to the theory of effective performance, when the mean tensile strain of the model was calculated under uniform tensile stress loading (along the z axis), the stress-strain behaviour of the composite could be modelled by FEA. With different micro-structural parameters considered in FEA, the correlation between tensile properties of the composite and its micro-structural parameters is discussed in this work. In this calculation, the fibre was taken as an elastic material with elastic modulus, E_f = 4.5, 75, 0.3 GPa for PP, glass and polyethylene (PE) fibre respectively and Poisson ratio of υ_f = 0.2. The matrix was a bi-linear material that obeyed the von Mises yielding criterion with Poisson ratio of υ_m = 0.33 and a tensile modulus of 1.05 GPa. No attempt was made to include a failure criterion or the effect of differential thermal deformation of the fibre and the matrix, as it was not necessary for the elastic model.

The 3D model could be subjected to loading in any direction to determine the corresponding properties and the stress-strain curve of the composite. The boundary conditions for the model include fixing one end of the model in all its three degrees of freedom and applying an axial load to the free end. The average composite stress and strain are given by Equations (2) and (3) [16, 17]:

$$\bar{\sigma} = \frac{1}{V}\sum_{n=1}^{k} V_n \sigma_{ij} \tag{2}$$

$$\bar{\varepsilon} = \frac{1}{V}\sum_{n=1}^{k} V_n \varepsilon_{ij} \tag{3}$$

where k is the total number of elements, σ_{ij} is the nth element stress, ε_{ij} is the n^{th} element strain and V is the total volume of composite. The contribution of each element of the composite model was taken into consideration according to Equations (2) and (3). This resulted in better estimates for the elastic moduli of various composites, than the estimates of other models, such as the rule of mixture [20, 21] and the Halpin-Tsai [22] (H-T) equation.

2.2. Variation of fibre composition

Mechanical properties used in these simulations were glass, PP and PE fibres with PPE matrix properties, since these materials were used in our experimental work and other published data. In this case, the same PPE matrix was considered for all composites to investigate the effect of the reinforcement on the mechanical properties of the composite. Finally, the FEA results were compared with experimental and published data [22].

2.3. Variation of fibre content

Mechanical properties used in these simulations were that of PP fibre and PPE matrix, the same materials used in our experiments, to show the effect of the fibre content on the mechanical properties of the composite. Reinforcement content affects the level of stress and stress distribution in fibre, matrix and fibre-matrix interphase. In this model, fibre content was varying from 20 to 50% v/v.

2.4. Numerical method

Two different composite systems have been considered in the present investigation. For the prediction of tensile properties of the two systems: (I) the same PP matrix and fibre content and, (II) the same PP reinforcement and matrix have been considered. This was to ensure better comparison with some published data and our experimental data as well as to show the effect of the properties of constituents on the composite properties. A comparative method has been performed [23].

3. Results and discussion

3.1. Stress distribution

Figure 4 illustrates the normal stress distribution for an all-PP composite. As can be seen the region surrounding the fibre and interphase exhibit complicated stress distribution. Figure 5 shows the level of stress in the fibre as well as in the fibre-matrix interface. There are two important zones of stress concentration, as shown in Figure 5: (1) fibre (especially fibre skin) (2) fibre-matrix interphase. The most important stress is at the interface. The von Mises stress shows high stress concentration in the fibre and interphase region. Figures 4 and 5 show that both the fibre and the interface in all-PP composites have uniform stress distribution. Figure 4 shows that there is a small difference between the concentrated stresses in fibre and surrounding matrix. Alternatively, glass-PP and PE-PP composites exhibit a level of concentrated stress that was not uniform in both constituents and the difference between the stress in the fibre and the surrounding matrix was very high. This can result in interfacial failure at low stress.

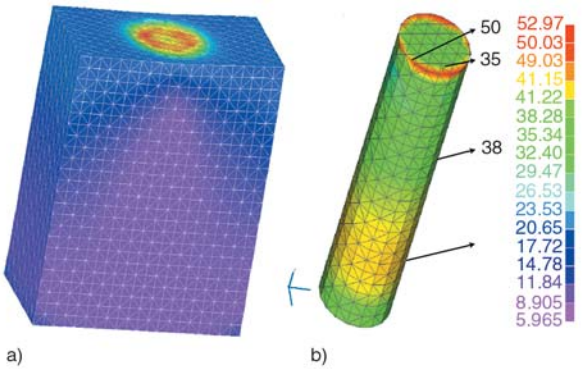

Figure 4. Stress distribution in (a) composite and (b) fibre

3.2. Variation of fibre content

Stress distribution for the composites with varying fibres content is shown in Figures 6 and 7. In Figure 6, the stress is plotted along the interface region, whereas Figure 7 shows stress as a function of the distance from the fibre centre to matrix. Although variation in fibre content had little effect on the stress at interphase, the difference in stress at the fibre and matrix was striking. If the fibres were packed too close, this would lead to stress concentrations and eventually de-bonding of the fibres. This means that there are detrimental effects in synergy arising from minimal matrix regions and high stress concentrations between adjacent fibres. Due to this, the composite with fibre content more than 50% v/v was not considered for modelling.

Figure 8 shows the stress distribution in fibres and surrounding matrix for composites with different fibre content. A rise in fibre content resulted in a more uniform stress distribution between fibre and surrounding matrix. Thus, whole fibres carried the main proportion of applied stress. However, for the

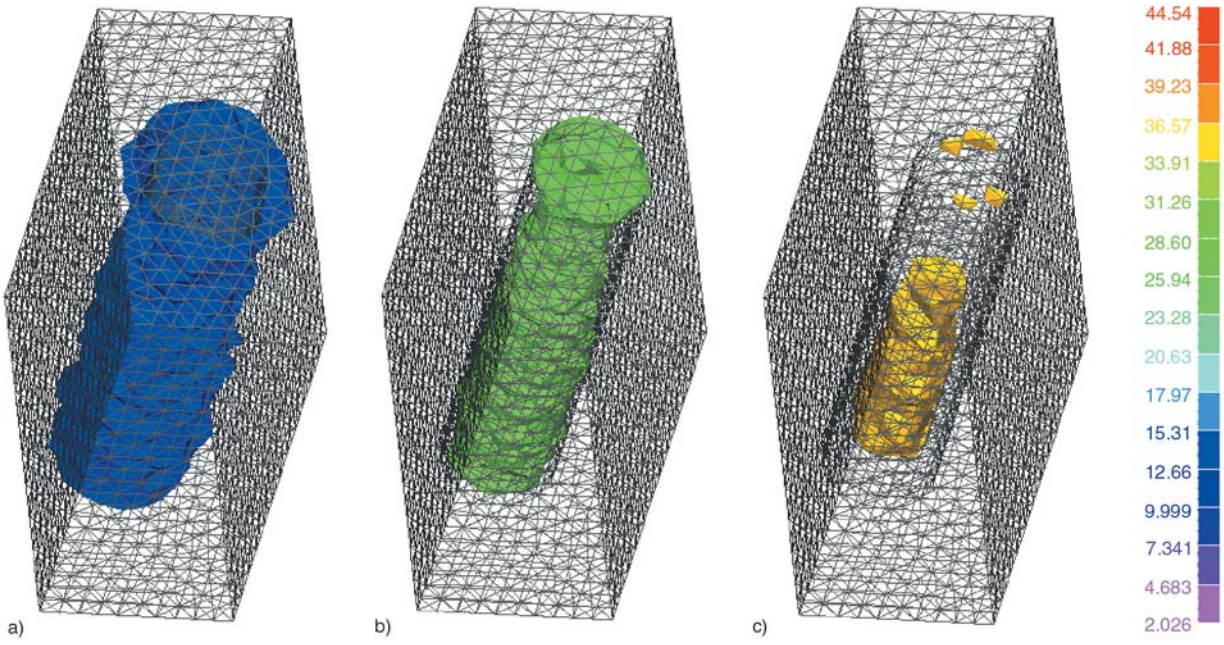

Figure 5. Details of the band illustration of normal stress at two high stress regions (a) interface and (b, c) fibre

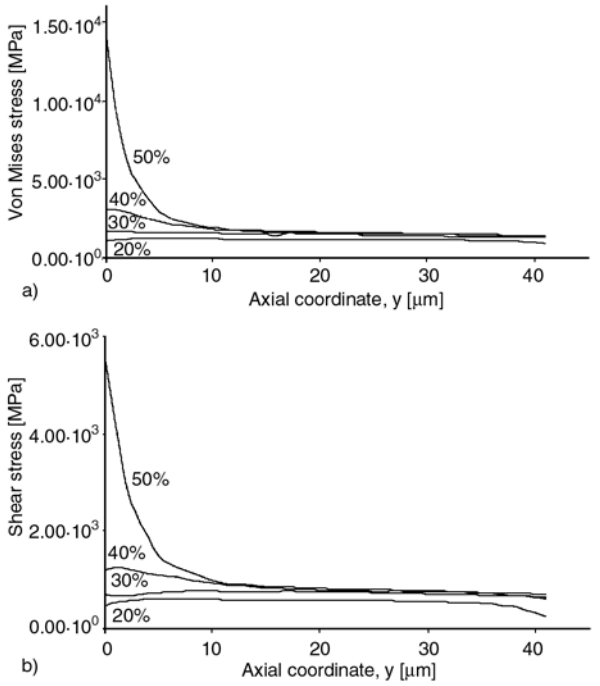

Figure 6. Distribution of axial stress in the composite with various fibre contents along the interface (a) von Mises stress and (b) shear stress

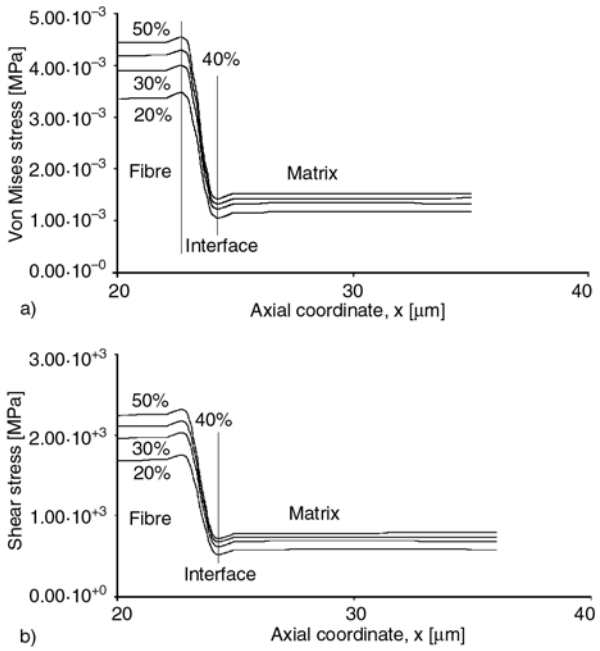

Figure 7. Distribution of axial stress in the composite with various fibre contents across the interface from 1 cm from the fibre end (a) von Mises stress and (b) shear stress

composite with low fibre content the matrix carried the main proportion of the applied load and tailed when the applied stress reached the matrix yield strength. The large scale yielding of the matrix resulted in increased fibre axial stress [8, 9]. This was consistent with the experimental results. In Figure 8, the load for the two composites is the same, but the level of stress in the fibres is lower and in the matrix is higher than in the composite with lower fibre content. This means the load applied to the composite will be carried by the fibre, compared with when there is a lower fibre content present. A higher shear stress appeared at the interface for the composite with low fibre content that lead to facile interfacial failure. The fibre content of the composite was an important factor controlling the mechanical properties of the composites.

There was a deviation at high fibre content more than a critical value (50%), because if the matrix was not adequately covering the fibres, efficient stress transfer from the matrix to the fibres was not obtained, causing a weakening effect rather than a reinforcing one in the presence of the fibres, and resulting in failure of the matrix. It is possible to reduce the stress concentration in the matrix and at the fibre-matrix interface by increasing fibre content to an optimum content. After this optimum level, the stress concentration increased at the fibre-matrix interface and in the matrix resulting in composite failure at lower stress, as predicted by FEA.

The simplest model for the micromechanics of fibre composites is that of Cox [20, 21] that is used in an analysis known as classical shear lag, where the theory required that simplifications are made. The assumptions are:

1. The interface between the two components is perfect;
2. The fibre and matrix remain elastic in their mechanical responses;
3. No axial load is transmitted through the fibre ends.

This gave the following equation, a simple rule of mixtures (Equation (4)):

$$E_c = V_f \cdot E_f + V_m \cdot E_m \tag{4}$$

where E is tensile modulus, V is volume fraction, and c, f and m represent composite, fibre and matrix, respectively. Following these assumptions a certain length of fibre is required for the transfer of shear stress from the matrix surrounding embedded fibres in a fibre composite under load.

Another model was introduced by Halpin, Tsai and Kardos, based on [22], which is an empirical

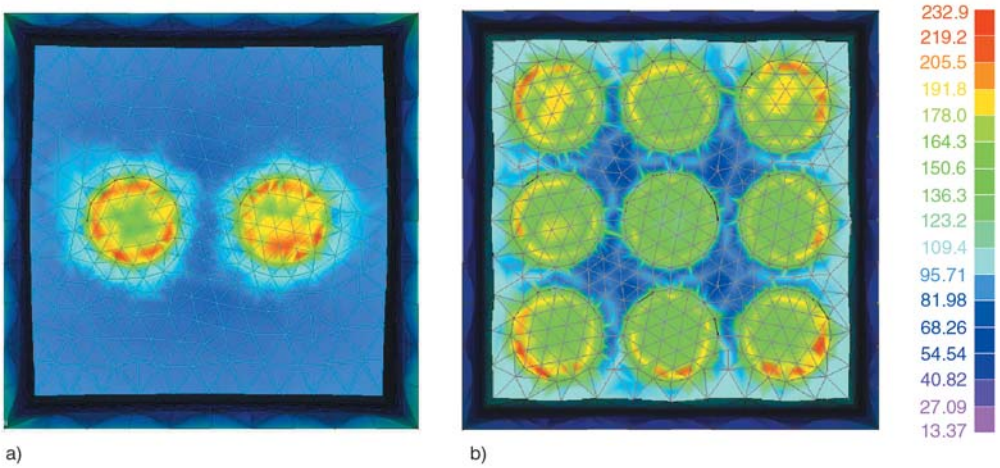

Figure 8. FEA representation of the normal stress distribution in the cross section of the composite with (a) 20 and (b) 50% wt fibre content

expression containing a geometric fitting parameter A, obtained by fitting with the numerical solution of formal elasticity theory. Composite moduli are put in the form (Equations (5) and (6)):

$$E_c = \frac{E_m(1+AB\Phi)}{1-B\Phi} \tag{5}$$

where

$$B = \frac{\frac{E_f}{E_m}-1}{\frac{E_f}{E_m}+A} \tag{6}$$

$A = 2(l/d)$ for tensile modulus. The ratio l/d is the aspect ratio. These equations are accurate for low fibre volume fractions. They are useful in determining the properties of composites that contain discontinuous fibres oriented in the loading directions

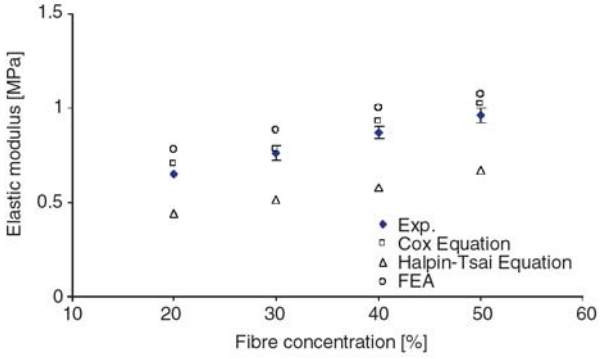

Figure 9. Comparison of the present FEA, rule of mixtures (Cox) equation, experimental data and the H-T equation predictions of Young's modulus of all-PP composites

Figure 9 shows the elastic modulus of the PP composite with different fibre concentrations and predictions of the H-T, rule of mixtures (Cox), FEA and the experimental data. As can be seen from this figure the results of both the present FEA and Cox equations agree well. However the results from the H-T were found to be lower than those predicted by FEA and Cox equations. Cox equation fit the data better because the experimental and model systems approximate to the three assumptions, while the H-T equation is not satisfied in that there is not a low fibre volume content and the fibres where not discontinuous in each system studied.

3.3. Variation of fibre composition

The von Mises and shear stress of the two important regions in the FEA model were analysed: (a) along the interfacial region, defined as the bonding line between the fibre and matrix; (b) along the specimen surface, where high stress was initiated by the applied force. Variation in fibre composition showed significant influence on the stress region in the composite, and on the resulting mechanical properties of the composite. The stresses in the interface regions in the three systems are shown in Figure 10.

When the fibre stiffness was too high or too low in comparison with the matrix, the load shared by the fibres significantly declined. There was a large difference between the level of stress in the fibres and matrix and high shear stress at the interface of the glass-PP composite leading to a high chance of interfacial de-bonding or failure at low stress. High

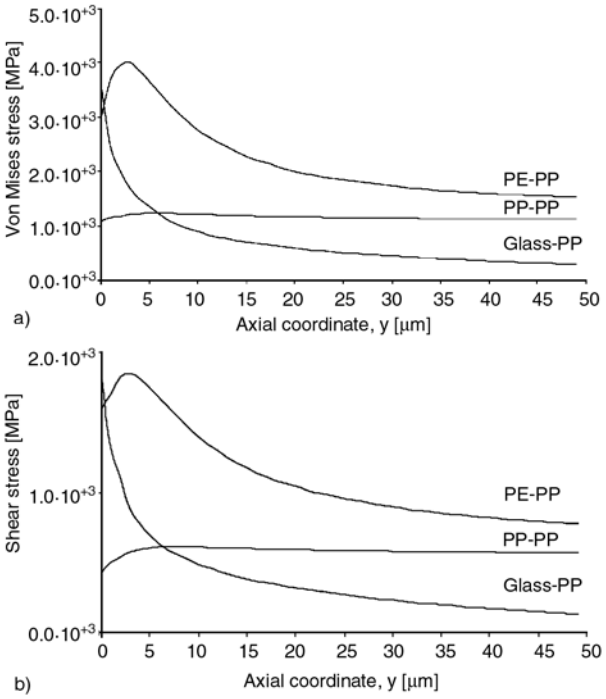

Figure 10. Distribution of axial stress in the composite with various fibre compositions along the interface (a) von Mises stress and (b) shear stress

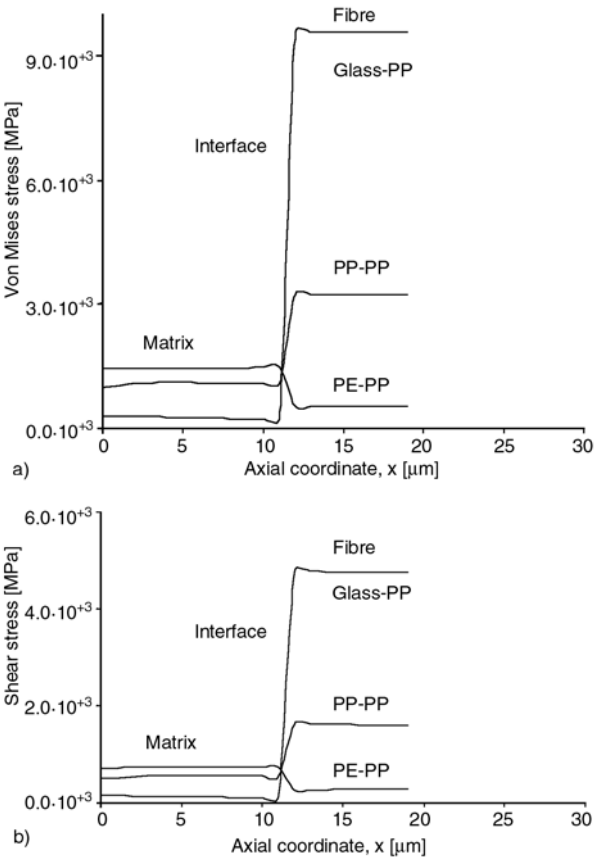

Figure 11. Distribution of axial stress in the composite with various fibre compositions across the interface (a) von Mises stress and (b) shear stress

fibre strength and stiffness are not an advantage, whereas in all-PP composites, the level of stress in fibre and matrix were close, leading to uniform stress distributions along the fibre-matrix interface and uniform performance of the composite. In this case, an applied load was transferred from the matrix to the fibre and the fibres retained a high proportion of the applied load in the composite during the test. According to the results for the PE-composites, the load did not transmit to the fibre from the matrix. PE fibre carried lower load than the matrix, which led to composite failure at low applied load. Figure 10 shows that the shear stress at the interface of this type of composite was more than that in the fibre and matrix. This increased the risk of premature interfacial failure and reduced the mechanical properties of the composite.

Figure 11 shows the von Mises and shear stress along the specimen surface. The figure supports the results from Figure 10 and shows an uneven stress distribution and a great difference between the level of stress in the surrounding matrix and the fibre in a glass-PP and PE-PP system in comparison with the all-PP system, leading to stress concentration in the interfacial region. This results in an easy separation of fibre from the matrix when a high load was applied. In this case, the shear stress at the interface was more than the normal stress. This means that interfacial shear de-bonding may occur under a critical applied stress, instead of the interfacial normal de-bonding. However, in the case of an all-PP system, the interfacial shear stress became lower than interfacial normal de-bonding. Thus, interfacial normal de-bonding, instead of interfacial shear de-bonding may occur when a critical applied stress was reached.

In glass-PP system the level of high stress on the interphase and the fibre cannot contribute to transmitting the load in the composite and the strength and stiffness of the fibre was not important. However, in PE-PP systems, the stress was high in the matrix and again the fibre could not reinforce the composite, due to the low stiffness and strength.

Figure 12 shows the 3D model of a glass-PP composite under an applied load. It can be seen from this figure that the stress concentrated at the fibre is 20 times more than the stress in the surrounding matrix. In this case (E_{matrix}/E_{fibre}) was too small, so a high shear stress appeared at the interface and

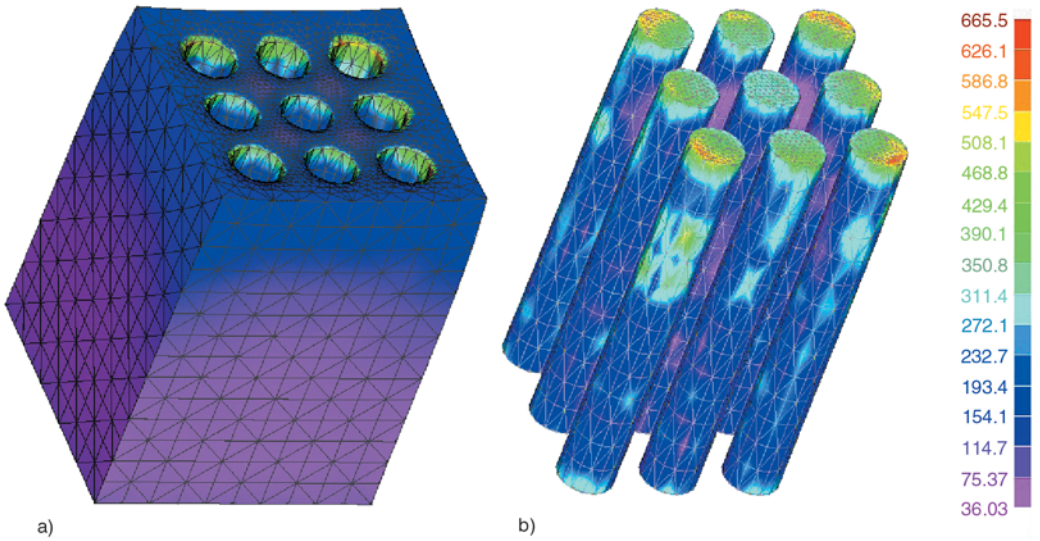

Figure 12. Stress distribution in (a) glass-PP composite and (b) glass fibre in the composite

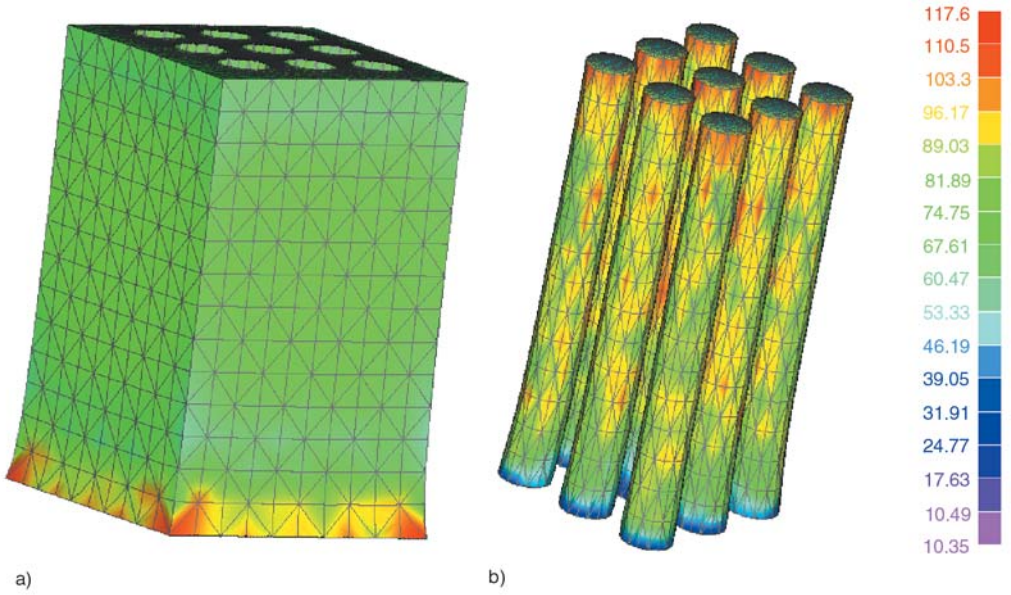

Figure 13. Stress distribution in (a) PE-PP composite and (b) PE fibre in the composite

interfacial shear failure would easily occur. Thus, this could be a weak point in mechanical properties of this system.

Figure 13 shows the 3D model for a PE-PP composite. The stress distribution and concentration are shown. In this composite the PE fibre has a lower stiffness than the matrix. The PE fibres cannot share a large portion of the applied stress and the matrix carried the main portion of the applied load. For example, the fibre took about 25% of the load carried by the surrounding matrix.

As observed from Figure 14, the stress distribution in an all-PP system is uniform in the fibres and surrounding matrix. In all-PP systems, fibre and matrix possess similar stiffness, and a significant portion of the applied load was transferred to the fibre. Thus, the stress concentration at the fibre-matrix interface was not too high, and posed no risk of premature interfacial failure. In this case, the fibres act as reinforcement for the lower stiffness matrix and improved the mechanical properties of the matrix. The results showed the advantages of using the same fibre and matrix in a composite.

4. Conclusions

It was shown using FEA, that the fibre content and composition had a dominant influence on stress distribution in polypropylene composites. The stress concentration at the fibre-matrix interface

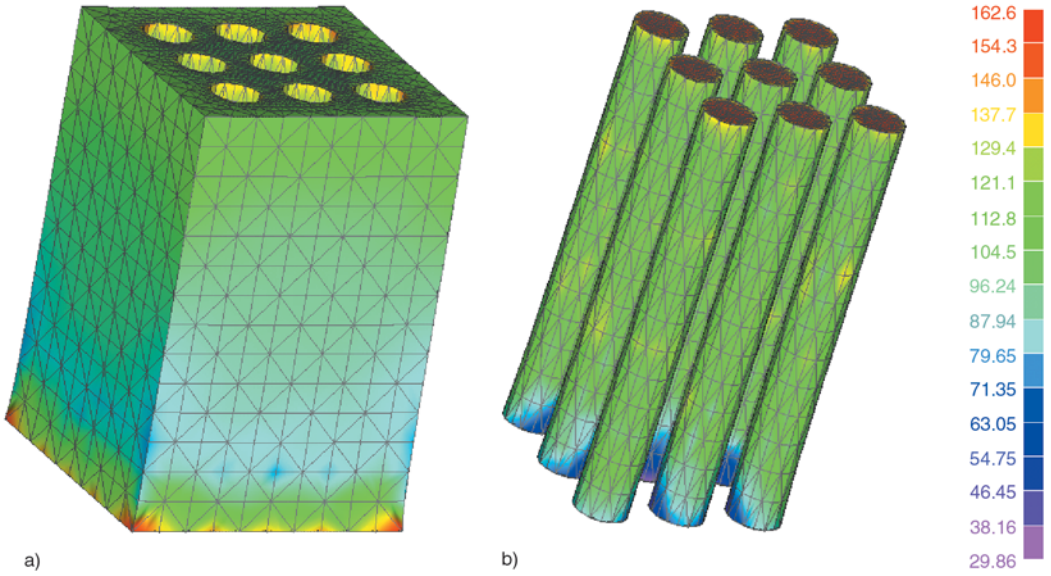

Figure 14. Stress distribution in (a) all-PP composite and (b) PP fibre in the composite

increased with decrease in fibre content. The variations in fibre composition influenced the higher stress region of the composites. As the fibre stiffness increased, the load shared by the fibres significantly declined and the shear stress at the fibre-matrix interface increased. As was observed for the all-PP system, the ratio between matrix and fibre stiffness was significant and the interfacial stress carried by both constituents acted to reduce the risk of premature interfacial failure and increased the mechanical properties of the composite. FEA results for this part of the investigation were consistent with prior experimental data.

The FEA model showed that with low fibre content, the fibre was not able to share a large portion of applied stress. The matrix carried the main portion of the applied stress and yielded over a large scale when the applied stress reached the matrix strength, resulting in increased fibre axial stress that was predicted by FEA. In the case of high fibre content, there was insufficient matrix to cover the fibre and stress transfer was inefficient. The predictions of the FEA model were consistent with experimental and published data.

Acknowledgements

Financial support from International Postgraduate Scholarship (IPRS) for Shadi Houshyar is acknowledged.

References

[1] Shanks R. A.: Alternative solutions: Recyclable synthetic fibre-thermoplastic composites. in 'Green Composites: Polymer Composites and the Environment' (ed.: Baillie C.) Woodhead Publishing, Cambridge 100–122 (2004).

[2] Wong S., Shanks R. A., Hodzic A.: Poly(L-lactic acid) composites with flax fibres modified by plasticizer absorption. Polymer Engineering and Science, **43**, 1566–1575 (2003).
DOI: 10.1002/pen.10132

[3] Houshyar S., Shanks R. A., Hodzic A.: The effect of fibre concentration on mechanical and thermal properties of fibre reinforced polypropylene composites. Journal of Applied Polymer Science, **96**, 2260–2272 (2005).
DOI: 10.1002/app.20874

[4] Houshyar S., Shanks R. A., Hodzic A.: Tensile creep behaviour of polypropylene fibre reinforced polypropylene composites. Polymer Testing, **24**, 257–264 (2005).
DOI: 10.1016/j.polymertesting.2004.07.003

[5] Houshyar S., Shanks R. A., Hodzic A.: Influence of different woven geometry in poly(propylene) woven composites. Macromolecular Materials and Engineering, **290**, 45–52 (2005).
DOI: 10.1002/mame.200400158

[6] Houshyar S., Shanks R. A.: Tensile properties and creep response of polypropylene fibre composites with variation of fibre diameter. Polymer International, **53**, 1752–1759 (2004).
DOI: 10.1002/pi.1569

[7] Houshyar S., Shanks R. A.: Morphology, thermal and mechanical properties of poly(propylene) fibre-matrix composites. Macromolecular Materials and Engineering, **288**, 599–606 (2003).
DOI: 10.1002/mame.200300023

[8] Abraham T., Banik K., Karger-Kocsis J.: All-PP composites (PURE®) with unidirectional and cross-ply lay-ups: Dynamic mechanical thermal analysis. Express Polymer Letters, **1**, 519–526 (2007).
DOI: 10.3144/expresspolymlett.2007.74

[9] Izer A., Bárány T.: Hot consolidated all-PP composites from textile fabrics composed of isotactic PP filaments with different degrees of orientation. Express Polymer Letters, **1**, 790–796 (2007).
DOI: 10.3144/expresspolymlett.2007.109

[10] Varga J., Ehrenstein G. W., Schlarb A. K.: Vibration welding of alpha and beta isotactic polypropylenes: Mechanical properties and structure. Express Polymer Letters, **2**, 148–156 (2008).
DOI: 10.3144/expresspolymlett.2008.20

[11] Cai L. F., Mai Y. L., Rong M. Z., Ruan W. H., Zhang M. Q.: Interfacial effects in nano-silica/polypropylene composites fabricated by in-situ chemical blowing. Express Polymer Letters, **1**, 2–7 (2007).
DOI: 10.3144/expresspolymlett.2007.2

[12] Turmanova S. Ch., Genieva S. D., Dimitrova1 A. S., Vlaev L.T.: Non-isothermal degradation kinetics of filled with rise husk ash polypropene composites. Express Polymer Letters, **2**, 133–146 (2008).
DOI: 10.3144/expresspolymlett.2008.18

[13] Prashantha K., Soulestin J., Lacrampe M. F., Claes M., Dupin G., Krawczak P.: Multi-walled carbon nanotube filled polypropylene nanocomposites based on masterbatch route: Improvement of dispersion and mechanical properties through PP-g-MA addition. Express Polymer Letters, **2**, 735–745 (2008).
DOI: 10.3144/expresspolymlett.2008.87

[14] Pannirselvam M., Genovese A., Jollands M. C., Bhattacharya S. N., Shanks R. A.: Oxygen barrier property of polypropylene-polyether treated clay nanocomposite. Express Polymer Letters, **2**, 429–439 (2008).
DOI: 10.3144/expresspolymlett.2008.52

[15] Bledzki A. K., Mamun A. A., Lucka-Gabor M., Gutowski V. S: The effects of acetylation on properties of flax fibre and its polypropylene composites. Express Polymer Letters, **2**, 413–422 (2008).
DOI: 10.3144/expresspolymlett.2008.50

[16] Shati F. K., Esat I. I., Bahai H.: FEA modelling of visco-plastic behaviour of metal matrix composites. Finite Elements in Analysis and Design, **37**, 263–272 (2001).
DOI: 10.1016/S0168-874X(00)00042-1

[17] Kang G. Z., Gao Q.: Tensile properties of randomly oriented short δ-Al_2O_3 fibre reinforced aluminium alloy composites: II. Finite element analysis for stress transfer, elastic modulus and stress-strain curve. Composites Part A, Applied Science and Manufacturing, **33**, 657–667 (2002).
DOI: 10.1016/S1359-835X(02)00006-4

[18] Hodzic A., Stachurski Z. H.: Droplet on a fibre: Surface tension and geometry. Composites and Interfaces, **8**, 415–425 (2001).
DOI: 10.1163/156855401753424451

[19] Huang A., Bush M. B.: Finite element analysis of mechanical properties in discontinuously reinforced metal matrix composites with ultra fine micro structure. Materials Science and Engineering, A, **232**, 63–72 (1997).
DOI: 10.1016/S0921-5093(97)00092-0

[20] Krenchel H.: Fibre reinforcement. Akademisk Forlag, Copenhagen (1964).

[21] He T., Porter R. S.: Melt transcrystallization of polyethylene on high modulus polyethylene fibres. Journal of Applied Polymer Science, **35**, 1945–1953 (1988).
DOI: 10.1002/app.1988.070350720

[22] Ibarra L., Macias M., Palma E.: Viscoelastic properties of short carbon fibre thermoplastic (SBS) elastomer composites. Journal of Applied Polymer Science, **57**, 831–842 (1995).
DOI: 10.1002/app.1995.070570707

[23] Maligno A. R., Warrior N. A., Long A. C.: Finite element investigations on the microstructure of fibre-reinforced composites. Express Polymer Letters, **2**, 665–676 (2008).
DOI: 10.3144/expresspolymlett.2008.79

eXPRESS Polymer Letters Vol.3, No.1 (2009) 13–18
Available online at www.expresspolymlett.com
DOI: 10.3144/expresspolymlett.2009.3

Short-chain grafting of tetrahydrofuran and 1,4-dioxane cycles on vinylchloride-maleic anhydride copolymer

A. G. Filimoshkin[1*], *A. S. Kuchevskaya*[1], *E. M. Berezina*[1], *V. D. Ogorodnikov*[2]

[1]Tomsk State University, Tomsk, 634050, Russia
[2]Institute of Petroleum Chemistry SB RAS, Tomsk, 634021, Russia

Received 27 October 2008; accepted in revised form 24 November 2008

Abstract. Mass increase of vinylchloride-maleic anhydride (VC-MA) copolymer samples aged in tetrahydrofuran (THF) or in 1,4-dioxane results from chemical interaction of VC-MA macromolecules with 1,4-dioxane or THF. Microstructure of the products of such modification was proved by infrared spectroscopy (IR-) and nuclear magnetic resonance spectroscopy (^{13}C NMR and ^{1}H NMR). Mechanism of modification has been proposed. The results of microstructure research of VC-MA samples aged in THF and in 1,4-dioxane coincide with already known data on the reactions of opening of these and other oxygen-containing cycles under mild conditions.

Keywords: *polymer synthesis, molecular engineering, graft copolymers, vinyl chloride-maleic anhydride copolymers, tetrahydrofuran, 1,4-dioxane*

1. Introduction

Alternating, statistical and graft copolymers of maleic anhydride (MA) exhibit quite a number of valuable properties. Thus MA and vinyl chloride (VC) copolymers easily enter into various reactions and are considered as convenient initial products for polymer synthesis of new substances utilized as biologically active materials and enzyme carriers, ionites, photographic, pharmaceutical, pore-forming, antifriction materials *etc* [1]. Copolymers of vinyl monomers with MA are applied in automotive industry [2] and they are also used as the initial reagents to produce novel composite materials. Sodium salts of succinic anhydride derivatives are widely used as dispersants, flocculants and soil modifiers [3]. Biomedical application of the MA copolymers as medicines and their carriers is also of interest.

The VC-MA copolymer easily reacts with water and alcohols [4, 5], sodium azide [6], carbonyl-containing solvents and dimethyl sulfoxide [7]. In deuterated acetone medium deuteroexchange was detected in the enol fragments of the macromolecules [8]. The reactions of the VC-MA copolymers with dimethyl formamide molecules proceed as regiospecific to form long-living solvate structures [9].

The present work is aimed at studying chemical modification of the VC-MA copolymer with such cyclic ethers as THF and 1,4-dioxane as a mode of molecular engineering.

2. Experimental

The samples of VC-MA copolymer were obtained by radical copolymerization of MA and VC at 80°C for 24 h in sealed tubes in 1,2-dichlorethane with benzoyl peroxide (1 mass%) and with a comonomer ratio of 1:1 [10]. The initial reagents and solvents were thoroughly refined [11]. The IR

*Corresponding author, e-mail: poly@ipc.tsc.ru

spectra were recorded on a FTIR-Spectrometer Nicolet 5700 (Thermo Electron, USA) in tablets with KBr (2 mg/300 mg KBr); ^{1}H and ^{13}C NMR spectra – on a Bruker Avance AV 300 NMR Spectrometer (Bruker, Germany) with operating frequency 300 and 75 MHz accordingly at 25°C in d_6-acetone (10 mass% solutions), where acetone was used as an internal standard. All experiments were carried out under conditions excluding any contact with atmospheric moisture to prevent hydrolysis of the succinic anhydride rings.

The process of grafting of THF and 1,4-dioxane was carried out in tightly closed flasks (0.5 g of VC-MA and 4 ml of the solvent). In a day homogeneous viscous solutions were carefully carried into the preliminary weighted Petri dishes and left for a week to remove the solvents. The formed films were dried *in vacuo* to constant mass. The mass of the aged samples increased by 8–10 mass% as compared to the mass of the initial VC-MA copolymer. Calculation of grafting efficiency: degree of polymerization is *ca* 600; 30 mol% (initial) of repeated units are tautomerized in the enol forms (see below) [12, 13]. If all enol forms had been involved in grafting the mass increase of the sample treated by THF would have been 12 mass%. The 8–10 mass% increase indicates that 60 mol% of the initial enol forms participate in grafting.

3. Results and discussion

Due to the action of different catalysts (HCl, $(CH_3CO)_2O$, ($POCl_3$ + H_2SO_4) and H_3PO_4) THF

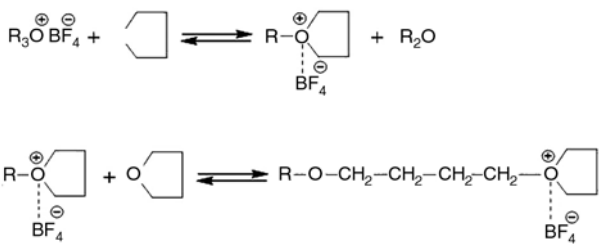

Figure 1. Mechanism of THF cycles breakage followed by polymerization

cycles open under mild conditions [14, 15]. As an example THF cycle opening in the presence of $R_3O{\cdot}BF_4$ is accompanied by polymerization (Figure 1). The other reactions of oxygen-containing cycle polymerization are also known [16].

Marked increase in the VC-MA copolymer mass after its aging in THF and in 1,4-dioxane media was unexpected. To explain this fact we supposed that certain tautomeric forms of the repeated units of VC-MA copolymer [10] interact with solvent molecules, which open with simultaneous grafting on them.

In the solvents of various nature VC-MA copolymer undergoes cycloanhydride-enol tautomerism resulting in dynamic micro structural heterogeneity in the form of enol Δ^6*en* (see *b*, *d*, *f* and *h* in Figure 2) and dienol derivatives of furan being tautomers of jointly VC and MA comonomer units, which afterwards appear in the macromolecular chains as succinic anhydride derivatives [10, 17]. Formation of Δ^6*en* tautomeric forms is accompanied by appearance of aromatic carbon atom signals in the ^{13}C NMR spectrum of the VC-MA

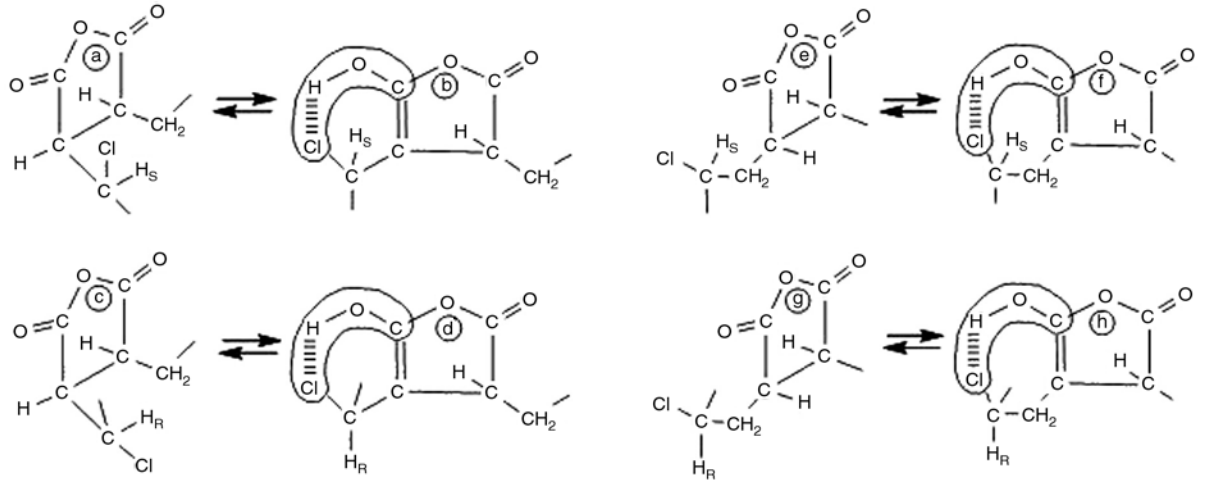

Figure 2. Dynamic microstructure of the VC-MA macromolecules (a, c, e and g – comonomeric units of VC and MA; b, d, f and h – Δ^6*en* tautomeric forms of the a, c, e and g units. H_S and H_R – hydrogen atoms attached to the S- or R-chiral carbon atoms).

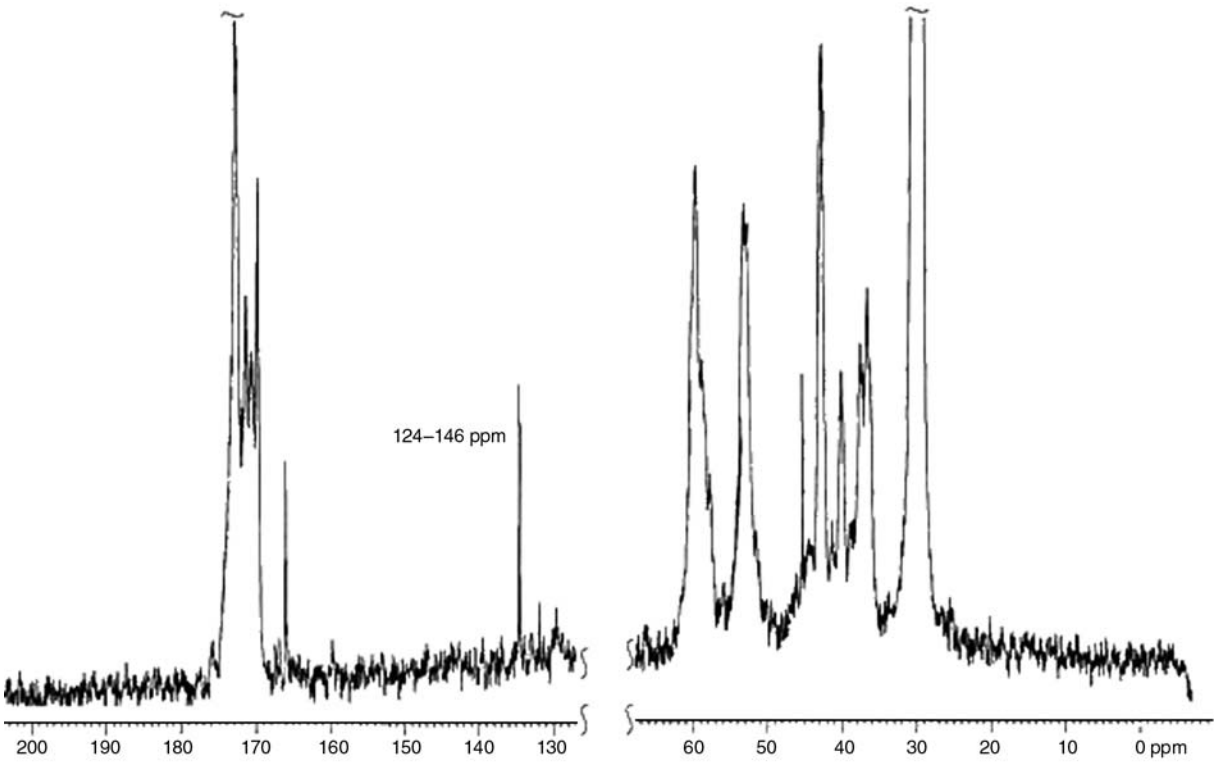

Figure 3. The ^{13}C NMR spectrum of the original VC-MA sample

sample in the region of 124–146 ppm (Figure 3) [18]. Under the selected synthesis conditions macromolecules of equimolar VC-MA copolymer were earlier found [12] to consist of the statistical sequence of the VC-MA repeat units (~67 mol%) and their Δ^6*en* tautomers (~33 mol%) (Figure 2) which was proved by mathematical modeling of the microstructure of the macromolecules in view [13]. It was suggested just the [Cl…H–O–C $^{\delta+}$]$^{\#}$ ensembles (Figure 2) that are the reaction centers causing cycle opening. Their high-energy transition state promotes formation of oxonium ions causing breakage of THF and 1,4-dioxane cycles: Figure 4 presents a mechanism of THF cycles grafting on the macromolecules of the VC-MA copolymer. As a result of nucleophilic attack at the C–Cl carbon atom (*a*) an oxonium compound is being formed (*b*) with simultaneous bonding breakage of the intramolecular hydrogen bond and hydrogen migration to its original position (*c*), THF cycle being opened at the same time (*d*).

To determine microstructure of VC-MA macromolecules modified with THF we used IR-, ^{13}C and ^{1}H NMR-spectroscopy. The IR spectrum of VC-MA aged in THF exhibits new bands: $\nu_{-C-O-C-}$ (1174 cm^{-1}), ν_{CH_2} (2588 and 2893 cm^{-1}), δ_{CH_2} (1368 cm^{-1}) and δ_{CH} (876 and 835 cm^{-1}), and the band intensity of δ_{CH_2} (1440 cm^{-1}) highly increases (see 1, 2 in Figure 5). The substantial change in the C–Cl carbon environment (Figures 4a and 4d) leads to the increased intensity of the ν_{CCl} absorption band (619 cm^{-1}). Besides one observes redistribu-

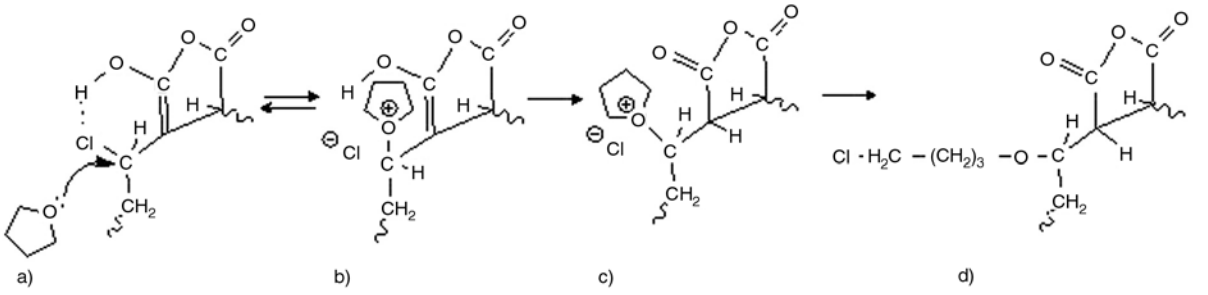

Figure 4. Mechanism of THF cycles grafting on the VC-MA macromolecules

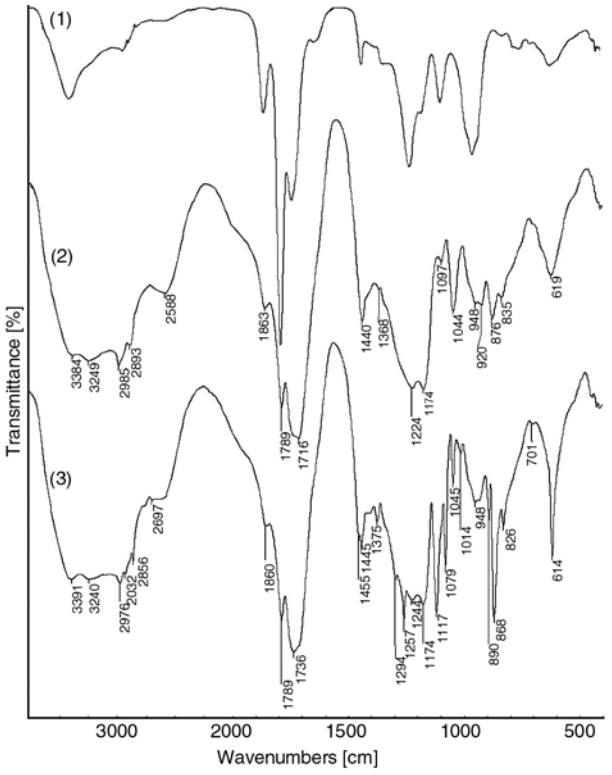

Figure 5. The IR spectra of the original VC-MA sample (1), of the VC-MA sample aged in THF (2) and of the VC-MA sample aged in 1,4-dioxane (3)

tion of band intensities at 1863, 1789 and 1716 cm^{-1} caused by $\nu_{C=O}$ of the succinic anhydride ring.

The ^1H NMR spectrum of the same VC-MA sample exhibits multiplets at 3.6–3.7 and 1.7–1.8 ppm (Figure 6b; unequivalent methylene groups of the attached THF molecules Cl–**CH_2**–CH_2–CH_2–**CH_2**–O–) absent in the spectrum of the initial VC-MA sample (Figure 6a). In the ^{13}C NMR spectrum two additional signals at 26 and 68 ppm of unequivalent CH_2 carbons are registered (Figure 7a).

If polymerization which is accompanied by THF cycles opening is well investigated, the six-member cycles of 1,4-dioxane are known to form peroxides rather easily [19], but they do not undergo polymerization [15]. After aging of the VC-MA samples in the freshly refined 1,4-dioxane its mass substantially increases. A probable mechanism of 1,4-dioxane interaction with Δ^6*en* reaction centers is presented in Figure 8.

The changes in the region of 4000–1500 cm^{-1} in the IR spectrum of VC-MA aged in 1,4-dioxane (see 3 in Figure 5) are identical to the above described changes observed in the IR spectrum of the VC-MA aged in THF. Besides new absorption

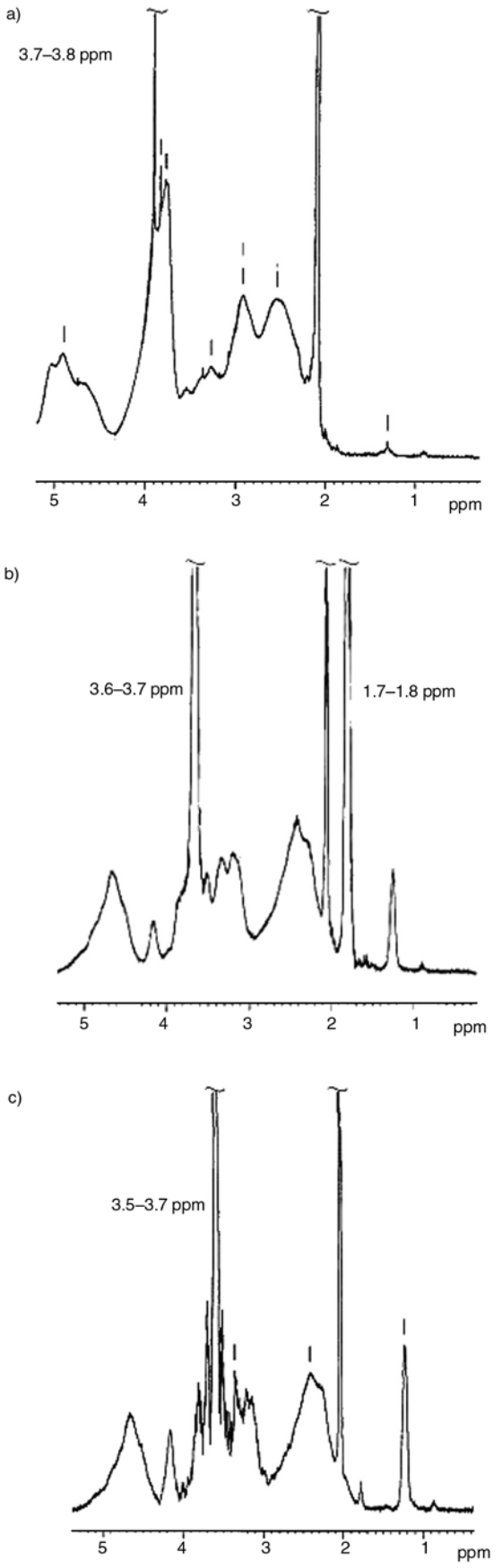

Figure 6. The ^1H NMR spectra the original VC-MA sample (a), of the VC-MA sample aged in THF (b) and of the VC-MA sample aged in 1,4-dioxane (c)

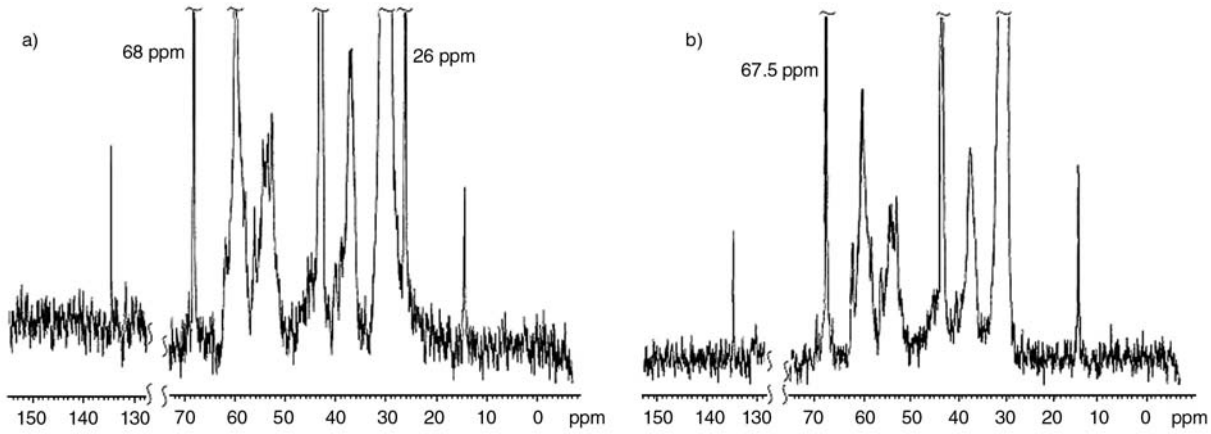

Figure 7. The ^{13}C NMR spectra of the VC-MA sample aged in THF (a) and of the VC-MA sample aged in 1,4-dioxane (b)

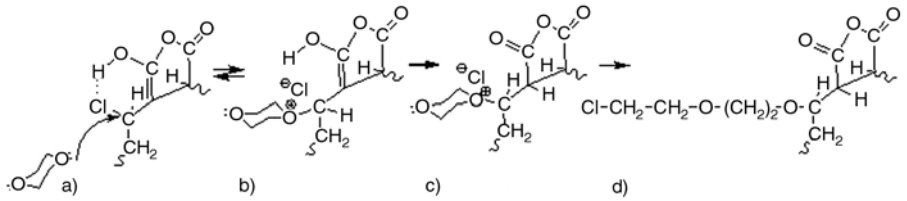

Figure 8. Mechanism of 1,4-dioxane grafting on the VC-MA macromolecules

bands $\nu_{-C-O-C-}$ (1117 cm^{-1}) and δ_{CH} (868 and 826 cm^{-1}) appear. Absorption bands of δ_{CH_2} (1375 cm^{-1}) and ν_{CCl} (614 cm^{-1}) become more pronounced. The intensity of the δ_{CH_2} absorption band (1445 cm^{-1}) increases.

The ^1H NMR spectrum of the VC-MA sample aged in 1,4-dioxane has an intensive multiplet at 3.5–3.7 ppm referred to the equivalent CH_2 protons of the dioxane fragments attached (Figure 6c). A new signal at 67.5 ppm of CH_2 carbon of the same fragments was registered in the ^{13}C NMR spectrum of the same sample (Figure 7b).

4. Conclusions

Thus reactive Δ^6*en* tautomeric forms of the repeat units of the VC-MA copolymer react with THF and 1,4-dioxane molecules to form short chain graft copolymers. In other words, the high energy transition state of the ensembles $[Cl\ldots H–O–C^{\delta+}]^{\#}$ appear to play the role of catalytic sites *in situ*. On an average *ca* 60 mol% of the Δ^6*en* tautomeric forms of macromolecules is involved in grafting.

References

[1] Trivedi B. C., Culbertson B. M.: Maleic anhydride. Plenum Press, New York (1982).

[2] Kaczmarek H., Felczak A., Szalla A.: Studies of photochemical transformations in polystyrene and styrene-maleic anhydride copolymer. Polymer Degradation and Stability, **93**, 1259–1266 (2008). DOI: 10.1016/j.polymdegradstab.2008.04.011

[3] Carja G., Chitanu G. C., Kameshima Y., Chiriac H., Okada K.: LDH-maleic anhydride copolymers as new hybrid materials and their textural organisation. Applied Clay Science, **41**, 107–112 (2008). DOI: 10.1016/j.clay.2007.10.002

[4] Bulantseva V. N., Berezina E. M., Chernov E. B., Filimoshkin A. G.: Characteristics of vinyl chloride-maleic anhydride copolymer hydrolysis. Vysokomolekulyarnye Soedinenya, Series B, **33**, 54–60 (1992).

[5] Pribytkov E. G., Eremina N. S., Terent'eva G. A., Chernov E. B., Filimoshkin A. G.: Esterification of vinyl chloride-maleic anhydride copolymer by alcohols. Russian Journal of Applied Chemistry, **71**, 313–317 (1998).

[6] Pavlova T. V., Terent'eva G. A., Chernov E. B., Filimoshkin A. G.: Interaction of vinyl chloride-maleic anhydride copolymer with sodium azide in dimethylformamide. Polymer Science, Series A, **36**, 631–636 (1994).

[7] Filimoshkin A. G., Chernov E. B., Terent'eva G. A., Berezina E. M., Telegin A. G.: Intermolecular interactions between vinyl chloride-maleic anhydride copolymer and carbonyl-containing solvents and dimethyl sulfoxide. Polymer Science, Series A, **39**, 1312–1316 (1997).

[8] Berezina E. M., Pavlova T. V., Terent'eva G. A., Chernov E. B., Filimoshkin A. G.: Effect of solvent on the structure of the solutions of poly(vinyl chloride-co-maleic anhydride). Polymer Science, Series A, **37**, 1254–1259 (1995).

[9] Safronova M. S, Berezina E. M., Terent'eva G. A., Chernov, E. B., Filimoshkin A. G.: Regiospecifity of reactions of vinyl chloride-maleic anhydride copolymer with dimethylformamide. Russian Journal of Applied Chemistry, **74**, 1554–1558 (2001).
DOI: 10.1023/A:1013725706655

[10] Filimoshkin A. G., Terent'eva G. A., Berezina E. M., Pavlova T. V.: A novel behavior of copoly (vinylchloride-maleic anhydride). Journal of Polymer Science, Part A: Polymer Chemistry, **31**, 1911–1914 (1993).

[11] Gordon A. J., Ford R. A.: The chemist's companion. Wiley, New York (1972).

[12] Filimoshkin A. G., Chernov E. B., Terent'eva G. A., Berezina E. M., Safronova M. S.: Microstructure of vinyl chloride-maleic anhydride copolymer in condensed state. Russian Journal of Applied Chemistry, **74**, 298–304 (2001).

[13] Pribytkov E. G., Berezina E. M., Eremina N. S., Terent'eva G. A., Chernov E. B., Filimoshkin A. G.: Mathematical modeling of the microstructure of a vinyl chloride-maleic anhydride copolymer in solution. Polymer Science, Series A, **39**, 932–937 (1997).

[14] Khimicheskaya entsiklopediya (Chemical encyclopedia). Edited by Zefirov N. S. Bol'shaya Rosiyskaya Entsiklopediya, Moscow, Vol 4 (1995).

[15] Odian G.: Principles of polymerization. Wiley, New York (2004).

[16] Ravve A.: Principles of polymer chemistry. Plenum Press, New York, London (1995).

[17] Filimoshkin A. G., Kosolapova V. F., Petrenko T. V., Aksenov V. S., Poleshchuk O. Kh.: New type of prototropic tautomerism involving carbon, hydrogen and oxygen atoms. Russian Journal of Organic Chemistry, **40**, 462–466 (2004).
DOI: 10.1023/B:RUJO.0000036062.82821.ab

[18] Pavlova T. V., Terent'eva G. A., Filimonov V. D., Chernov E. B., Filimoshkin A. G.: New views on the microstructure of vinyl chloride-maleic anhydride copolymer in solution. Russian Journal of Applied Chemistry, **72**, 1600–1603 (1999).

19] Khimicheskaya entsiklopediya (Chemical encyclopedia). Edited by Knunyants I. L. Sovetskaya Entsiklopediya, Moscow, Vol 2 (1990).

eXPRESS Polymer Letters Vol.3, No.1 (2009) 19–24
Available online at www.expresspolymlett.com
DOI: 10.3144/expresspolymlett.2009.4

High temperature tensile properties and deep drawing of fully green composites

R. Nakamura[1*], *K. Goda*[2], *J. Noda*[2], *J. Ohgi*[3]

[1]GraduateSchool of Science and Engineering, Yamaguchi University, Tokiwadai, Ube, Yamaguchi 755-8611, Japan
[2]Department of Mechanical Engineering, Yamaguchi University, Tokiwadai, Ube, Yamaguchi 755-8611, Japan
[3]Department of Applied Medical Engineering Science, Yamaguchi University, Tokiwadai, Ube, Yamaguchi 755-8611, Japan

Received 15 October 2008; accepted in revised form 5 December 2008

Abstract. In recent years, research and development of materials using biomass sources are much expected to construct a sustainable society. The so-called green composite consisting of natural fibers and biodegradable resin, is one of the most promising materials in developing biomass products. In this study, especially, we focus on the tensile deformation behavior of the green composites reinforced with ramie woven fabrics at high temperature. The results show that the fracture strain at high temperatures increases larger than that of room temperature, and initial deformation resistance of the composites seen at room temperature does not appear at high temperatures. Thus, several conditions to cause more deformability of the green composites were found. Finally, in order to utilize such deformability, Lankford-values of the green composites were clarified, and deep drawing was carried out for sheet materials made of the green composites.

Keywords: *polymer composites, green composite, natural fiber, deep drawing, tensile strength*

1. Introduction

Development of materials technology using biomass is anticipated for creation of a sustainable society. Especially, composites consisting of plant-based natural fibers and biodegradable resin, so-called fully green composites, are highly anticipated for practical use [1, 2]. Advantages of natural fibers include their excellent specific strength and stiffness properties, low cost, and low density. They are more abundant in nature and more eco-friendly in contrast to conventionally used glass and fossil-fuel-based fibers. Consequently, many studies examining the mechanical and interfacial properties of natural fiber reinforced composites have been carried out [3–5]. To date, kenaf-fiber-reinforced polylactic acid (PLA) matrix composites have been used for spare tire covers [6], circuit boards [7], and so on, of which the processing is based on injection molding. The merit of this technique is known to be generation of near-net shape products, even if they have a complex shape. However, the reinforcing natural fibers are broken and shortened during extrusion and/or injection molding processes. Consequently, the strength and stiffness of the fibers are not well reflected in the resultant mechanical properties of the products. Therefore, we specifically investigated green composites reinforced with woven fabrics of ramie fiber yarns and examined their deformation behavior [8]: the composites can be extended somewhat through yarn twisting and crimps of fabrics, and can be extended much more through mercerization [8, 9]. If such properties could be used effectively, green composites using woven fabrics might be a

*Corresponding author, e-mail: j006wc@yamaguchi-u.ac.jp

new plastic processing product that is mechanically superior to conventional polymer products.

The purpose of this study is to explore if the green composites can be applied for plastic processing. First, high-temperature tensile properties and the Lankford-value [10] (*r*-value) of the composites were explored. Then, deep drawing of the composite laminates was carried out.

2. Experimental procedure

2.1. Materials

A woven ramie fabric (No.25, single yarn, 44 warp /inch, 46 weft/inch) supplied from TOSCO Co. Ltd., Japan was used as a reinforcement material. The fabric surface is shown in Figure 1. Physical characteristics of ramie fibers are shown in Table 1. The resin used in this study is a biodegradable resin (Ecoflex; BASF Japan Ltd.) that was originally shaped as a pellet. A 2 mm thick sheet of this resin was preliminarily prepared through compression molding, and was used as a matrix material. Density and mechanical properties of the resin are shown in Table 2.

2.2. Fabrication method

Green composites were fabricated using a hot-press machine (mini Test Press-10; Toyo Seiki Seisaku Sho Ltd., Japan). Three fabrics of 220×220 mm^2 size were overlapped with one resin sheet of the same size. We used two kinds of stacking sequence as 0–90°/0–90°/0–90° (UT) and ±45°/±45°/±45° (UT-45).One set of these constituents was pressed with 9.8 MPa at 170°C for 5 min. Then they were cooled down to room temperature with the same pressure. Cross sectional optical micrograph of a composite used in this study is shown in Figure 2. Tensile specimens were cut off from the fabricated composite laminates. The shape and dimension of the tensile specimens are shown in Figure 2. Hereinafter, this composite laminate is denoted as UT composite. In addition, the composite laminates reinforced with alkali-treated woven fabrics were tensile-tested in identical fabrication conditions. To make ductility, alkali treatment using a high concentration sodium hydroxide solution was performed [11, 12]. In this case, the ramie woven fabrics were alkali-treated in advance in 21.5 wt% sodium hydroxide solution for two hours. And then they were washed in water including a small quantity of acetic acid. Hereinafter, this composite laminate is denoted as AT composite. Fiber volume fractions of UT and AT composites fabricated in this study were in the range of 44 to 52%.

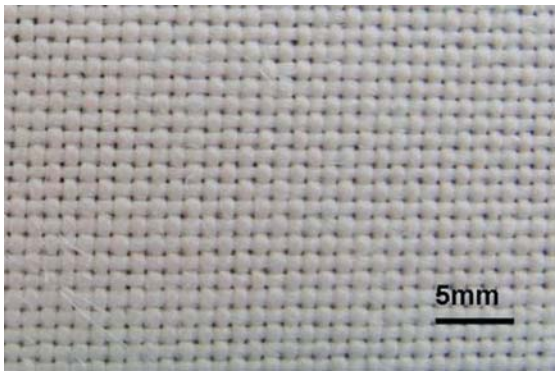

Figure 1. Ramie woven fabric

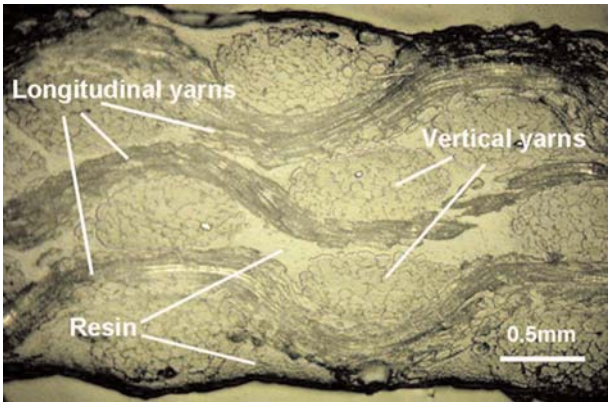

Figure 2. Optical micrograph of the longitudinal cross-section of a green composite reinforced with untreated ramie woven fabrics

Table 1. Properties of ramie fibers

Density [Mg/m^3]	Cellulose [wt%]	Lignin [wt%]	Hemicellulose [wt%]	Pectin [wt%]	Wax [wt%]	Microfibrillar angle [°]	Moisture content [wt%]
1.50	68.6–76.2	0.6–0.7	13.1–16.7	1.9	0.3	7.5	8.0

Table 2. Mechanical properties of the biodegradable resin (Eco-flex)

Density [Mg/m^3]	Melting point [°C]	Tensile Strength* [MPa]	Fracture Strain* [%]	Young's modulus* [GPa]
1.25–1.27	105–115	19.8	197.2	0.14

*value of the properties is obtained in the tensile test

2.3. Tensile test

Tensile tests of composite laminates were carried out along their weft directions at room temperature at the crosshead speed of 0.5 mm/min using an Instron-type testing machine (Autograph IS-5000; Shimadzu Corp.); they were also carried out at 100, 115 or 130°C at 1.5 mm/min using a hydraulic testing machine (Servo-pulser EHF-EB10; Shimadzu Corp.). In the latter case, the specimen was tensile-tested 10 min after fixing the specimen in the electronic furnace of the machine. The number of tensile specimens shown in Figure 3. was 4–6 for each condition. In addition, to explore the plastic anisotropy of the composite laminates, their *r*-values were investigated at 115°C in the conditions described above.

The *r*-value expresses a measure of the plastic anisotropy of a sheet material and is often used for evaluating the quality of deep drawing products. Lankford *et al*. proposed this idea in 1950 [10] and nowadays it is used widely in the field of metal rolling process. A schematic of strain states during deep drawing is shown in Figure 4. The *r*-value is defined as a ratio of the true strain in the width direction, ε_w, to the true strain, ε_t, in the thickness direction, when a sheet material is pulled in uniaxial tension beyond its elastic limit, as follows in Equation (1):

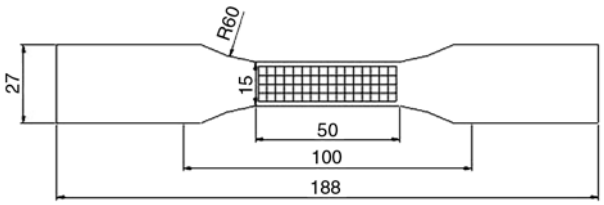

Figure 3. Shapes and dimensions of the tensile specimen

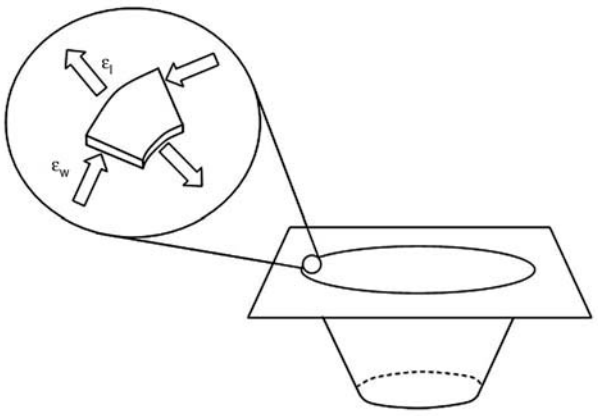

Figure 4. Schematic of strain states during deep drawing

$$r \equiv \frac{\varepsilon_w}{\varepsilon_t} \tag{1}$$

where $\varepsilon_w=\ln(w/W)$, $\varepsilon_t=\ln(t/T)$, w and t are final width and thickness of the material, respectively. W and T are initial values of w and t. The *r*-value means an index of deep drawing, and higher *r*-value yields more deeply drawn products. In general it is difficult to measure precisely change of the thickness of thin plate specimens. Therefore, the *r*-value is estimated as Equation (3), by changing ε_t as Equation (2):

$$\varepsilon_t = (\varepsilon_l + \varepsilon_w) \tag{2}$$

$$r = -\frac{\varepsilon_w}{\varepsilon_l + \varepsilon_w} = -\frac{\ln\frac{w}{W}}{\ln\frac{l}{L} + \ln\frac{w}{W}} \tag{3}$$

Equation (2) follows the law of volume constant.

To check the degree of degradation of ramie fibers at high temperatures, single fiber tensile tests were also carried out at room temperature, and at 100, 130, 160, and 200°C at the speed of 2.0 mm/min. Single ramie fibers were extracted carefully from a ramie sliver (Tosco Co. Ltd., Japan). The tensile testing machine used here was a hand-made testing machine, to which a fine capacity load-cell and hand-made small electrical furnace was attached. The tensile testing method for single fibers follows the Japanese Industrial Standard (JIS R 7606; Carbon fibre determination of the tensile properties of the single-filament specimens). The gage length of the tensile specimen was 20 mm. The number of single fiber specimens was 20–25 for each condition.

2.4. Deep drawing

Deep drawing processing was applied to composite laminates using a hotplate-attached press machine (20 t capacity; Yamamoto Suiatsu Kogyosho Co. Ltd.). In this experiment, the composite laminate described earlier was first cut out to 220×220 mm^2. Next, the laminate was fixed on a square metal frame, in which a hole of 70 mm diameter was provided at the center. The composite laminate was heated in an electrical furnace of 130°C for 10 min. In this condition, we found from an infrared ther-

mometer that the surface temperature of the composite laminates achieved 115°C. Furthermore, the composite laminate was shifted promptly to the press machine and drawn at the depth of 10 or 20 mm using a 50 mm diameter cylindrical punch or a 50×50 mm^2 square punch.

3. Results and discussion

3.1. Tensile properties of fully green composite laminates and natural fibers at high temperatures

Figure 5 shows typical stress-strain diagrams of UT composites at room temperature and high temperature. The UT composite tested at room temperature exhibits a typical diagram that resembles those of previously reported composites reinforced with the same woven fabrics, in which there are three stages: 1) elastic deformation through matrix stress transfer, 2) crimps of fabrics extension, and 3) yarn extension. The result showed that Young's modulus of 1.67 GPa and tensile strength of 75.9 MPa at room temperature. Tensile strengths at 100, 115 and 130°C are clearly less than those tested at room temperature. Furthermore, regarding their initial behavior, the deformation resistance does not appear at 115 and 130°C because the resin cannot transfer its shear stress to the fibers at high temperatures. As inferred from these results, plastic processing of the composite laminates might be possible at 115–130°C.

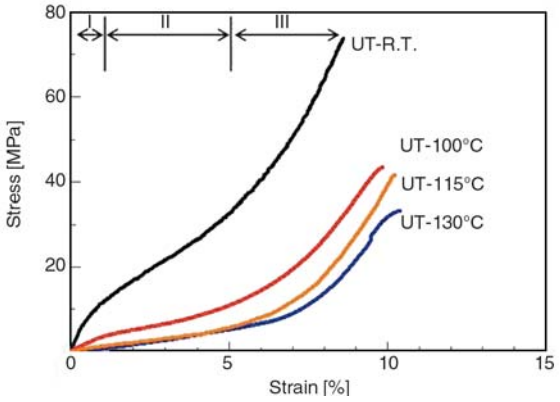

Figure 5. Typical stress-strain diagrams of UT composites at room temperature and elevated temperatures

Tensile properties of single fibers at R.T., 100, 130, 160 and 200°C are shown in Table 3. Tensile strength decreases greatly at 100–130°C; it does not change so much at temperatures higher than 130°C. Therefore, we must devote attention to such a strength decrease of the single fibers during plastic processing of the composites.

3.2. *r*-values of fully green composite laminates

To investigate a deep drawability of fully green composite laminates, their *r*-values were investigated through a tensile test. The test temperature was selected as 115°C from the results described above. Table 4 shows deformability and *r*-values of the composite laminates. In this experiment, testing was stopped at the tensile strain of 25% for the specimens, showing that the fracture strain was greater than 25%. As shown in the Table 4, the *r*-value of the green composites at 115°C is 8.42, which is much higher than the value range of approximately 0.7–2.1, as indicated in sheet metals. On the other hand, although the AT composites and ±45° composites show larger longitudinal strains [8], their *r*-values are lower than those of the others. Especially, it is noteworthy that the *r*-value of ±45° composites is negative. Therefore, a more trans-

Table3. Tensile properties of single fibers

	Fiber diameter [μm]	Young's modulus [GPa]	Tensile strength [MPa]	Fracture strain [%]
R.T.	33.6	24.0	494	2.57
100°C	26.7	22.6	448	2.25
130°C	39.6	17.7	268	2.10
160°C	36.9	21.7	291	1.74
200°C	29.8	18.9	307	1.82

Table 4. Deformability and *r*-values of the green composite laminates at 115°C

	Longitudinal strain [%]	Transverse strain [%]	*r*-value
UT-115°C	5.79	–4.90	8.42
UT-45°–115°C	7.31	12.0	–2.60
AT-115°C	15.6	–4.65	0.43
GFRP	2.0	–	0.01

verse compressive strain occurred than with a longitudinal tensile strain. In Table 4, the result for the AT-115°C composite is also shown. In this composite, a large increase in the fracture strain at the longitudinal direction is obtained. Consequently, the *r*-value of the composite decreases compared to that of UT-115°C. The *r*-value of GFRP using a plane fabric at 0–90° direction is 0.01 [13]. Therefore the green composite laminates used here are superior to GFRP from the perspective of plastic processing.

3.3. Results of deep drawing

Deep drawing processing was applied for the green composite laminates. Figures 6a and 6b depict typical deep drawing products. Table 5 shows the classification of deep drawability by cylindrical and square punches. When alkali-treated woven fabrics are used as reinforcement, the product can achieve 20 mm depth for both punches. For untreated woven fabrics, the drawing was only 10 mm for the cylindrical punch; it was not achieved for the square punch. Figures 6a and 6b show that about 1 and 2 mm wrinkles in height, respectively, were brought into UT and AT composites along the diagonal direction. As described earlier, the negative *r*-value of ±45° composite means that the deformation along the transverse direction is greater than the longitudinal deformation. Therefore, the wrinkle pattern is brought into the products. To reduce wrinkles in the products, the 0–90° direction of AT composite was placed in the diagonal direction. Then the process was applied in the same condition. As depicted in Figure 6c, the result shows that the wrinkle pattern disappears clearly. The reason is that contraction force at the circumferential direction becomes small due to the short distance between punch and square metal frame, as compared to Figure 6a.

The results described above demonstrate that the fully green composites can produce stronger and stiffer deep drawing products than usual polymeric materials.

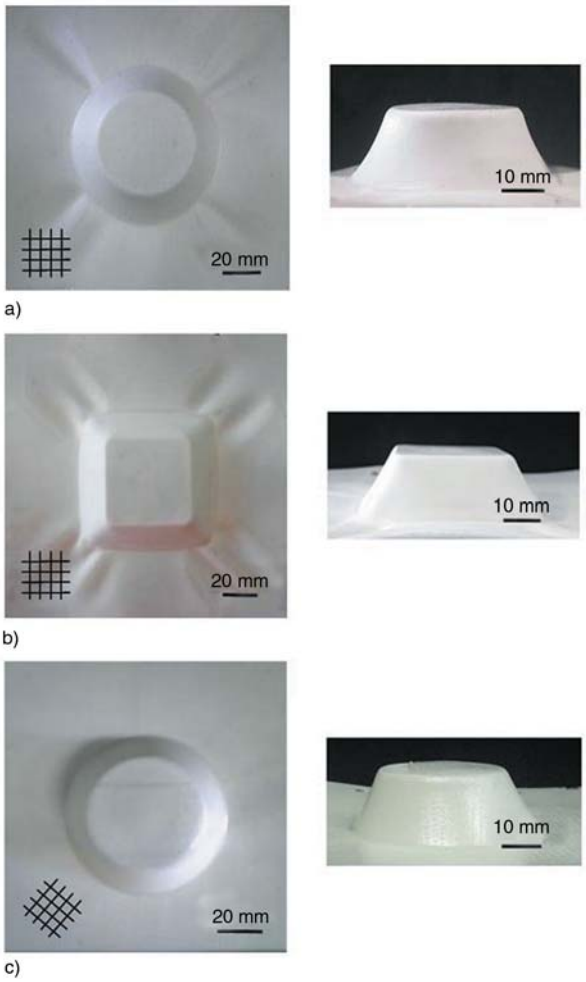

Figure 6. Photographs of deep drawn products using AT composite (a) 0–90°/0–90°/0–90° laminate processed using a cylindrical punch, (b) 0–90°/0–90°/0–90° laminate processed using a square punch, and (c) ±45°/±45°/±45° laminate processed using a cylindrical punch

4. Conclusions

High-temperature tensile properties and deep drawability of fully green composites reinforced with ramie woven fabrics were explored. Based on the initial deformation resistance at high temperatures of the composites and high temperature tensile strength of the single fibers, it was concluded that the optimum temperature range of plastic processing for the composites was 100–115°C.

Table 5. Classification of deep drawability

Depth	AT composite		UT composite	
	Cylindrical punch	Squared punch	Cylindrical punch	Squared punch
10 mm	o	o	o	–
20 mm	o	o	×	×

o; possible, ×; not possible

Deep drawing of the composite laminates was carried out at 115°C using cylindrical and square punches. The results show that, when alkali-treated ramie woven fabrics were used as reinforcement, deep drawing was achieved at the depth of 20 mm. Consequently, the development of plastic processing such as deep drawing for the green composites is expected.

Acknowledgements

The authors wish to acknowledge the Research Fellowship of the Japan Society for the Promotion of Science (JSPS) for Young Scientists for supporting this research.

References

[1] Luo S., Netravali A. N.: Interfacial and mechanical properties of environment-friendly 'green' composites made from pineapple fibers and poly (hydroxybutyrate-co-valerate) resin. Journal of Material Science, **34**, 3709–3719 (1999).
DOI: 10.1023/A:1004659507231

[2] Wambua P., Ivens J., Verpoest I.: Natural fibers: Can they replace glass in fibre reinforced plastics? Composites Science and Technology, **63**, 1259–1264 (2003).
DOI: 10.1016/S0266-3538(03)00096-4

[3] Netravali A. N., Chabba S.: Composites get greener. Materials Today, **6**, 22–29 (2003).
DOI: 10.1016/S1369-7021(03)00427-9

[4] Bledzki A. K., Gassan J.: Composites reinforced with cellulose based fibers. Progress in Polymer Science, **24**, 221–274 (1999).
DOI: 10.1016/S0079-6700(98)00018-5

[5] Goda K., Cao Y.: Research and development of fully green composites reinforced with natural fibers. Jounal of Solid Mechanics and Materials Engineering, **1**, 1073–1084 (2007).
DOI: 10.1299/jmmp.1.1073

[6] Inoh T.: Industrial products of plant origin material-effective use of plastics for recycling society (in Japanese). Journal of the Japan Society of Mechanical Engineers, **109**, 51–52 (2006).

[7] Iji M., Serizawa S., Inoue K.: Development of polylactic acid with kenaf and its application to electronic products (in Japanese). Journal of the Japan Society of Polymer Processing, **15**, 602–604 (2003).

[8] Nakamura R., Sreekala M. S., Jyouyou H., Goda K.: Creation of plasticity in textile green composites using ramie woven fabrics. International Journal of Plastics Technology, **9**, 406–415 (2005).

[9] Nakamura R., Sreekala M. S., Goda K., Jyouyou H.: Plastic deformation behavior of textile green composites using a plain woven ramie fabric. in 'Proceedings of 12th European Conference on Composite Materials, Biarritz, France' 432–434 (2006).

[10] Lankford W. T., Snyder S. C., Bauscher I. A.: New criteria for predicting the press performance of deep drawing sheet. Transactions of the American Society for Metals, **42**, 1197–1232 (1950).

[11] Goda K., Sreekala M. S., Gomes A., Kaji T., Ohgi J.: Improvement of plant based natural fibers for toughening green composites -Effect of load application during mercerization of ramie fibers. Composites Part A, **37**, 2213–2220 (2006).
DOI: 10.1016/j.compositesa.2005.12.014

[12] Sao K. P., Samantray B. K., Bhattacherjee S.: X-ray study and disorder in ramie fiber. Journal of Applied Polymer Science, **52**, 1687–1694 (1994).
DOI: 10.1002/app.1994.070521203

[13] Omura M., Okamoto K.: Relation between plastic workability and fraction of fibers on GFRP sheet (in Japanese). Journal of the Society of Material Science, Japan, **47**, 452–457 (1998).

eXPRESS Polymer Letters Vol.3, No.1 (2009) 25–32
Available online at www.expresspolymlett.com
DOI: 10.3144/expresspolymlett.2009.5

Swelling characterization and drug delivery kinetics of polyacrylamide-co-itaconic acid/chitosan hydrogels

A. Martínez-Ruvalcaba[1], *J. C. Sánchez-Díaz*[1], *F. Becerra*[2], *L. E. Cruz-Barba*[1], *A. González-Álvarez*[1*]

[1]Chemical Engineering Department, University de Guadalajara, Guadalajara 44430, Mexico
[2]Chemistry Department, University de Guadalajara, Guadalajara 44430, Mexico

Received 14 October 2008; accepted in revised form 6 December 2008

Abstract. Hybrid polymeric networks composed of polyacrylamide and chitosan were developed to determine their swelling and ascorbic acid delivery kinetics at various chitosan concentrations. The hybrid acrylamide/chitosan hydrogels were synthesized in aqueous itaconic acid solution (1% w/w). Young's modulus was also evaluated for the hydrogels, and the results were correlated with the swelling properties. Swelling experiments were carried out using three different pH solutions: acidic (pH 4 buffer solution), neutral (distilled water) and basic (pH 10 buffer solution). The results of the swelling study showed that the swelling properties of the network varied with the changes of the pH in the swelling solution, as well as concentration of chitosan. When chitosan concentration increased, the swelling capacity diminished, and therefore Young's modulus increased. The results indicated that the swelling process followed a second order kinetics. The ascorbic acid diffusion inside the hydrogel follows a Fickian mechanism. The ascorbic acid diffusion coefficients are reported as a function of chitosan concentration.

Keywords: *polymer gels, chitosan, swelling kinetics, mechanical properties, drug delivery*

1. Introduction

Hydrogels are three-dimensional polymeric networks that have a solid-like appearance, formed by two or more components, one of which is a liquid present in high quantity. The capability of hydrogels to swell in water is due to the hydrophilic groups present in the polymer chains, while its mechanical resistance is due in part to the physical or chemical network cross-linking [1–3]. Interpenetrating polymer networks are defined as a combination of two or more polymers forming a network, which are synthesized in juxtaposition. However, most interpenetrating polymer networks do not interpenetrate on a molecular scale. Studies of reversible volume changes in response to pH, ionic concentration, etc. have been carried out for several kinds of polymeric networks [3–5].

The swelling behavior of any polymer network depends upon the nature of the polymer, polymer-solvent compatibility and degree of cross-linking. However, in the case of ionic networks, swelling kinetics depends upon mass transfer limitations, ion exchange and ionic interaction [6]. Swelling kinetics of hydrogels can be classified as diffusion-controlled (Fickian) or relaxation-controlled (non-Fickian). When diffusion into the hydrogel occurs much faster than the relaxation of the polymer chains, the swelling kinetics is said to be diffusion-controlled [7].

Hydrogels can swell to profitable rates when placed into an appropriate environment, which means a

*Corresponding author, e-mail: agonzalezalvarez@gmail.com

specific pH, temperature, electric field, light, pressure or specific molecule [6–12]. Several researchers have studied the swelling of pH-sensitive hydrogels and the influence of this parameter in chemical, biological and physiological systems [13]. Hydrogels exhibiting pH-sensitive swelling behavior have been usually swollen from ionic networks that can contain acidic or basic pendant groups. When these groups are ionized, a swelling osmotic pressure inside the material is built up, and fixed charges are trapped in the gel. As a result of the electrostatic repulsion, the uptake of solvent in the network is increased [14, 15].

Polyacrylamide forms a hydrogel with an outstanding swelling capacity, which is not substantially affected by the pH and the presence of electrolytes. Polyacrylamide gels are obtained by free-radical cross-linking copolymerization of acrylamide and N,N'-methylenebis(acrylamide) monomers. The properties of polyacrylamide hydrogels strongly depend on the initial degree of dilution of the monomers and, if the amount of water present at polymerization increases, the network's structure would not be firm [16]. Due to their high water retention, polyacrylamide hydrogels are widely used as biomaterials, and have been extensively studied for biomedical applications, such as drug delivery systems [17–19]. Different polymeric networks with a polyacrylamide basis have been synthesized and used for various applications [20–22]. Krusic *et al*. prepared semi-interpenetrating polymeric networks based on polyacrylamide/ poly(itaconic acid) and demonstrated that poly(itaconic acid) interacts with the polyacrylamide gel mainly by hydrogen bonding, resulting in the formation of an interpolymer complex [21].

Chitosan is a copolymer of N-acetyl-glucosamine and N-glucosamine units distributed randomly or in blocks throughout the biopolymer chain, depending on the processing method used to obtain the biopolymer. Several interesting properties of chitosan, such as gel and film forming ability, bioadhesion, biodegradability and biocompatibility have been reported. Chitosan has received a great deal of attention in the pharmaceutical field due to its promising properties [23, 24]. Because of the properties of chitosan and polyacrylamide, several works have explored the feasibility of a polyacrylamide/chitosan blend. These studies have reported different aspects of the characterization, biocompatibility, and release properties of polyacrylamide/chitosan hydrogels [25–27].

Synthesis method, swelling kinetics, and Young's moduli for a polyacrylamide/chitosan hybrid polymeric network at various chitosan concentrations, and different swelling media are reported in this work. A study to determine the ascorbic acid delivery behavior was also carried out, and the diffusion coefficients of ascorbic acid in the hydrogels were obtained as a function of chitosan concentration.

2. Experimental

2.1. Materials

Acrylamide (AM) 99% and chitosan (CS) 99% from Aldrich Chemical; 2,2'-azobis(2-amidinopropane) dihydrochloride (V-50) from Wako Chemicals; itaconic acid 98.5% from Acros; and ascorbic acid 99% from Merck were used as received. N,N'-methylenebisacrylamide (NMBA) from Scientific Polymer was recrystallized from a methanol solution. Doubly distilled deionized water was used.

2.2. Preparation of hydrogels

The polyacrylamide/chitosan (PAM-CS) hydrogels were synthesized using five different mass ratios (m_{AM}/m_{CS}: 100/0, 95/5, 90/10, 85/15, 80/20). First a chitosan powder was dispersed in a 1.0 wt% itaconic acid aqueous solution, in order to obtain a solution with a concentration of 1.0 wt% chitosan. Then an AM/NMBA aqueous solution was prepared ($m_{NMBA}/m_{AM} = 0.02$). Both solutions were then perfectly mixed and left to polymerize at 50°C for 24 hr in the presence of V-50 ($m_{V\text{-}50}/m_{AM} = 0.02$). The total solids concentration in the system was 6% relative to water.

The hydrogels, obtained in the shape of rods, were cut into disks, which were then immersed in water and left for several days to wash out any residual monomer. After washing, the hydrogels were left to dry at room temperature. In order to produce materials with similar dimensions, the dried disks were carefully sanded until the thickness ranged from 1.5 to 2 mm with diameters between 10 and 12 mm.

2.3. Swelling behavior

In order to study the swelling behavior, the disk samples (approximately 0.05 g) were immersed in three different swelling solutions: water, pH 4.0 buffer solution, and pH 10.0 buffer solution. The samples were placed in the swelling solution and the weight of the swollen samples was measured against time after the excess surface water was removed by gently tapping the surface with a dry piece of filter paper. The degree of swelling (H) for each disk sample at time t was calculated using Equation (1):

$$H = \frac{w_t - w_0}{w_0} \tag{1}$$

where w_t and w_0 are the sample's weight at any given time, and in the dry state, respectively.

2.4. Mechanical properties

Compression tests were done on the hydrogel disks once they were swollen to equilibrium conditions at 20°C. These tests were carried out in a thermo-mechanical analyzer (TMA-7 Perkin-Elmer). Hydrogels swollen to equilibrium conditions were cut to yield rectangles and were properly measured. Young's modulus was obtained from the slope of the initial linear zone (less than 5% strain) of the stress-strain curve according to Equation (2) [28]:

$$\tau = -E(\lambda - 1) \tag{2}$$

where τ is the applied stress, and λ is the deformation given by the ratio of the deformed (h) to the initial thickness (h_0) of the hydrogel disks, $\lambda = -h/h_0$.

2.5. Drug delivery measurements

Previously measured (weight and dimensions) xerogels were loaded with ascorbic acid by immersing them in a drug saturated aqueous solution (333 g/l) until equilibrium was reached. The loaded hydrogels were then dried at room temperature for a week and weighed to obtain the concentration of V-C in the xerogels.

To study the drug delivery kinetics the loaded xerogels were immersed in 200 ml of distilled water at 30°C which were continuously stirred. In order to follow the delivery kinetics, the conductivity of the solution [μS/cm] was measured at different times using an Orion Star 4 conductometer. The swelling experiments were carried out keeping the disks immersed. Conductivity vs. ascorbic acid concentration calibration curves were obtained using standard solutions (0–30 mg/l) at 30°C. The amount of drug released at any given selected time (M_t) was obtained from the calibration curve. The maximum amount of drug available for release (M_∞) was determined by gravimetric measurements.

3. Results and discussion

3.1. Swelling properties and Young's modulus

Polymerization of the acrylamide-chitosan system using low concentrations of cross-linking agent (NMBA), and using itaconic acid aqueous solutions to dissolve the chitosan creates a hybrid polymeric network [2]. The swelling media and the amount of chitosan were changed in order to determine the influence of pH and chitosan concentration in the polymeric network. The hydrogel samples were immersed in swelling solutions with different pH. The amount of solution that penetrated into the hydrogel until equilibrium was reached (equilibrium swelling, H_∞) was determined during the swelling process. An example of swelling kinetics (water uptake versus time) for the hydrogels at different polyacrylamide/chitosan mass ratios is depicted in Figure 1. This figure corresponds to hydrogels swollen in a basic environment. The figure shows a decrease in the equilibrium swelling when the hydrogel's chitosan content is increased

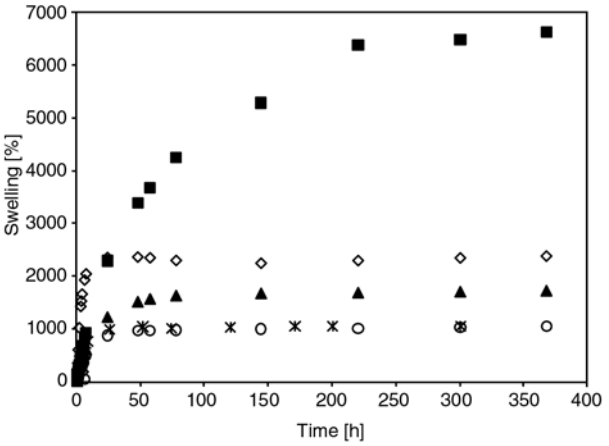

Figure 1. Swelling [%] as function of time for hydrogels with different acrylamide/chitosan mass ratio (m_{AM}/m_{CS}) (■ 100/0, ◇ 95/5, ▲ 90/10, O 85/15, ★ 80/20)

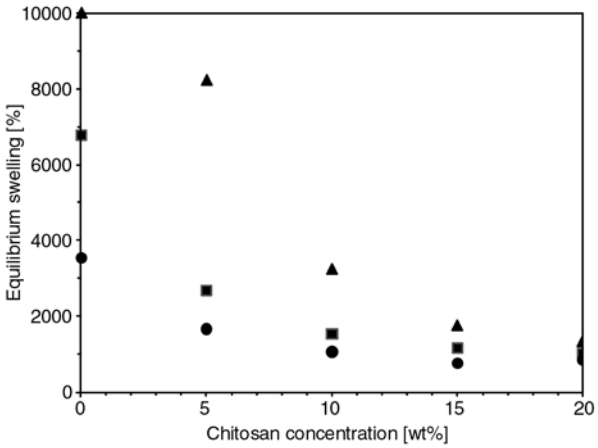

Figure 2. Equilibrium swelling [%] as function of the chitosan concentration for the three different swelling media (• acid, ▲ water, ■ basic)

(decrease of m_{CS}). This behavior suggests that the chitosan trapped in the hydrogel occupies more of the free space volume in the polymeric network, thus decreasing the volume available for swelling [2]. Besides, considering that the chitosan has a hydrophobic nature, when the chitosan concentration is increased, the hydrophilic character of the hydrogel is decreased. We can also observe how the mechanical properties (Young's modulus) of the hydrogel reach higher values when the chitosan concentration is increased [15] (Figures 2 and 3).

Figures 2 and 3 show the variation of H_∞ and the Young's modulus, respectively, as a function of chitosan concentration. Addition of chitosan decreases the swelling capacity of the hydrogels and increases Young's modulus. This phenomenon may be explained due to the presence of ionizable groups in both, chitosan and itaconic acid. In acidic environments the amine groups in chitosan are ionized to form NH_3^+ groups, which allow chitosan to form networks through ionic links with the carboxy groups in the itaconic acid. When the chitosan concentration increases the cross-linking density increases, swelling capacity decreases and Young's modulus increases. In basic environments, the carboxy groups in the itaconic acid are ionized, while the chitosan NH_3^+ groups change back to NH_2 groups. Under these conditions chitosan does not form ionic links and the cross-linking density decreases, the swelling capacity increases, and Young's modulus decreases. In a neutral pH environment (distilled water), the carboxy groups in the itaconic acid are ionized and the chitosan is not, therefore there is no ionic links, thus decreasing the cross-linking density. The ionic strength in the neutral swelling medium is smaller than that in acidic and basic media, therefore having the higher swelling capacities [29, 30]. The hydrogels that are sensitive to the pH changes usually have ionizable groups; when these groups are ionized, for example in the chitosan amine groups at low pH, is generated a swelling osmotic pressure inside the hydrogel. In addition, when ionized groups are deionized, the swelling osmotic pressure disappears, in the case of the amine groups of the chitosan it happens at high pH's.

Figure 4 shows an example of the effect of the swelling medium's pH. The figure corresponds to a hydrogel with an acrylamide/chitosan mass ratio of 90/10. In water, H_∞ is about 3500%, while in a basic medium is just 1700%, and in an acid medium is 1200%. Considering that the swelling

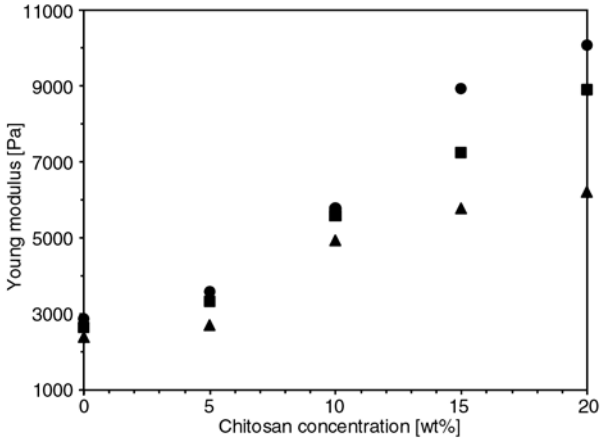

Figure 3. Young's modulus [Pa] as function of the chitosan concentration for the three different swelling media (• acid, ▲ water, ■ basic)

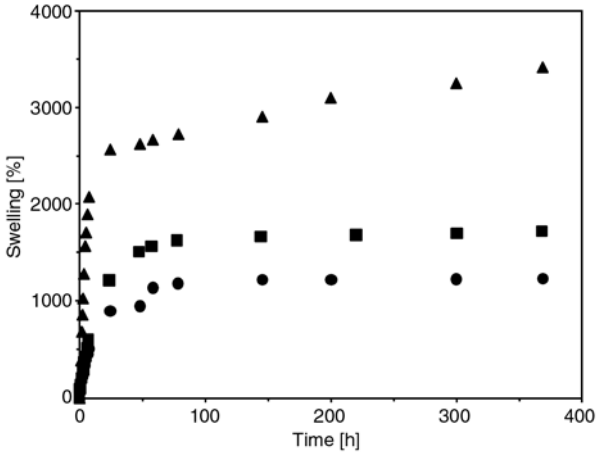

Figure 4. Effect of the swelling media over the swelling [%] for the hydrogel with a mass ratio: m_{AM}/m_{CS} = 90/10 (• acid, ▲ water, ■ basic)

process in the polymeric network is influenced by the swelling media's ionic strength, when the ionic strength increases, the concentration of ions in the hydrogel must increase in order to satisfy the Donnan equilibrium condition [15]; which establishes that the hydrogel swelling is diminished when the interactions of the material with the counter-ions of the swelling media increase.

3.2. Swelling kinetics

For most of the pharmaceutical applications it is important to know the swelling kinetics of the hydrogels, which will be used as drug release agents, because this process has a direct impact on drug release/delivery. There are a few rigorous theories dealing with hydrogel swelling kinetics; some authors have proposed that swelling can be described by a second order kinetics [30], as indicated in Equation (3):

$$\frac{dH}{dt} = k(H_\infty - H)^2 \tag{3}$$

where k is the swelling rate constant.
By integration of Equation (3), and applying the initial conditions, we have Equations (4) and (5):

$$\frac{t}{H} = \frac{1}{k_\infty} + \frac{t}{H_\infty} \tag{4}$$

$$k_\infty = kH_\infty^2 \tag{5}$$

where k_∞ is the equilibrium swelling rate constant. When the swelling kinetics corresponds to a second order kinetics, Equation (4) is a linear relationship, and H_∞ and k corresponds to the slope and intercept of the line, respectively [31]. The results obtained in this study agree with this behavior. Table 1 summarizes the second order swelling rate constants (k) obtained.

Considering that the swelling process is affected by specific relations between the molecules of the swelling medium and the polymer pendant groups (amines, amides, carboxy), one can expect many kinds of polymer-solution interactions, and probably a complex kinetics. The decrease in the swelling rate when the chitosan concentration increases (k increases) suggests that specific interactions between the polymeric network loaded with chitosan and the medium are weaker when compared to the interactions that occur with the polymeric network without chitosan.

3.3. Ascorbic acid delivery

Results obtained from the tests of ascorbic acid release from the PAM/CS hydrogels in aqueous medium are shown in Figure 5. This figure shows the dependence of the release on the acrylamide/chitosan mass ratio used. In addition to the PAM/CS hydrogels, results for a chitosan free sample (polyacrylamide hydrogel) are also shown. The figure shows that at constant time the drug released is lower when the chitosan concentration is higher. Taking into account that the swelling kinetics is

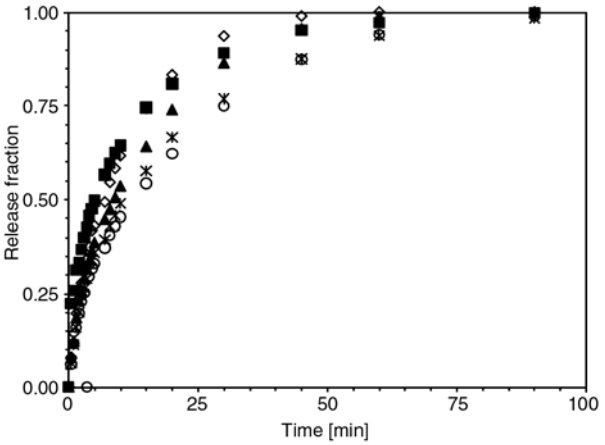

Figure 5. Release fraction versus time for hydrogels with different acrylamide/chitosan mass ratio (m_{AM}/m_{CS}) immersed in a basic medium (■ 100/0, ◇ 95/5, ▲ 90/10, O 85/15, ★ 80/20)

Table 1. Values of the swelling rate constant k (g xerogel/g water·hr) for the PAM-CS hydrogels swelled in different aqueous media

Chitosanconcentration [wt%)]	k (acid medium)	k (water)	k (basic medium)
0	0.028	0.025	0.020
5	0.038	0.046	0.050
10	0.085	0.077	0.088
15	0.123	0.097	0.134
20	0.289	0.610	0.340

determined by the hydrogel porosity (volume of the free spaces in the polymeric network) [2], when the chitosan chains are trapped into the polymeric network, the chitosan occupies a fraction of that free space in the network. This causes a decrease in the hydrogel porosity, which is evidenced by the fact that the quantity of drug released decreases when chitosan concentration is increased. Considering that the ascorbic acid delivery is also governed by specific dipole-dipole interactions and hydrogen bonds between water molecules and the ions present in the solution, the decrease in the drug released when the chitosan concentration is increased is also influenced by the decrease in the chitosan degree of deionization, which improves hydrogel link formation, and therefore increases cross-linking density. That is the same phenomena observed for Young's modulus, which are higher when the chitosan concentration is increased.

Diffusion from the gel phase to the surroundings can be considered as a one-dimensional isothermic process for hydrogel samples with a small thickness respect to its diameter (the relationship between diameter and thickness must range between 5 and 8) [32]. In order to produce materials with appropriate dimensions, the sample diameters varied between 10 and 12 mm, and thickness ranged from 1.5 to 2 mm.

For a process controlled by diffusion in thin disks, Equation (6) is used to determine the nature of diffusion [33]:

$$F=\frac{M_t}{M_\infty}=k_1 t^n \tag{6}$$

where the release fraction (F) is defined as M_t/M_∞, M_t is the amount of drug released at any given time, M_∞ is the maximum amount (weight) available for release, t is the release time, k_1 is the kinetic constant of the system, and n is a characteristic power for the drug release.

Equation (6) describes the release kinetics of a drug and is only valid for the first 60% of the fractional uptake. When n is equal to 0.5 the drug is said to diffuse with Fickian behavior. For n = 1 the behavior is called Case II diffusion. Finally, anomalous transport behavior, which is intermediate between Fickian and Case II, is known as non-Fickian diffusion [34]. For Fickian behavior, k_1 is given by Equation (7):

Table 2. Parameters k_1, n and diffusion coefficients for the PAM-CS hydrogels at different chitosan concentrations

Chitosan concentration [wt%]	k_1	n	D [$cm^2 \cdot s^{-1}$]
0	0.0296	0.495	$1.48 \cdot 10^{-5}$
5	0.0235	0.507	$1.15 \cdot 10^{-5}$
10	0.0198	0.514	$8.33 \cdot 10^{-6}$
15	0.0191	0.506	$7.74 \cdot 10^{-6}$
20	0.0172	0.512	$3.19 \cdot 10^{-6}$

$$k_1=4\left(\frac{D_i}{\pi h^2}\right)^{\frac{1}{2}} \tag{7}$$

where D_i is the diffusion coefficient for the drug delivery mechanism and h is the thickness of the loaded sample.

The power n in Equation (6) was determined from slope of the release fraction (F) vs. time log-log plot. The values of n shown in Table 2 indicate that the ascorbic acid release from the hydrogel follows a Fickian diffusion for all chitosan concentrations. This behavior suggests that the release process is controlled by diffusion only [2]. The values of n are used together with Equation (6) in order to calculate the release kinetic constant (k_1), which are also reported in Table 2 for different chitosan concentrations. The kinetic constants are lower when the chitosan concentration increases, and this fact suggests that the diffusion rate decreases when chitosan quantity increases due to the decrease in size of the free spaces in the network.

The diffusion coefficient (D_i) for the ascorbic acid was determined using Equation (7), due to the fact that kinetic constants suggest Fickian behavior. Table 2 shows the D_i values for different chitosan concentrations.

The diffusion coefficients obtained are inversely proportional to the chitosan concentration, and therefore the release rate decreases when the chitosan amount increases. This behavior confirms that an increase in the hydrogel's chitosan concentration reduces the swelling in neutral medium, and release rate and Young's modulus increase.

4. Conclusions

The synthesis of a hybrid polymeric network based in polyacrylamide and chitosan in acidic solution (itaconic acid) was carried out in order to determine

its swelling kinetics and ascorbic acid release. Swelling capacity, equilibrium swelling and Young's modulus reached at different pH environments, as well as release fractions and diffusion coefficients for the ascorbic acid release were reported. It was found that the swelling capacity decreases and the Young's modulus increases when the chitosan concentration is increased, most probably due to the changes in the hydrogel porosity, which in turn causes an increase in the cross-linking density, as well as the hydrophobic character of chitosan, which reduces the hydrophilicity of the hydrogel.

The swelling kinetics and mechanical properties were studied using three different swelling media: acidic, neutral, and basic. In acidic medium the swelling capacity decreases due to the chitosan NH_3^+ groups that is ionically linked with the itaconic acid COO^- group, and this ionic bond increases the cross-linking density. In aqueous medium, the NH_3^+ group loses a proton and becomes NH_2, thus reducing the cross-linking density. In basic medium the swelling capacity decreases relative to the aqueous medium, because the itaconic acid is ionized and is forming hydrogen bonds with the nitrogen of the amine groups. The swelling of the hydrogels follows a second order kinetics, and the swelling rate constants obtained confirm the presence of different polymer-solution interactions in the system, which do not exist in the chitosan-free hydrogel.

The ascorbic acid release follows Fick's second law of diffusion, and the characteristic power, n, is about 0.5. The kinetic constant (k_1) and the diffusion coefficients decrease when the chitosan concentration in the hydrogel is increased, mainly due to a rise in the cross-linking density and a decrease on the volume of free spaces available in the hydrogel. The diffusion coefficients are between 10^{-5} and 10^{-6} cm^2/s, which suggest that the hydrogels studied have a good potential for their use in applications such as drug release, since similar values have been reported in papers with a pharmaceutical approach.

References

[1] Almdal K., Dyre J., Hvidt S., Kramer O.: What is a gel? Macromolecular Symposia, **76**, 49–51 (1993).

[2] Berger J., Reist M., Mayer J. M., Felt O., Peppas N. A., Gurny R.: Structure and intereactions in covalently and ionically crosslinked chitosan hydrogels for biomedical applications. European Journal of Pharmaceutics and Biopharmaceutics, **57**, 19–34 (2004). DOI: 10.1016/S0939-6411(03)00161-9

[3] Sperling L. H.: Interpenetrating polymer networks and related materials. Plenum Press, New York (1981).

[4] Jeong S., Park S. J., Shin M-S., Kim S. I.: Characteristics of electrical responsive chitosan/polyallylamine interpenetrating polymer network hydrogel. Journal of Applied Polymer Science, **86**, 2290–2295 (2002). DOI: 10.1002/app.11217

[5] Kim S. J., Shin S. R., Lee Y. M., Kim S. I.: Swelling characterizations of chitosan and polyacrylonitrile semi-interpenetrating polymer network hydrogels. Journal of Applied Polymer Science, **87**, 2011–2015 (2003). DOI: 10.1002/app.11699

[6] Frank S., Lauterbur P. C.: Voltage-sensitive magnetic gels as magnetic resonance monitoring agents. Nature, **363**, 334–336 (1993). DOI: 10.1038/363334a0

[7] Peppas N. A., Colombo P.: Analysis of drug release behavior from swellable polymer carriers using the dimensionality index. Journal of Controlled Release, **45**, 35–40 (1997). DOI: 10.1016/S0168-3659(96)01542-8

[8] Tanaka T.: Phase transitions of gels. in 'Polyelectrolyte gels: Properties, preparation and applications' (eds.: Harland R. S., Prud'homme R. K.) American Chemical Society, Washington, Vol 480, 1–21 (1992).

[9] Suzuki A., Ishii T., Maruyama Y.: Optical switching in polymer gels. Journal of Applied Physics, **80**, 131–136 (1996). DOI: 10.1063/1.362768

[10] Khare A. R., Peppas N. K.: Swelling/deswelling of anionic copolymer gels. Biomaterials, **16**, 559–567 (1995). DOI: 10.1016/0142-9612(95)91130-Q

[11] Zhong X., Wang Y-X., Wang S-C.: Pressure dependence of the volume phase-transitions of temperature-sensitive gels. Chemical Engineering Science, **51**, 3235–3239 (1996). DOI: 10.1016/0009-2509(95)00344-4

[12] Peppas N. A., Huang Y.: Polymer and gels as molecular recognition agents. Pharmaceutical Research, **19**, 578–587 (2002). DOI: 10.1023/A:1015389609344

[13] Peppas N. A., Khare A. R.: Preparation, structure and diffusional behavior of hydrogels in controlled release. Advanced Drug Delivery Reviews, **11**, 1–35 (1993). DOI: 10.1016/0169-409X(93)90025-Y

[14] Brannon-Peppas L., Peppas N. A.: Equilibrium swelling behavior of pH-sensitive hydrogels. Chemical Engineering Science, **46**, 715–722 (1991). DOI: 10.1016/0009-2509(91)80177-Z

[15] Peppas N. A., Bures P., Leobandung W., Ichikawa H.: Hydrogels in pharmaceutical formulations. European Journal of Pharmaceutics and Biopharmaceutics, **50**, 27–46 (2000).
DOI: 10.1016/S0939-6411(00)00090-4

[16] Naghash H. J., Okay O.: Formation and structure of polyacrylamide gels. Journal of Applied Polymer Science, **60**, 971–979 (1996).
DOI: 10.1002/(SICI)1097-4628(19960516)60:7<971::AID-APP7>3.0.CO;2-J

[17] Blanco M. D., Garcia O., Olmo R., Teijon J. M., Katime I.: Release of 5-fluorouracil from poly(acrylamide-co-monopropyl itaconate) hydrogels. Journal of Chromatography B: Biomedical Sciences and Applications, **680**, 243–253 (1996).
DOI: 10.1016/0378-4347(95)00401-7

[18] Chen J., Haesun P., Park K.: Synthesis of superporous hydrogels: Hydrogels with fast swelling and superabsorbent properties. Journal of Biomedical Materials Research Part A, **44**, 53–62 (1999).
DOI: 10.1002/(SICI)1097-4636(199901)44:1<53::AID-JBM6>3.0.CO;2-W

[19] Ferreira L., Vidal M. M., Gil M. H.: Design of a drug-delivery system based on polyacrylamide hydrogels. Evaluation of structural properties. The Chemical Educator, **6**, 100–103 (2001).
DOI: 10.1333/s00897010461a

[20] Muniz E. C., Geuskens G.: Compressive elastic modulus of polyacrylamide hydrogels and semi-IPNs with poly(N-isopropylacrylamide). Macromolecules, **34**, 4480–4484 (2001).
DOI: 10.1021/ma001192l

[21] Krusic K. M., Dzunuzovic E., Trifunovic S., Filipovic J.: Semi-IPNs based on polyacrylamide and poly(itaconic acid). Polymer Bulletin, **51**, 159–166 (2003).
DOI: 10.1007/s00289-003-0203-7

[22] Mishra S., Bajpai R., Katare R., Bajpai A. K.: Radiation induced crosslinking effect on semi-interpenetrating polymer networks of poly(vinyl alcohol). Express Polymer Letters, **1**, 407–415 (2007).
DOI: 10.3144/expresspolymlett.2007.58

[23] Khor E., Lim L. Y.: Implantable applications of chitin and chitosan. Biomaterials, **24**, 2339-2349 (2003).
DOI: 10.1016/S0142–9612(03)00026-7

[24] Boonsongrit Y., Mitrevej A., Mueller B. W.: Chitosan drug binding by ionic interaction. European Journal of Pharmaceutics and Biopharmaceutics, **62**, 267–274 (2006).
DOI: 10.1016/j.ejpb.2005.09.002

[25] Risbud M. V., Bhonde R. R.: Polyacrylamide-chitosan hydrogels: In vitro biocompatibility and sustained antibiotic release studies. Drug Delivery, **7**, 69–75 (2000).
DOI: 10.1080/107175400266623

[26] Yazdani-Pedram M., Lagos A., Retuert P. J.: Study of the effect of reaction variables on grafting of polyacrylamide onto chitosan. Polymer Bulletin, **48**, 93–98 (2002).
DOI: 10.1007/s00289-002-0006-2

[27] Xia Y., Guo T., Song M., Zhang B., Zhang B.: Hemoglobin recognition by imprinting in semi-interpenetrating polymer network hydrogel based on polyacrylamide and chitosan. Biomacromolecules, **6**, 2601–2606 (2005).
DOI: 10.1021/bm050324l

[28] Ferry J. D.: Viscoelastic properties of polymers. Wiley, New York, (1980).

[29] Lárez C., Canelón F., Millán E., Katime I.: Interpolymeric complexes of poly(itaconic acid) and chitosan. Polymer Bulletin, **48**, 361–366 (2002).
DOI: 10.1007/s00289-002-0049-4

[30] Lee J. W., Kim S. Y., Kim S. S., Lee Y. M., Lee K. H., Kim S. J.: Synthesis and characteristics of interpenetrating polymer network hydrogel composed of chitosan and poly(acrylic acid). Journal of Applied Polymer Science, **73**, 113–120 (1999).
DOI: 10.1002/(SICI)1097-4628(19990705)73:1<113::AID-APP13>3.0.CO;2-D

[31] Katime I. A., Katime O., Katime D.: Smart materials of this millenium: Macromolecular hydrogels (in Spanish). Servicio Editorial de la Universidad del País Vasco, Bilbao (2004).

[32] Leanirith Y., Bunel C., Vairon J. P.: Reversible immobilization of drugs on a hydrogel matrix, 2. Diffusion of free chloramphenicol from poly(2-hydroxyethyl methacrylate) hydrogels. Die Makromolekulare Chemie, **191**, 1119–1129 (1990).
DOI: 10.1002/macp.1990.021910514

[33] Mathur A. M., Moorjani S. K., Scranton A. B.: Methods for synthesis of hydrogel networks: A review. Polymer Reviews, **36**, 405–430 (1996).
DOI: 10.1080/15321799608015226

[34] Karadag E., Saraydin D., Sahiner N., Guven O.: Radiation induced acrylamide/citric acid hydrogels and their swelling behaviors. Journal of Macromolecular Science Part A: Pure and Applied Chemistry, **38**, 1105–1121 (2001).
DOI: 10.1081/MA-100107132

eXPRESS Polymer Letters Vol.3, No.1 (2009) 33–38
Available online at www.expresspolymlett.com
DOI: 10.3144/expresspolymlett.2009.6

Electrostatic stretching of grafted maleic acid copolymer chains

L. Renner[1], *T. Pompe*[1*], *C. Werner*[1,2,3]

[1]Leibniz Institute of Polymer Research Dresden, Max Bergmann Center of Biomaterials Dresden, Hohe Str. 6, 01069 Dresden, Germany
[2]Center for Regenerative Therapies Dresden, Germany
[3]Institute of Biomaterials and Biomedical Engineering, University of Toronto, Toronto, Ontario, Canada

Received 3 November 2008; accepted in revised form 9 December 2008

Abstract. We report on the swelling behaviour of thin maleic acid copolymer films in dependence of pH and ionic strength. The response of the polymer films was studied by quartz crystal microbalance with dissipation monitoring. It was found that solution's pH and ionic strength can be separately used to adjust the swelling of the maleic acid copolymer films. While the pH affects the degree of dissociation of the maleic acid groups, ionic strength triggers the interaction of the resulting charges along the polymer chains. The dominance of electrostatic interactions in the system was obvious from the maximal extension of the grafted polymer chains at very low ionic strength. Tuning the expansion of grafted polymer chains by pH and ionic strength can be utilized in various applications of biointerfacial research to adjust the physicochemical properties of polymer thin film coatings.

Keywords: *coatings, swelling, grafting density, ionic strength, QCM-D*

1. Introduction

Maleic acid copolymer films are versatile polymer platforms [1] that can be applied to study many aspects in biointerfacial science such as blood compatibility [2], protein adsorption [3], cell and tissue engineering [4, 5], and supported lipid bilayer membranes [6]. This versatility stems from several facts: the maleic anhydride is highly reactive towards primary amines and alcohols, the maleic acid functionalities can be reversibly converted into maleic anhydride moieties, and the density of anhydride moieties can be adjusted by the choice of the comonomer [1]. The reactivity of the anhydride groups offers exciting options for the covalent attachment of proteins and other biomolecules while the hydrolyzed copolymers allow for the physical adsorption of biomolecules with different anchorage strength [1, 3, 5].

The kinetic and static swelling of maleic acid copolymer films in phosphate buffered saline (pH 7.4 and pH 3) was subject of an earlier study [7]. It was found that the different time stages of swelling could be described according to polymer theory [8] of free polymer chains pointing to a very low number of grafting points per polymer chain. The low number of grafting points was also supported by the observed scaling laws in dependence on molecular weight of the polymer chains at high and low pH. These scaling laws correlated very well to swelling of free polymer chains in good and bad solvent conditions [9, 10]. An intermediate swelling step was found to be affected by the chemical conversion of the maleic anhydride to the

*Corresponding author, e-mail: pompe-tilo@ipfdd.de

maleic acid moieties which accelerated the swelling kinetics. The swelling kinetics of polymer films readily accounted for the variation in hydrophilicity and polarity of the polymer chains due to the variation of the comonomer and were in excellent agreement with swelling studies of maleic anhydride copolymers in solution [11].

The response of the copolymer films to varying properties of aqueous environments is of crucial importance for intended further applications in biointerfacial science [14]. In addition to the variation of the pH changes of the ionic strength often occur and need to be considered when applying thin polymer films e.g. in biosensor devices to gain the optimum activity of immobilized enzymes within a copolymer-supported lipid bilayer membrane. Therefore we set off to address the question how maleic acid copolymer films swell at varied ionic strength. The swelling behavior was analyzed for buffer solutions across a broad range of different ionic strength at pH 7 using a quartz crystal microbalance with dissipation monitoring. The observed layer thickness changes revealed an electrostatically driven expansion of the grafted polymer chains causing almost fully stretched polymer molecules at the conditions of maximum repulsion.

2. Experimental section

2.1. Polymer thin film preparation

Thin films of poly(propene-*alt*-maleic anhydride) (PPMA) (Leuna-Werke AG, Germany) (MW 6 000, 0.06%) and poly(ethene-*alt*-maleic anhydride) (PEMA) (Aldrich, Munich, Germany) (MW 125 000, 0.1–0.3%) were produced by spin-coating (RC5, Suess Microtec, Garching, Germany) copolymer solutions in methylethylketone (Fluka) or THF/acetone (Acros Organics, Geel, Belgium) mixture with a ratio of 1:1, respectively, on top of quartz crystals (Q-Sense AB; Gothenburg, Sweden) with 50 nm SiO_2 coatings (GeSiM GmbH, Dresden, Germany). Before polymer coating the SiO_2 surface was freshly oxidized in a mixture of aqueous solutions of ammonia (Acros Organics, Geel, Belgium) and hydrogen peroxide (Merck, Darmstadt, Germany) and were subsequently surface-modified with 20 mM 3-aminopropyl-triethoxy-silane (ABCR, Karlsruhe, Germany) in isopropanol/water (9:1) for 2 h prior to spin-coating of the copolymer solutions to allow a covalent attachment of the thin copolymer films. Stable covalent binding of the polymer films to the crystals was achieved by a heating step at 120°C for 2 h. To adjust the grafting density of PEMA chains

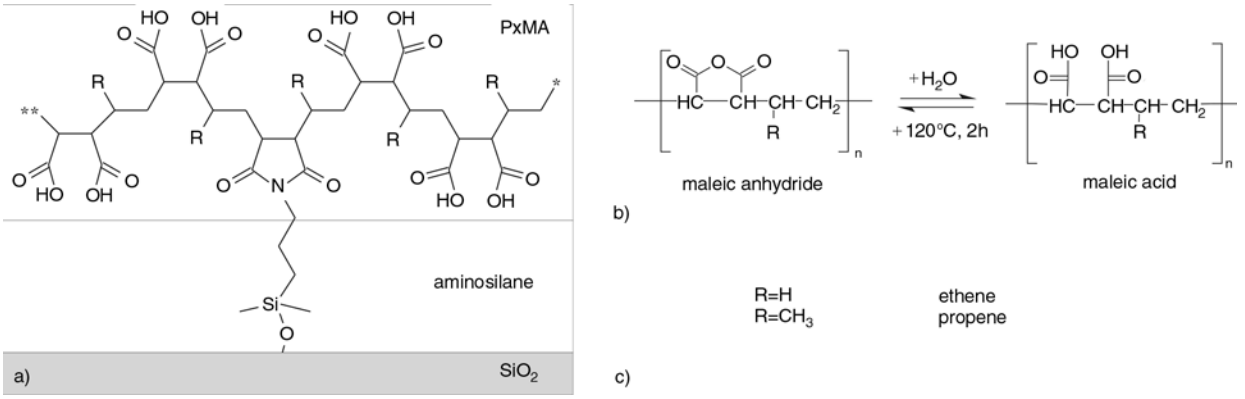

Figure 1. Schematic view of the covalently immobilized maleic acid copolymer layers (a), the reversible hydrolysis between maleic acid and anhydride functionalities (b). The side chains *R* vary with the type of comonomer unit (propene or ethene) (c).

Table 1. A summary of maleic anhydride copolymer film properties taken from [1, 7]

	PPMA	**PEMA**
RMS roughness[1]	0.34 nm	0.8 nm
thickness[2] pH 3 (±0.5 nm) (hydrolyzed)	20 nm	45 nm
COOH group surface density[3]	$7 \cdot 10^{14}$ cm^{-2}	$1.2 \cdot 10^{15}$ cm^{-2}
water contact angle[4] (±3 deg)	38°	26°
isoelectric point[5] (1 mM KCl)	1.9	1.9

[1]determined by scanning force microscopy; [2]ellipsometry measurements; [3]determined by XPS after methionine amide conversion; [4]measurement of hydrolyzed copolymer surfaces; [5]electrokinetic measurements

the PEMA solution concentrations were adjusted to 0.03, 0.1, and 0.3%. The polymer films were thoroughly characterized with respect to water contact angle, film thickness, surface roughness, and chemical composition in dry and wet conditions, as recently published [1, 7]. A schematic of the polymer platform is given in Figure 1. Important film properties are summarized in Table 1.

2.2. Quartz Crystal Microbalance with Dissipation Monitoring (QCM-D)

Swelling studies were performed on a QCM-D 300 (Q-Sense AB) with dissipation monitoring. The method is described in detail elsewhere [12]. In short, frequency changes are directly correlated to mass changes. Dissipation is attributed to dissipative energy losses of the attached layers on an oscillating crystal surface. The frequency and dissipation data were fitted to the Voigt-Voinova model to calculate the corresponding thickness changes [13].

2.3. Swelling studies

To test the influence of different ionic strengths and pH on the thickness of polymer films distinct solutions have been applied. The substrates have been immersed in HEPES (4-(2-hydroxyethyl)-1-piperazineethanesulfonic acid) buffer in order to change the ionic strength, HEPES buffer (pH 7.2) was diluted 1:10 (10^{-1} HEPES), 1:100 (10^{-2} HEPES), or 1:1 000 (10^{-3} HEPES) at room temperature. Swelling of the thin copolymer films was further determined in dependence on the solution's pH using phosphate buffered saline (PBS) at pH 7.4 (Sigma, Munich, Germany) or unbuffered saline solution at pH 4 using the same ionic strength.

3. Results and discussion

QCM-D measurements on PPMA and PEMA polymer films in aqueous solutions were performed to unravel the influence of pH and ionic strength of buffer solutions on the swelling of the polymers. As found in earlier studies [14] switching from low pH (pH 4) to high pH (pH 7) increases the charge density along the polymer chain due to an increased dissociation of the carboxylic acid groups. The charged moieties on the polymer chains are shielded by counterions in the solution over distances (Debye screening lengths) that exponentially decrease with increasing ionic strength of the solution. Therefore, we expect a substantially stronger electrostatic repulsion between charged polymer chains at lower ionic strength. It is furthermore hypothesized that the increased electrostatic repulsion between the negatively charged carboxylic acid groups should affect the balance between electrostatic and entropic forces of the polymer chains. Infinitely small solution concentrations of ions $c_{ions} \rightarrow 0$ may lead to a maximum extension of the polymer chains.

This hypothesis was scrutinized by QCM-D experiments. The effect of ionic strength variations is demonstrated on hydrolyzed PPMA and PEMA films (Figure 2a and 2b, respectively). The corresponding thickness values are listed in Table 2 and given in Figure 3. The data show a minor decrease

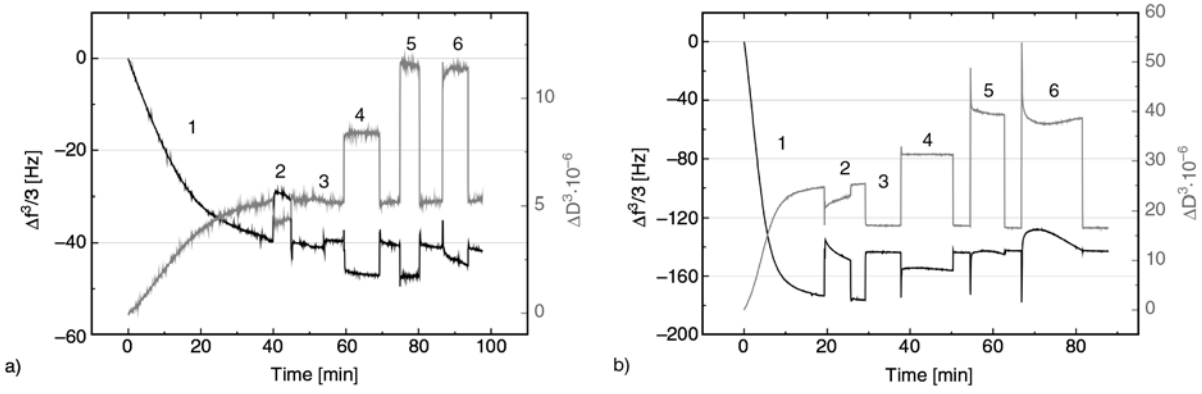

Figure 2. QCM-D measurements on (a) 0.06% PPMA and (b) 0.1% PEMA films depending on pH and ionic strength. The conditions have been varied in the following order: (1) swelling in PBS pH 7.4, (2) pH 4 solution, (3) HEPES buffer pH 7.2, (4) 10× diluted HEPES, (5) 100× diluted HEPES and (6) 1 000× diluted HEPES. After each step the solution was recalibrated with HEPES buffer (solution 3).

Table 2. Thickness variations of copolymer films PPMA and PEMA with various grafting density in dependence of pH and ionic strength of the solution. For the study of the influence of ionic strength HEPES buffer was diluted 10× (HEPES 10×), 100× (HEPES 10×), and 1 000× (HEPES 1 000×)

	Thickness [nm]					
Polymer Film	**PBS**	**pH 4**	**HEPES**	**HEPES 10×**	**HEPES 100×**	**HEPES 1 000×**
PPMA 0.06%	9	7	9	12	14	14
PEMA 0.03%	12	8	6	8	14	14
PEMA 0.1%	34	28	28	36	40	40
PEMA 0.3%	170	137	150	175	212	225

in the film thickness occurring upon changing from pH 7.4 (PBS) to pH 4 (unbuffered saline solution). This is in excellent agreement with scanning force microscopy data reported earlier [7]. Both pH solutions closely resembled each other with respect to ion concentration and ionic strength. Hence, the change in the layer thickness can be attributed to the partial protonation of the carboxylic acid groups. As reported in an earlier study [14] the pK_a values of the two adjacent carboxylic acid groups of maleic acid ($pK_{a1} = 3$ and $pK_{a2} = 7$) explain an only partial dissociation of the acidic groups at pH 4. Therefore, the electrostatic repulsion along (and between) the grafted polymer chains is lowered at pH 4 which leads to the reported change from good solvent conditions to bad solvent conditions [7].

The impact of electrostatic repulsion on the swelling of the thin polymer films was further shown by changing the ionic strength of the buffer solution. This was accomplished by diluting the HEPES buffer. When changing from PBS to HEPES buffer a slight change in thickness was observed at first, which was attributed to the different electrolyte compositions of the two buffer solutions. The dilution of HEPES buffer led to sudden and significant thickness increases (Table 2). Interestingly, the change from 100× dilutions to 1000× dilution did not lead to a further increase in the film thickness, which points to a saturation behaviour: The stretching of the grafted polymer chains was already maximized at the ionic strength of 100× buffer dilution and the repulsive electrostatic interactions fully overwhelm the entropic contributions. In earlier studies [1, 7] PEMA films spin coated from 0.3% solutions and PPMA films from 0.06% solutions, respectively, were concluded to contain polymers with very few grafting points per chain only. At these concentrations the grafting-to process occurring during spin-coating resulted in the highest possible packing density with singular grafting points per polymer chain to the substrate. Thus, the layer thickness data of the swollen films can be compared with a theoretical chain length of the polymer molecules. The contour length of an ideal polymer chain with the number of repeating units N (compare Table 1) can be calculated with simple geometrical considerations $D_{max} = N \cdot l \cdot \cos(\theta/2)$ assuming no steric hindrance between the polymer chains [15]. For PEMA with a molecular weight of 125 000 and PPMA with a molecular weight of 6000 this would lead to a maximum contour length D_{max} of 506 and 22 nm, respectively, assuming a distance of 1.54 Å and a tetrahedral bond angle of $\theta = 68°$ between C–C bonds [16]. The maximum thickness values of the swollen polymer films correspond to almost one half of the length of a fully stretched polymer chain. As pointed out earlier the polymer chains in the reported case are grafted by very few grafting points to the surface. An estimation for one grafting point per chain which is randomly distributed along the chain would exactly give a mean effective chain length of the grafted chains of one half of the calcu-

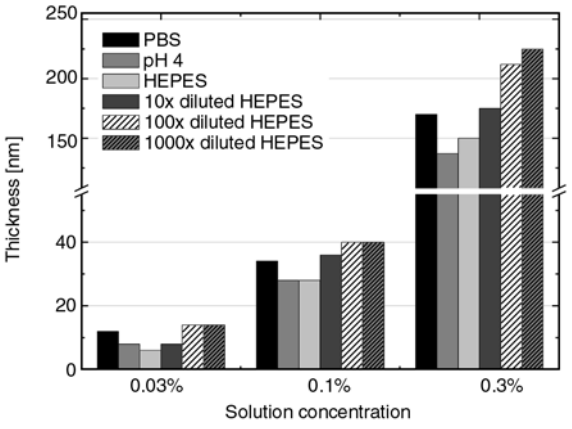

Figure 3. Thickness of the PEMA polymer films as a function of the polymer solution concentration during spin coating (resulting in varied grafting density), the applied pH, and ionic strength

lated fully stretched polymer chain. Hence, our findings clearly indicate that electrostatic repulsion determines the polymer chain conformation resulting in fully stretched chains at low ionic strength and high pH values. The results furthermore confirm the very low density of grafting points per polymer chain.

This interpretation is supported by the measurements of polymer films prepared out of different spin-coating concentrations. As found earlier [7] the decreased concentration of polymer chains in the solution leads to a larger available space for the adsorbed molecules on the substrate surface during the spin-coating process. The higher spreading of the adsorbed molecules was found to increase the number of grafting points per polymer chain. Hence, it is expected that the effective free chain length which can expand upon swelling should be lowered. Our results of the PEMA film swelling at low ionic strength perfectly match with this expectation, see Table 2. While the maximum layer thickness was significantly lower than for the highest spin-coating concentration it was again found that in HEPES buffer diluted more than 100× the film swelling does no longer increase pointing to the maximum possible stretch of the polymer chains.

4. Conclusions

In this work different maleic acid copolymer films were analyzed regarding their swelling behaviour in dependence on grafting density and solvent interactions. In aqueous solutions around neutral pH the maleic acid functionalities are completely de-protonated leading to a high charge density along the polymer chain. Because of that electrostatic repulsion governs the stretching of the grafted polymer chains resulting in a full expansion at low ionic strength. In this context the grafting density of polymer chains on the substrate (affecting the number of grafting sites per chain) modulates the swollen film thickness by variation of the effective free polymer chain length. The reported findings extend our knowledge about important structural characteristics of a versatile set of polymer grafted surfaces.

References

[1] Pompe T., Zschoche S., Herold N., Salchert K., Gouzy M., Sperling C., Werner C.: Maleic anhydride copolymers – A versatile platform for molecular biosurface engineering. Biomacromolecules, **4**, 1072–1079 (2003).
DOI: 10.1021/bm034071c

[2] Sperling C., Salchert K., Streller U., Werner C.: Covalently immobilised thrombomodulin inhibits coagulation and complement activation of artificial surfaces in vitro. Biomaterials, **25**, 5101–5113 (2004).
DOI: 10.1016/j.biomaterials.2003.12.014

[3] Renner L., Pompe T., Salchert K., Werner C.: Fibronectin displacement at polymer surfaces. Langmuir, **21**, 4571–4577 (2005).
DOI: 10.1021/la046801n

[4] Alberti K., Davey R. E,, Onishi K., George S., Salchert K., Seib F. P., Bornhäuser M., Pompe T., Nagy A., Werner C., Zandstra P. W.: Functional immobilization of signaling proteins enables control of stem cell fate decisions. Nature Methods, **5**, 645–650 (2008).
DOI: 10.1038/nmeth.1222

[5] Pompe T., Renner L., Werner C.: Nanoscale features of fibronectin fibrillogenesis depend on protein-substrate interaction and cytoskeleton structure. Biophysical Journal, **88**, 527–534 (2005).
DOI: 10.1529/biophysj.104.048074

[6] Renner L., Osaki T., Chiantia S., Schwille P., Pompe T., Werner C.: Supported Lipid bilayers on spacious and pH-responsive polymer cushions with varied hydrophilicity. The Journal of Physical Chemistry B, **112**, 6373–6378 (2008).
DOI: 10.1021/jp711479f

[7] Pompe T., Renner L., Grimmer M., Herold N., Werner C.: Functional films of maleic anhydride copolymers under physiological conditions. Macromolecular Bioscience, **5**, 890–895 (2005).
DOI: 10.1002/mabi.200500097

[8] Pitard E., Bouchaud J-P.: Glassy effects in the swelling/collapse dynamics of homogeneous polymers. The European Physical Journal E, Soft Matter, **5**, 133–148 (2001).
DOI: 10.1007/s101890170070

[9] de Gennes P. G.: Polymers at interfaces: A simplified view. Advances in Colloid and Interface Science, **27**, 189–209 (1987).

[10] Binder K.: Scaling concepts for polymer brushes and their test with computer simulation. The European Physical Journal E, Soft Matter, **9**, 293–298 (2002).
DOI: 10.1140/epje/i2002-10076-2

[11] Rätzsch M., Zschoche S., Steinert V.: Kinetic investigations of reactions with maleic anhydride copolymers and model compounds. Journal of Macromolecular Science, **24**, 949–965 (1987).
DOI: 10.1080/00222338708076928

[12] Rodahl M., Höök F., Krozer A., Brzezinski P.: Quartz crystal microbalance setup for frequency and Q-factor measurements in gaseous and liquid environments. Review of Scientific Instruments, **66**, 3924–3930 (1995).
DOI: 10.1063/1.1145396

[13] Voinova M. V., Rodahl M., Jonson M., Kasemo B.: Viscoelastic acoustic response of layered polymer films at fluid-solid interfaces: Continuum mechanics approach. Physica Scripta, **59**, 391–396 (1999).
DOI: 10.1238/Physica.Regular.059a00391

[14] Osaki T., Werner C.: Ionization characteristics and structural transitions of alternating maleic acid copolymer films. Langmuir, **19**, 5787–5793 (2003).
DOI: 10.1021/la034439r

[15] Rubinstein M., Colby R. H.: Polymer physics. Oxford University Press, USA (2003).

[16] Huntley D. R., Markopoulos G., Donovan P. M., Scott L. T., Hoffmann R.: Squeezing C–C bonds. Angewandte Chemie International Edition, **44**, 7549–7553 (2005).
DOI: 10.1002/anie.200502721

eXPRESS Polymer Letters Vol.3, No.1 (2009) 39–48
Available online at www.expresspolymlett.com
DOI: 10.3144/expresspolymlett.2009.7

Structure-property effects on mechanical, friction and wear properties of electron modified PTFE filled EPDM composite

M. S. Khan[1,], D. Lehmann[1], G. Heinrich[1], U. Gohs[1], R. Franke[2]*

[1]Leibniz Institute of Polymer Research Dresden, Hohe Str. 6, 01069 Dresden, Germany
[2]IMA Materialforschung und Anwendungstechnik GmbH Dresden, Wilhelmine-Reichard-Ring 4, 01109 Dresden, Germany

Received 5 November 2008; accepted in revised form 9 December 2008

Abstract. Tribological properties of Ethylene-Propylene-Diene-rubber (EPDM) containing electron modified Polytetrafluoroethylene (PTFE) have been investiagted with the help of pin on disk tribometer without lubrication for a testing time of 2 hrs in atmospheric conditions at a sliding speed and applied normal load of 0.05 m·s^{-1} and F_N = 1 N, respectively. Radiation-induced chemical changes in electron modified PTFE powders were analyzed using Electron Spin Resonance (ESR) and Fourier Transform Infrared (FTIR) specroscopy to characterize the effects of compatibility and chemical coupling of modified PTFE powders with EPDM on mechanical, friction and wear properties. The composites showed different friction and wear behaviour due to unique morphology, dispersion behaviour and radiation functionalization of PTFE powders. In general, EPDM reinforced with electron modified PTFE powder demonstrated improvement both in mechanical and tribological properties. However, the enhanced compatibility of PTFE powder resulting from the specific chemical coupling of PTFE powder with EPDM has been found crucial for mechanical, friction and wear properties.

Keywords: *mechanical properties, PTFE, EPDM, electron irradiation, friction*

1. Introduction

Elastomers are special class of polymeric materials with exceptional elastic mechanical properties. The high elastic memory, high ultimate elongation and low elastic modulus in comparison to engineering thermoplastics recommend elastomers in wide range of special purpose applications. However, their significantly poor friction and wear properties restrict their use for tribological applications. This characteristic of rubber compound is not only required for tire performance but also in non-tire rubber goods where elastomeric component is in direct contact with a counter-surface. For this reason, a renewed interest can be noticed for rubber tribology because of the property requirement for rubber in engineering applications such as for dynamic and static sealing, automotive stripping and as gasket etc. [1].

This necessitates exploring on how the requested performance can be achieved by the formulation of rubber compounds. Different elastomeric compositions containing various kinds of friction-modifiers such as fibrous (glass, carbon, asbestos) and reinforcing fillers (molybendium disulfide, silica, graphite) have been investigated [2–5]. More recently Karger-Kocsis *et al.* have carried out detailed tribological investigations on rubbers containing novel reinforcing fillers such as organophilic nanoclay [6], carbon nanofibers and carbon nanotubes [7, 8]. Besides this, Polytetrafluoroethyl-

*Corresponding author, e-mail: khan@ipfdd.de

ene (PTFE) with its remarkably low friction coefficient has also gained interest for use in tribological applications [9–12]. In rubbers, PTFE was initially used as a reinforcing additive in Silicone and Fluorosilicone rubbers [13–15] and afterwards in Styrene-butadiene-rubber, Acrylonitrile-butadiene-rubber and Butyl rubber [16]. New PTFE-based rubber compounds and compounding procedures have been introduced in improving mechanical properties of both low-strength (ethylene propylene, silicone) and high-strength (nitrile) rubbers for O-rings, sealing and valves etc. [17]. However, PTFE especially in rubbers have not been achieved with any commercially significant success. This is mainly due to the intractability of PTFE in providing homogeneous formulation because of its poor wetting and dispersion characteristic. This problem results from the unique properties of PTFE, most probably its highly hydrophobic surface which resists wetting. There is indeed a strong motivation to investigate new techniques and procedures for the use of PTFE powder in rubber compound as solid lubricant for tribological applications.

More recently, chemically coupled PTFE-polyamide [18] and PTFE-rubber [19] compounds based on the modification of PTFE powder by high energy electrons has opened a new way in producing materials for tribological applications. Radiation functionalization produces PTFE micropowders containing persistent trapped-radicals radicals and functional groups on the surface of PTFE powder can be easily compounded into elastomers such as EPDM rubber. A detailed characterization related to the mechanical, friction and wear properties of PTFE-based EPDM compounds have been presented by the authors in [20, 21]. In previous attempts the spectroscopic investigations revealed that during peroxide vulcanization the radiation-induced chemical changes in PTFE powder result in lower crosslinking efficiency and ultimately poor bulk properties of PTFE-EPDM composites [22, 23]. The present study focuses on using electron irradiation for crosslinking the EPDM rubber containing PTFE powder to obtain elastomeric composites with comparable hardness and bulk properties. PTFE based composites were produced in a specific controlled manner so that the influence of morphology, dispersion and surface activity of different PTFE powders on mechanical and especially on friction and wear properties of elastomeric composites could be realized. These investigations are of significant importance regarding the application of PTFE powder in rubber compounds.

2. Experimental

2.1. Materials and radiation modification of PTFE powder

EPDM (Buna EP G 6850) with ethylidene norbornene (ENB) content 7.7 wt%; ethylene content 51 wt%; Mooney viscosity, ML (1+4) at 125°C, 60; ash content 0.2 wt%; specific gravity, 0.86 g·cm^{-3}; was supplied from Lanxess Deutschland GmbH, Leverkusen, Germany. The properties and producers of PTFE powders investigated in this study are listed in Table 1. PTFE powder L100X grade was modified with an absorbed dose of 500 kGy at an average dose rate of about 10 kGy/h using electron accelerator (ELV-2) from Budker Institute of Nuclear Physics, Novosibirsk, Russia, installed at the Leibniz Institute of Polymer Research Dresden. The electron treatment was carried out in air and at room temperature. The transportation tray carrying PTFE powder passes to and fro under the beam exit-window (scanner) of electron accelerator. A 100 kGy dose requires a pro-

Table 1. Properties of PTFE powders

PTFE powder properties	L100X*	MP1100**	MP1200**
Producers	Solvay Solexis, Italy	DuPont, Wilmington USA	
Polymerization process	emulsion	emulsion	suspension
Irradiation dose [kGy]	500	500	500
Primary particle size [nm]	70–80	200	unknown
Mean agglomerate size [μm]	3.65	4	3
Carboxylic groups (C=O)	44.13	15.13	15.48
Radical concentration [%]***	100	125.6	56.3
Specific surface area [g/m^2]	26	7–10	1.5–3

*irradiated in the institute

**commercially irradiated powders

***radical concentration normalized to L100X PTFE powder

cessing time of 3 hrs to perform 40 passes (each pass delivers 2.5 kGy). A shut down time of at least 8 hrs was necessary after every successive 100 kGy to allow sufficient diffusion of air in PTFE powder. For 500 kGy dose, five steps each comprising of 100 kGy dose were performed. The total time to achieve 500 kGy dose was approx. 50 hrs, including 8 hrs shutdown intervals. These treatment parameters have been chosen in order to avoid excess temperature rise which might favour deactivation of the radical formation as well as to influence the chemical structure of PTFE powder.

2.2. Spectroscopic investigation of PTFE powder

The relevant concentration of free radicals was determined with the help of MiniScope MS200 Electron Spin Resonance (ESR) instrument from Magnettech Limited, Berlin, Germany. Spin numbers for each PTFE grade were calculated prior to mixing with EPDM. Fourier Transform Infrared Spectrometer (FTIR) spectra were recorded on Vertex 80v (Bruker) FTIR spectrometer (4000–400 cm^{-1}, resolution = 2 cm^{-1}, 32 scans per measurement) from Bruker Optik GmbH, Ettlingen, Germany in transmission mode on 10 μm thin PTFE foils to observe the chemical changes induced in different PTFE powders. The concentration of carboxylic groups (–COOH) was calculated using mathematical integration tool for the calculation of the area under the curve. The FTIR spectra have been normalized to Carbon-Fluorine (CF) upper vibration band at 2365 cm^{-1}.

2.3. Specimen preparation

EPDM and 30 phr (parts per hundred of rubber) PTFE powder were first pre-mixed in an internal mixer (PolyLab Haake Rheomix) from Thermo Electron GmbH, Karlsruhe, Germany for 5 minutes at 100°C and at a rotor speed of 50 rpm. The material from internal mixer was placed in between non-sticking polyesters films for press molding at a temperature of 150°C and a pressure of 5 MPa in an electrically heated press for 3 min to obtain rubber blocks of dimension 110 mm×110 mm×2 mm. The molded samples of PTFE-EPDM were then crosslinked with energy rich electrons at 200 kGy dose in atmospheric conditions and at room temperature of 25°C. Crosslinking with 200 kGy dose was accomplished in 5 passes with an absorbed dose of 40 kGy per pass and at an average dose rate of about 25 kGy/min. The processing time was 8 min with an electron energy and current of 1.5 MeV and 4 mA, respectively.

2.4. Characterization

Mechanical properties including tensile strength at break, relative elongation at break and modulus at 100% (M100) and 200% (M200) were determined according to ISO 527 at a cross-head speed of 200 mm/min using tensile testing machine from Zwick GmbH, Ulm Germany. Hardness values were measured according to DIN 53505, using a Shore (A) Durometer from Heinrich BAREISS GmbH, Oberdischingen, Germany. Indentations were made at several points for each specimen for measurements of average hardness values.

The frequency-temperature dependent viscoelastic mechanical property of the compounds, the loss factor or tan delta (E''/E') was measured with the help of a dynamic mechanical analyzer, EPLEXOR® 150 N (Gabo Qualimeter Testanlagen GmbH, Ahlden, Germany) using a 2 mm thick rectangular rubber block having an area of 15 mm×8 mm. The temperature scans were run from –100°C to 150°C at a heating rate of 4 $K \cdot min^{-1}$. The measurements were done in tension mode at a strain and frequency of 0.5% and 10 Hz, respectively.

Micro-structure morphology and dispersion analysis of PTFE powder were determined with the help of LEO 435 scanning electron microscope (SEM – acceleration voltage 20 kV) from LEO Electron Microscopy Ltd, Cambridge, England. Cryogenically fractured composites were used for the dispersion analysis of PTFE powder in EPDM. SEM was also used to assess the wear mechanisms involved rubber composites.

2.5. Friction and wear testing

A pin on disk tribometer according to ASTM G 99–2005 (ISC 200 from Implant Sciences, Wakefield, USA) was used as shown in Figure 1. Hardened carbon steel balls (type 100 KU 15 KL3, Wälzlagertechnik Dresden, Germany) made of the steel 100Cr6 (German standard 100Cr6, near AISI L3 steel) with a diameter of 15 mm served as coun-

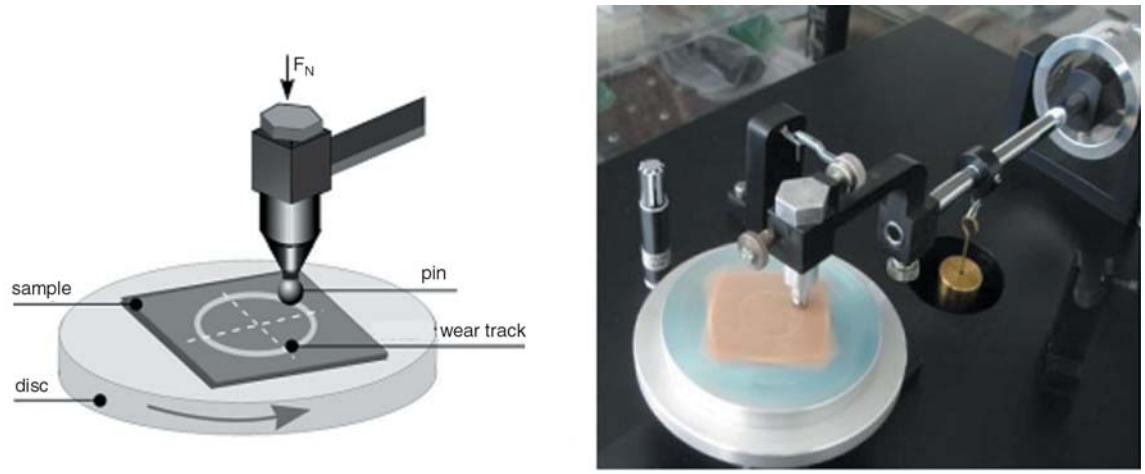

Figure 1. Schematic (left) of the pin-on-disk tribometer (right) illustrating the testing set-up for the friction and wear characterization of rubber sample (mounted on disk) against a counter-surface (pin/steel ball)

terpart. The surface of the steel balls were grinded with an arithmetic average roughness of R_a = 0.47 μm. The compound specimens were manufactured as square plates with dimensions 40 mm× 40 mm, thickness h = 2 mm and bonded on the steel disc using double-sided tesafilm®. A sliding speed of 0.05 m·s^{-1} was applied. The diameter of the circle rotation was 10 mm in each case. The tribological investigations were performed at a constant load of F_N = 1 N over a testing time of t_B = 2 h. The tests were carried out at a temperature of 22.9°C and a relative humidity of 31%. Profilometry of the wear track was conducted with profilometer (Perthometer CONCEPT 6.2, Mahr, Göttingen, Germany) at four different locations. In each case the point was shifted around 90° angle. For determination of the specific wear rate (k), the cross-sectional area of wear track was calculated by approximating the shape of the wear scar with a segment of circle. Specific wear rate was calculated as per Equation (1):

$$k = \frac{W_V\,[\mathrm{mm}^3]}{F_N \cdot s\,[\mathrm{N{\cdot}m}]} \tag{1}$$

where W_V is the volume of the removed material, F_N is the normal load and s is the sliding distance. The friction coefficient (μ) was determined directly by measuring the tangential force with a strain gauge load cell and recorded continuously with a sampling rate of 100 Hz. In case of stick slip effect, the experimental data strongly fluctuated and therefore for qualitative analysis of the friction behaviour of different composites the average values of friction coefficients are reported. The average friction coefficient was calculated as mean of maximum and minimum friction coefficient values, i.e. $\mu = (\mu_{max}-\mu_{min})/2$. For all series the mass wear loss of the counterpart ball was lower than the detection limit of the weighing balance (RC 1 from Satorius AG, Göttingen, Germany) which works with an accuracy of 0.1 mg.

3. Results and discussion

3.1. Optimization of crosslinking irradiation dose

In order to investigate the effect of morphology, dispersion and chemical coupling, the composites should have hardness higher than the critical value of 58 Shore (A) as determined in [22, 23]. Peroxide vulcanization of PTFE-EPDM composites containing electron modified PTFE powder is strongly influenced by the irradiation-induced changes in PTFE powder. Hardness of PTFE-EPDM compounds vary according to absorbed dose of PTFE powder. For this reason, EPDM has been vulcanized using electron irradiation in order to suppress this undesired effect on composite's hardness. The dose for electron crosslinking was determined relative to the required hardness values of PTFE-EPDM compounds. This was achieved by monitoring the influence of crosslinking dose on hardness of composites. Figure 2 shows the influence of absorbed dose on hardness of EPDM rubber and PTFE-EPDM composites. It can be seen that the optimum dose for crosslinking of EPDM rubber amounts to about 80 to 120 kGy. Above 120 kGy,

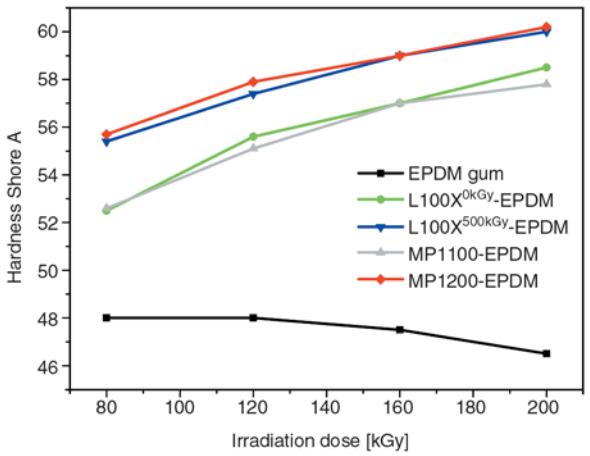

Figure 2. Comparison of hardness values of EPDM gum and PTFE-EPDM composites as a function of crosslinking irradiation dose

hardness decreases due to chain scission of EPDM. However, in the presence of PTFE powder, hardness of EPDM-PTFE composites increases as expected. L100X^{500kG}y-EPDM and MP1200-EPDM show highest while L100X^{0kGy}-EPDM and MP1100-EPDM show lowest hardness. This behaviour is in contradiction to that observed in peroxide induced vulcanization of L100X^{500kGy}-EPDM composite [22, 23]. It suggests that the variation in hardness of different composites at any specific absorbed dose results from differences in the chemical coupling mechanism of PTFE powders. This can be clearly seen in the different hardness values of L100X^{0kGy}-EPDM and L100X^{500kGy}-EPDM composites. However, at an optimum crosslinking dose of 200 kGy all of the PTFE-EPDM composites attained the required minimum hardness value of 58 Shore (A).

3.2. Mechanical and dynamic mechanical properties

The effects of PTFE powders on mechanical properties of PTFE-EPDM composites are shown in Figure 3. As expected modified PTFE-EPDM composites compared to non-modified (L100X^{0kGy}-EPDM) shows enhanced properties. There is no significant variation in tensile strength and elongation at break values of all modified PTFE-EPDM composites. However, L100X^{500kGy}-EPDM shows the highest M100 and M200 followed by MP1200-EPDM and MP1100-EPDM while L100X^{0kGy}-EPDM (horizontal broken line) shows the lowest. M200 was not achieved by L100X^{0kGy}-EPDM. This reinforcement effect in case of L100X^{500kGy}-EPDM is due chemical coupling of PTFE powder with EPDM. The effect of reinforcement can also be seen in the tan delta curves of composites shown in Figure 4. As can be seen the glass transition temperature (T_g) is only slightly influenced by addition of different PTFE powders to EPDM. The peak-height increases from MP1200-EPDM to L100X^{500kGy}-EPDM and reaches the maximum value for L100X^{0kGy}-EPDM and MP1100-EPDM. L100X^{0kGy}-EPDM, MP1100-EPDM and MP1200-EPDM show similar T_g of about –38°C whereas L100X^{500kGy}-EPDM has a higher T_g value of about –35°C. This shift in T_g to higher temperature is due to the restricted mobility of the polymer chains. Figure 4 also shows the mag-

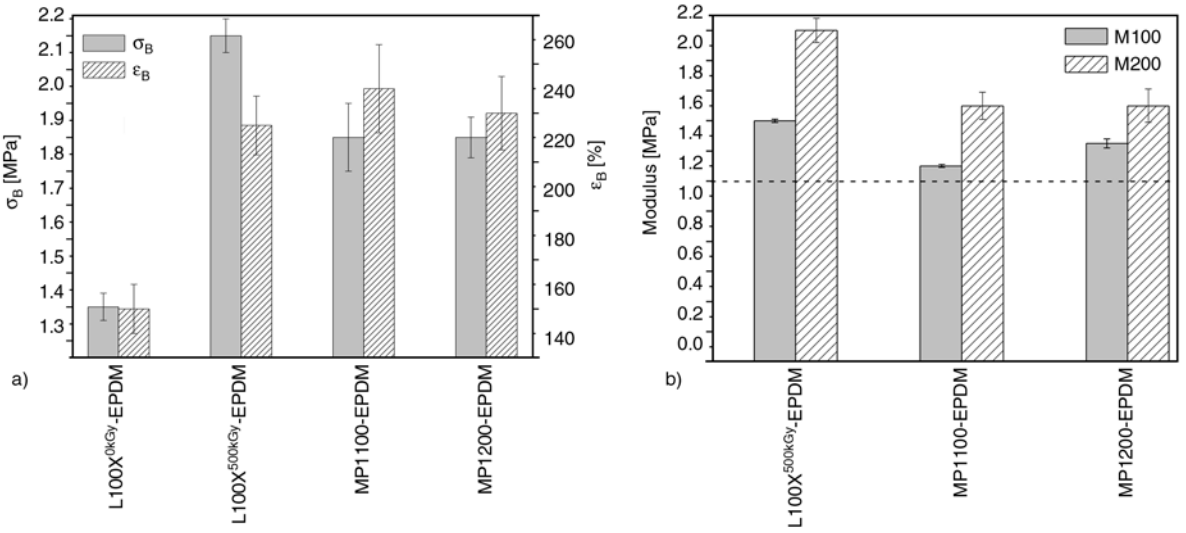

Figure 3. Tensile strength at break (σ_B) and elongation at break (ε_B) are shown in figure (a) while modulus, M100 and M200 are shown in figure (b). The horizontal broken lines indicate M100 of L100X^{0kGy}-EPDM.

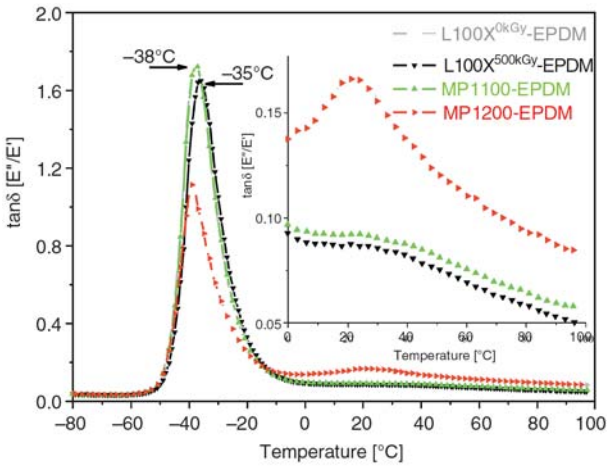

Figure 4. Tan delta behaviour of PTFE filled EPDM composites as a function of temperature

nified tan delta curves of the compounds in the temperature range of friction and wear testing where L100X^{500kGy}-EPDM shows the lowest tan delta while L100X^{0kGy}-EPDM and MP1100-EPDM shows similar behaviour at slightly higher level. The upturn in tan delta behavior of MP1200-EPDM could be due to the relaxation processes associated with the radiation-induced effects on crystallites structure of PTFE powder.

3.3. Compatibility and dispersion

Table 1 shows the relative concentration of C=O groups determined in the region 1840–1740 cm^{-1}. It can be observed that C=O concentration varies in different PTFE powders. L100X^{500kGy} PTFE powder shows the highest concentration of C=O groups while both MP1100 and MP1200 being three times less than L100X^{500kGy} PTFE powder have almost similar concentration of C=O groups. Higher concentration of C=O groups in case of L100X^{500kGy} PTFE powder suggests significantly lower contact angle or higher wettability. Lower contact angle corresponds to higher surface energy and enhanced interaction with polar compounds such as water. However, the enhanced compatibility of irradiated PTFE and EPDM cannot be explained by the presence of these functional groups since EPDM being a non-polar compound does not interact via polar or H-bonding forces. The other influencing factor is the relative concentration of persistent free radicals trapped in the crystalline structure at the surface of modified PTFE powders as shown in Table 1. The trapped radicals affect the properties through radical coupling with the olefinic unsaturation diene in rubber compound. The overall (bulk and surface) radical concentration of PTFE powders normalized to L100X^{500kGy} PTFE powder (100%) suggest that MP1100 has the highest (125.6%) while MP1200 (56.3%) indicates the lowest radical concentration. However, the degree of chemical coupling might also depend on the amount of radicals available on the surface of PTFE powders for chemical coupling with EPDM rather than the bulk concentration. In such case the surface to available radical concentration is of significant importance.

Figure 5 shows the scanning micrographs of PTFE-EPDM composites. It can be seen that L100X^{0kGy}-EPDM demonstrates poor compatibility and dispersion. It shows bigger agglomerates with poor dispersion behaviour in EPDM. This is due to the highly inert and hydrophobic surface of PTFE powder which lacks chemical compatibility with EPDM matrix. For this reason PTFE powder is modified with electron irradiation in order to enhance simultaneously its poor compatibility and dispersion characteristic. As observed in Figure 5, L100X^{500kGy} PTFE powder in comparison to L100X^{0kGy} PTFE powder shows improved dispersion and compatibility. The enhanced compatibility due to the chemical coupling by radical mechanism helps in de-agglomeration and dispersion of PTFE agglomerates during the reactive processing. Grafted EPDM chains on the surface of PTFE particles interact with the EPDM matrix and as such extensive shearing and de-agglomeration provides new active sites for chemical coupling with the olefinic unsaturated diene of EPDM. This helps in reinforcement and simultaneously improves the properties of L100X^{500kGy}-EPDM as shown in Figures 3 and 4. MP1100 shows the most excellent dispersion amongst the PTFE powders investigated. This is mainly due to the ability of this special grade of PTFE powder to de-agglomerate to its primary particle size of 0.2 μm. Both MP1100 and L100X^{500kGy} PTFE powders are embedded firmly in EPDM matrix. However, L100X grade is difficult to disperse uniformly compared to MP1100 even though both are produced by emulsion polymerization. On the other hand MP1200 PTFE powder having solid morphology is difficult to de-agglomerate even under high shearing. The agglomerates are pulled out of EPDM on application of stress. This clearly indicates the lower or

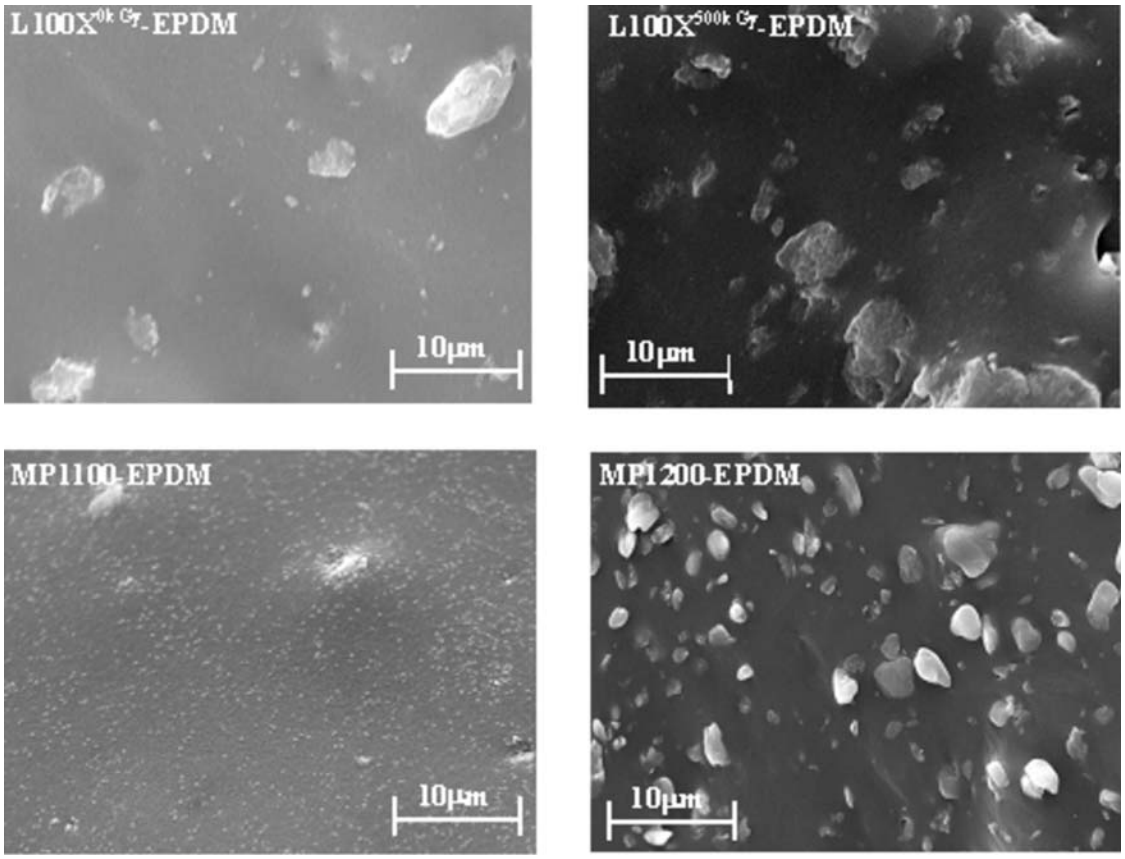

Figure 5. Scanning micrographs of the cryogenically fractured surfaces showing PTFE morphology and dispersion in EPDM

insufficient degree of compatibility of the bigger MP1200 agglomerates. The surface of EPDM indicates the presence of many PTFE particles. This clearly shows the difficulty in obtaining uniform dispersion of MP1200 in EPDM matrix.

3.4. Friction properties

Figure 6 shows the friction behaviour of PTFE-EPDM composites sliding against a hard spherical ball. The friction curves demonstrate that the friction coefficients of all vulcanizates decreases during the course of testing. The friction coefficient values decreases from initial to the final fiction values with in a range of 4 to 100%. As can be seen the elastomeric composites show different behaviour both at the beginning and during the course of testing time. MP1100-EPDM shows the highest friction in comparison to the other composites. Moreover, a sudden decrease in initial friction coefficient is observed for all compounds except for MP1100-EPDM. After a steady state is achieved, friction coefficient of MP1200-EPDM and L100X^{0kGy}-EPDM remains almost constant up to the end of measurement. On the contrary, MP1100-EPDM shows a gradual decrease in friction coefficient. This behaviour can be approximated by a linear function having a negative slope.

Similarly, L100X^{500kGy}-EPDM shows the same behaviour after steady state condition has been achieved. However, the slope of the friction curve is less than MP1100-EPDM. This clearly shows the

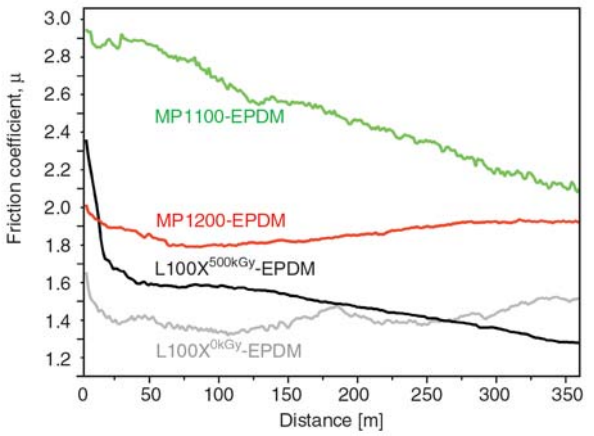

Figure 6. Comparison of the friction behaviour of different PTFE-EPDM composites as a function of sliding distance

influence of PTFE powders on friction behaviour of EPDM matrix. The higher friction values of MP1100-EPDM could be due to the direct interaction of the counter-body with EPDM. As is obvious in Figure 5, the surface of MP1100-EPDM is the smoothest of all the investigated composites due to its enhanced compatibility and excellent dispersion. There is almost no indication of PTFE particles on the surface. Only a few agglomerates are visible. Thus there is a rare possibility for MP1100 PTFE powders to form a transfer film during sliding contact against the counter-body. This results in a significantly higher friction coefficient throughout the testing time. On the other hand, all other composites show significantly lower friction values. This is due to the presence of PTFE agglomerates on the surface which allows a direct interaction with the counter-surface once EPDM layer is removed. This can be clearly seen in the sudden decrease in friction coefficients as shown in Figure 6. Moreover, a further decrease in case of L100X^{500kGy}-EPDM compared to L100X^{0kGy}-EPDM and MP1200-EPDM is observed. This is due to the interaction of the embedded PTFE agglomerates in wear track of L100X^{500kGy}-EPDM with counter-body. This facilitates in easy sliding of the counter-body against a wear track covered with PTFE particles.

3.5. Wear properties

Figure 7 shows the specific wear rates (k) of PTFE filled EPDM composites. Specific wear rates respond in accordance with the friction behaviour. The specific wear rate changes with in a range of 40% (L100X^{500kGy}) to 400% (MP1100-EPDM). MP1100-EPDM with its significantly high friction coefficient suffered from higher wear rate. Similarly, L100X^{0kGy}-EPDM and MP1200-EPDM having low friction coefficients show comparatively lower wear rates.

Figure 8 shows scanning micrographs of the wear scars of composites after repeated sliding with the counter-body. It can be seen that different wear mechanisms have occurred in the composites. In case of L100X^{0kGy}-EPDM, wear behaviour is characterized by the detachment of PTFE agglomerates from EPDM due to its significantly poor compatibility with EPDM. At higher magnification it also

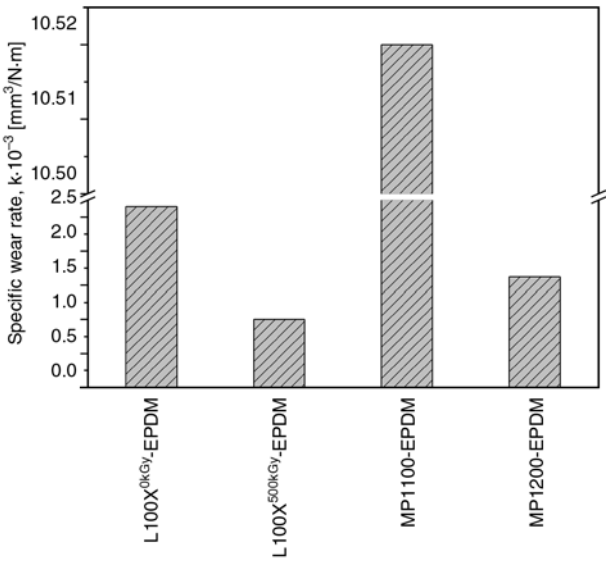

Figure 7. Comparison of the specific wear rates (k) of PTFE filled EPDM composites during friction testing

shows the presence of flattened agglomerates. This indicates that PTFE powder may have been transferred to the counter-surface. However, in case of L100X^{500kGy}-EPDM, the wear track is smooth. It shows the presence of significant amount of embedded PTFE agglomerates that have been flattened or abraded by repeated sliding of the counter-body. This is in accordance with the friction mechanism described before. The interaction of counter-body with PTFE agglomerates results in both the lowest wear rate and friction coefficient. In contradiction, MP1100-EPDM shows a rough wear track due to the detachment of significantly large lumps from the top of the surface. The wear mechanism is similar to the de-lamination type wear that has occurred in the deep regions of EPDM. At higher magnification one can observe that no PTFE agglomerates are visible for contact with counter-body. Thus almost no PTFE has been transferred to the counter-surface. MP1200-EPDM suffered from wear mechanism similar to MP1100-EPDM and L100X^{0kGy}-EPDM. A comparatively smaller lumps compared to MP1100-EPDM have been removed from the top of the surface. On the other hand, MP1200 being bigger and less compatible agglomerates have been removed from EPDM similar to L100X^{0kGy}-EPDM. One can observe the presence of these detached PTFE agglomerates on the wear track surface.

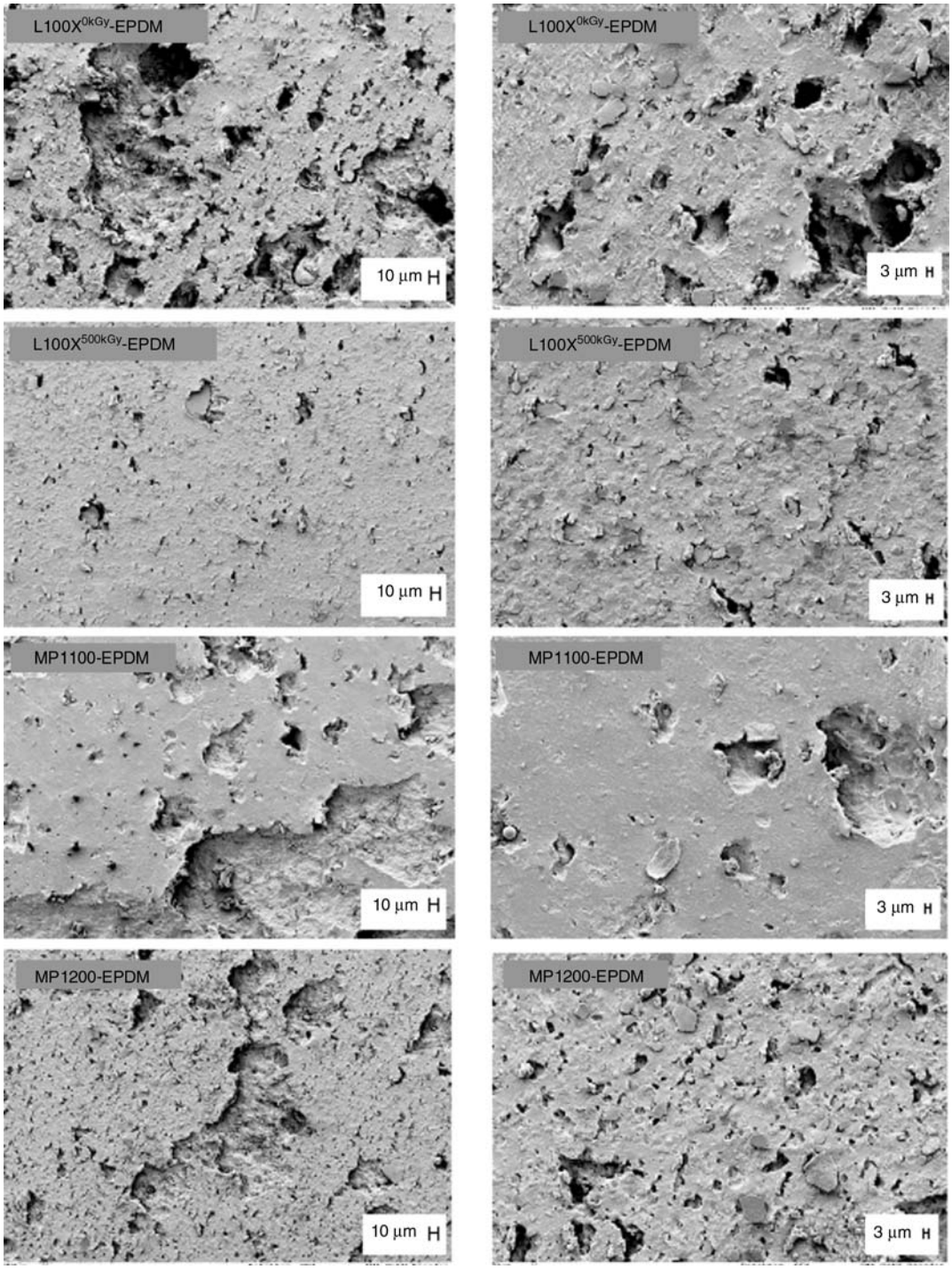

Figure 8. Scanning micrographs of wear track (contact area) showing the wear mechanisms involved in different PTFE-EPDM composites

4. Conclusions

The specific interaction of different PTFE powders with EPDM as well as with the counter-surface (steel-ball) controls mechanical as well as friction and wear properties of PTFE filled EPDM vulcanizates. L100X^{500kGy}-EPDM shows improved mechanical, dynamic mechanical and tribological properties due to enhanced chemical compatibility with EPDM. The significant improvement in friction and wear properties results from the embedment of L100X^{500kGy} PTFE agglomerates in EPDM matrix. This enable the counter-surface in easy sliding against a wear track covered with embedded PTFE particles. Friction and wear properties are strongly influenced by PTFE dispersion, PTFE transfer film formation and the corresponding chemical interaction between PTFE powder and EPDM matrix. MP1100-EPDM shows signifi-

cantly poor friction and wear properties but maintains excellent dispersion while MP1200-EPDM and L100X^{0kGy}-EPDM with comparatively improved friction and wear properties are characterized with poor dispersion and chemical compatibility of PTFE powder with EPDM. The described approach opens the route for potential use of electron modified PTFE powder in a variety of rubber compounds for tribological applications. However, a direct evidence of the existence, nature and the influence of chemical coupling between electron modified PTFE powder and EPDM rubber is necessary in order to design materials for tribological applications based on PTFE in technical rubber formulations.

Acknowledgements

The authors thank Solvay Solexis S.p.A. Italy and DuPont, Wilmington, DE, USA for the free of charge supply of PTFE powders.

References

[1] Bock E.: Sealing systems in a combustion engine (in German). Gummi Fasern Kunststoffe, **3**, 180–187 (2004).

[2] Bjerk R., Brandon W., Engelkin F., Jero J.: Fluoroelastomer-based composite material. U.S. Patent 3898361, USA (1975).

[3] Scher I. H., Ungar S. I.: Abrasion-resistant laminate. U.S. Patent 4400423, USA (1983).

[4] Bjerk R., Brandon W., Engelkin F., Jero J.: Fluoroelastomer-polyacrylate based friction material. U.S. Patent 4045402, USA (1977).

[5] Defrank M. P.: Epoxy-rubber based friction material. U.S. Patent 4131590, USA (1978).

[6] Gatos K. G., Kameo K., Karger-Kocsis J.: On the friction and sliding wear of rubber/layered silicate nanocomposites. Express Polymer Letters, **1**, 27–31 (2007).
DOI: 10.3144/expresspolymlett.2007.6

[7] Karger-Kocsis J., Felhős D., Thomann R.: Tribological behavior of a carbon nanofiber modified santoprenes thermoplastic elastomer under dry sliding and fretting conditions against steel. Journal of Applied Polymer Science, **108**, 724–730 (2008).
DOI: 10.1002/app.27429

[8] Felhős D., Karger-Kocsis J., Xu D.: Tribological testing of peroxide cured HNBR with different MWCNT and silica content under dry sliding and rolling conditions against steel. Journal of Applied Polymer Science, **108**, 2840–2851 (2008).
DOI: 10.1002/app.27624

[9] Tanaka K., Kawakami S.: Effect of various fillers on the friction and wear of PTFE-based composites. Wear, **79**, 221–234 (1982).
DOI: 10.1016/0043-1648(82)90170-3

[10] Bahadur S., Tabor D.: The wear of filled polytetrafluoroethylene. Wear, **98**, 1–13 (1984).
DOI: 10.1016/0043-1648(84)90213-8

[11] Friedrich K., Lu Z., Hager A. M.: Recent advances in polymer composites' tribology. Wear, **190**, 139–144 (1995).
DOI: 10.1016/0043-1648(96)80012-3

[12] Burris D. L., Boesl B., Bourne G. R., Sawyer W. G.: Polymeric nanocomposites for tribological applications. Macromolecular Materials Engineering, **292**, 387–402 (2007).
DOI: 10.1002/mame.200600416

[13] Crandell W. H.: Evaluation of silicon rubber modified with teflon. Rubber World, **133**, 236–240 (1955).

[14] Kaufman M. H., Gonzales J.: Reinforcement of fluoroelastomers with halopolymers. Rubber Chemistry and Technology, **41**, 527–532 (1968).

[15] Magner L. M., Punderson J. O.: Blends of fluorinated polymers. U.S. Patent 3484503, USA(1969).

[16] Kaufman M. H.: Hydrocarbon polymers. U.S. Patent 3940455, USA (1976).

[17] Stewart C. W.: Elastomeric compositions containing treated PTFE. U.S. Patent 4507439, USA (1985).

[18] Franke R., Lehmann D., Kunze K.: Tribological behaviour of new chemically bonded PTFE polyamide compounds. Wear, **262**, 242–252 (2007).
DOI: 10.1016/j.wear.2006.05.001

[19] Haberstroh E., Linhart C., Epping K., Schmitz T.: Improving the tribological properties of elastomers by PTFE powder (in German). Kautschuk Gummi Kunststoffe, **59**, 447–453 (2006).

[20] Khan M. S., Lehmann D., Heinrich G.: Properties of the EPDM with modified PTFE Nanopowder. Kautschuk Gummi Kunststoffe, **60**, 226–234 (2007).

[21] Khan M. S., Lehmann D., Heinrich G.: Modification of PTFE nanopowder by controlled electron beam irradiation: A useful approach for the development of PTFE coupled EPDM compounds. Express Polymer Letters, **2**, 284–293 (2008).
DOI: 10.3144/expresspolymlett.2008.34

[22] Khan M. S., Lehmann D., Heinrich G., Franke R.: Tribological studies of peroxide-cured EPDM rubber filled with electron beam irradiated PTFE powder. Wear, **266**, 200–207 (2009).
DOI: 10.1016/j.wear.2008.06.014

[23] Khan M. S., Franke R., Gohs U., Lehmann D., Heinrich G.: Friction and wear behaviour of electron beam modified PTFE filled EPDM compounds. Wear, **266**, 175–183 (2009).
DOI: 10.1016/j.wear.2008.06.012

eXPRESS Polymer Letters Vol.3, No.1 (2009) 49–61
Available online at www.expresspolymlett.com
DOI: 10.3144/expresspolymlett.2009.8

Factors affecting the properties of PLA/$CaSO_4$ composites: homogeneity and interactions

K. Molnár[1,2], J. Móczó[1,2], M. Murariu[3], Ph. Dubois[3], B. Pukánszky[1,2]*

[1]Laboratory of Plastics and Rubber Technology, Department of Physical Chemistry and Materials Science, Budapest University of Technology and Economics, H-1521 Budapest, P. O. Box 91, Hungary
[2]Institute of Materials and Environmental Chemistry, Chemical Research Center, Hungarian Academy of Sciences, H-1525 Budapest, P. O. Box 17, Hungary
[3]Laboratory of Polymeric and Composite Materials, Center of Innovation and Research in Materials and Polymers (CIRMAP), Materia Nova Research Center, University of Mons-Hainaut, Place du Parc 20, 7000 Mons, Belgium

Received 29 October 2008; accepted in revised form 9 December 2008

Abstract. Composites were prepared from poly(lactic acid) (PLA) and a natural $CaSO_4$ filler to study the developed structure and the interaction of the components. The filler was characterized very thoroughly by several techniques and the results indicated that the filler contains a considerable amount of small particles with size much below the volume average size of 4.4 μm. The presence of these small particles did not result in inhomogeneity, considerable extent of aggregation was not observed in the composites. The filler was coated with stearic acid to modify interactions and optimum coverage corresponded to the amount estimated from the specific surface area of the filler. Mechanical properties changed only slightly with increasing amounts of the uncoated filler, but coating resulted in a drastic change of tensile properties and deformation behavior. Considerable plastic flow was observed around filler particles on the fracture surface of broken specimens. The quantitative estimation of interfacial interactions and their comparison to existing data proved that the interaction of PLA and $CaSO_4$ corresponds to values observed in other mineral filled polymers. On the other hand, the reinforcing effect of the coated filler is extremely poor indicating almost zero interaction. Additional experiments proved that considerable amount of stearic acid dissolves in PLA and plasticizes the polymer. Stearic acid seems to desorb also from the surface of the filler, dissolve in the polymer and modify matrix properties.

Keywords: *mechanical properties, PLA/$CaSO_4$ composites, surface modification, homogeneity, interfacial interaction*

1. Introduction

Recently the interest in poly(lactic acid) (PLA) as well as in its copolymers [1–7], blends [8, 9] and composites [10–21] increased enormously for various reasons. PLA has several advantages compared to fossil fuel based polymers. Among others it can be produced from renewable resources, its production consumes CO_2, it is recyclable and compostable, and its properties can be modified and adjusted to a large number of applications in various ways. Increasing production capacity decreases its price thus PLA may represent a reasonable alternative to commodity polymers in several application areas. During the purification of the lactic acid monomer considerable amount of calcium sulfate forms as a byproduct, thus it is reasonable to attempt to use this mineral filler for the modification of poly(lactic) acid. The use of this material may result in a reasonable application of the byproduct and allow the modification of PLA as well. PLA/$CaSO_4$ composites were reported to have advantageous properties including good strength, impact resistance and decreased price [18].

*Corresponding author, e-mail: bpukanszky@mail.bme.hu

Recently several papers were published by some of the authors showing the advantages of $CaSO_4$ as filler [18–22]. It was shown that the β-anhydrite II (AII) form of gypsum is thermally stable, does not absorb significant amounts of water and its use as filler in PLA results in composites with good thermal, mechanical and impact properties. The study of several $CaSO_4$ types with different particle characteristics indicated that good homogeneity and advantageous properties can be achieved at an average particle size of 9 μm. The good performance of the composites was attributed to favorable interactions developing between the filler and the polymer matrix [18]. However, this relatively large particle size usually results in easy debonding especially in such stiff matrices like PLA [23]. In the paper cited above [18] the strength of interaction was estimated from the Young's modulus of composites and from tensile strength using the Nicolais-Narkis equation [24]. Unfortunately stiffness is not very sensitive to changes in interaction [25] and the Nicolais-Narkis model [24] does not include the effect of interaction, in fact it assumes complete debonding and zero load-bearing of the matrix.

Considering these open questions, the goal of our study was to shed more light onto the effect of particle characteristics and interaction on the structure and properties of PLA/$CaSO_4$ composites. A gypsum sample with smaller particle size (see Ref. [18]) was selected for the study, since debonding is very easy at large particle size especially in stiff matrices [23]. Interfacial interactions were estimated with the help of an appropriate model and compared to well-established materials, to PP/$CaCO_3$ composites extensively used in practice. Interactions were modified by coating the surface of the filler with stearic acid. Such surface modification results in a decrease of interactions which is advantageous for homogenization by decreasing aggregation, but it decreases matrix/filler interaction as well [26]. We hoped to obtain valuable information about interaction-structure-property correlations in the studied composites and to develop guidelines for the preparation of new materials with favorable properties.

2. Experimental

The PLA used in the experiments was obtained from NatureWorks (USA). The selected grade with M_n = 88 500 g/mol and M_w/M_n = 1.8 is recommended for extrusion. The polymer (<2% D isomer) has a density of 1.3 g/cm^3, while its MFI is 3.9 g/10 min at 190°C and 2.16 kg load. The CAS-20-4 calcium sulfate filler was supplied by the United States Gypsum Company (USA). The filler, manufactured from high purity gypsum rock using controlled calcination and fine grinding, has a volume average particle size of 4.4 μm, specific gravity of 2.96 g/cm^3 and calcium sulfate content >99%. The $CaSO_4$ content of the PLA composites was changed from 0 to 30 vol% in 5 vol% steps.

The filler was surface coated with various amounts of stearic acid to determine optimum coating, which corresponds to monolayer coverage [26, 27]. Coating was carried out in a Haake Rheomix 600 mixer fitted with blades for dry-blending. Coating was done at 120°C for 10 min at 100 rpm rate with stearic acid amounts ranging from 0.1 to 5 g/100 g filler in 9 steps. The surface characteristics of uncoated and coated fillers were studied by inverse gas chromatography. The fillers were aggregated in methanol, then the dried samples were grinded and sieved. The size of the grinded filler particles covered a wide range, the fraction between 400 and 800 μm size was used for the filling of the column. Columns were conditioned at 140°C for 16 hours and measurements were done at 100°C with the injection of various n-alkanes. An attempt was made to determine monolayer coverage by a dissolution method developed earlier [26, 28]. DSC traces were also recorded on coated fillers; free stearic acid can be determined from the appearance of its melting peak as shown by an earlier study [29]. The particle size and particle size distribution of the filler was determined with a Malvern Mastersizer 2000, while its specific surface area with an Autosorb 1 (Quantachrome, USA) apparatus.

Poly(lactic acid) was dried at 110°C for 4 hours in a vacuum oven before composite preparation. Homogenization of the components was carried out at 190°C and 50 rpm for 10 min in a Brabender W 50 EH internal mixer attached to a Haake Rheocord EU 10 V driving unit. The melt was transferred to a Fontijne SRA 100 compression molding machine to produce 1 mm thick plates used for further testing. As a result of fast cooling with water, the plates were mostly amorphous with a negligible amount of crystalline phase (see also DSC traces later). Rheological measurements were carried out using a

Paar Physica UDS 200 apparatus at 220°C in oscillatory mode in the frequency range of 0.1–600 1/sec on discs with 25 mm diameter and 0.5 mm thickness. The amplitude of the deformation was 5%. Mechanical properties were characterized by tensile testing on standard ISO 527 specimens using an Instron 5566 apparatus. Stiffness (E) was determined at 0.5 mm/min cross-head speed and 115 mm gauge length. Tensile strength (σ), and elongation-at-break (ε) were calculated from force vs. deformation traces measured on the same specimens at 5 mm/min cross-head speed. The melting and crystallization characteristics of PLA and its composites were determined using a Perkin Elmer DSC 7 apparatus. Two heating and a cooling runs were done on 5 mg samples with heating and cooling rates of 10°C/min. The particle characteristics of $CaSO_4$ and the structure, as well as the deformation mechanism of the composites were studied by SEM (JEOL JSM-6380 LA). Micrographs were taken both from fracture surfaces created at liquid nitrogen temperature and during the failure of the specimens in the tensile testing machine. 10 μm slices were cut from composites and studied by polarization optical microscopy (POM) using a Leica DFC 320 microscope to determine the distribution of the filler in the polymer and the possible presence of aggregates.

3. Results and discussion

The results of the study are presented in several sections. The first two deal with the particle characteristics of the filler and surface coating, two factors which are crucial for the structure of the composites and for the interactions between the components. Mechanical properties are presented next, followed by the discussion of structure and interfacial interactions in the two final sections of the paper.

3.1. Particle characteristics of the filler

Previous experience showed that fillers with large particle size debond very easily from the matrix [23, 30]. Debonding results in the formation of voids that may merge into large cracks leading to the catastrophic failure of the material. Studies done on PP/$CaCO_3$ composites showed that fillers with an average particle size below 1 μm strongly

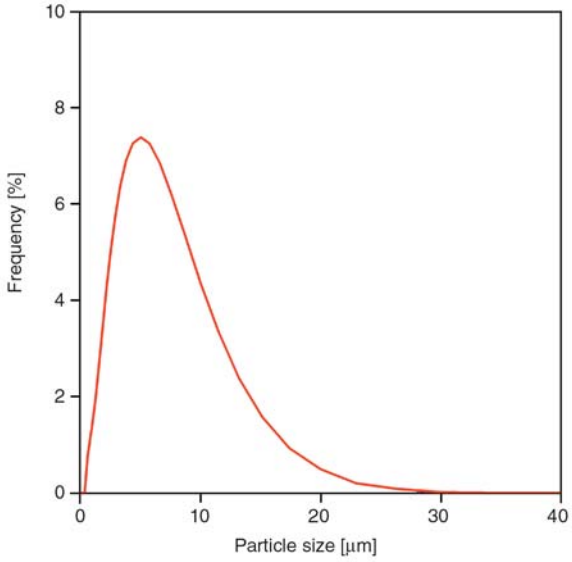

Figure 1. Particle size distribution of the $CaSO_4$ filler used in the experiments

aggregate, and the optimum particle size in PP is around 2–3 μm. As a consequence, we selected a $CaSO_4$ with a nominal median particle size of 4 μm from the available assortment. However, besides average size, also the size distribution is very important for the reasons mentioned above, i.e. large particles debond very easily, while small particles aggregate. The particle size distribution of the selected filler is presented in Figure 1. Its volume average size is 4.4 μm, but it contains a large number of relative large particles up to 25–30 μm size. Unfortunately, the presence and amount of very small particles cannot be estimated from the figure because of its scale.

Further information can be obtained about the particle characteristics of the $CaSO_4$ filler from SEM micrographs as shown in Figure 2. The large particles are clearly visible in the micrograph, but a large number of very small particles with size below the micrometer level are also seen. These particles are attached to the larger ones and the apparatus used for particle size analysis cannot distinguish them. Small particles may aggregate deteriorating mechanical properties. Further information about particle characteristics can be deduced from the specific surface area of the filler. BET adsorption measurements yielded a specific surface area of 5.38 m^2/g for our $CaSO_4$ sample. Assuming perfectly spherical particles of uniform size, this surface area corresponds to a particle size of 0.4 μm. Similarly, the 4.4 μm average particle size would correspond to 0.46 m^2/g specific surface

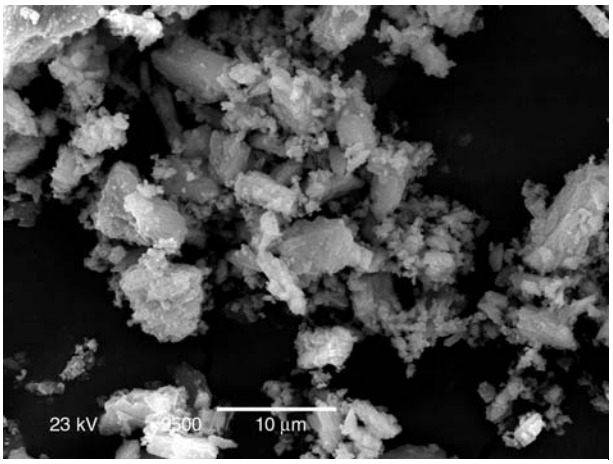

Figure 2. SEM micrograph showing the particle characteristics of the filler

area. These considerations indicate that in accordance with the SEM micrograph of Figure 2, our filler contains a large number of small particles not detected by the laser diffraction equipment. The presence of these particles might influence interactions, structure and properties of the PLA composites.

3.2. Surface coating

Fillers are often coated to modify interactions between the filler and the matrix polymer. Particulate fillers are usually coated with a surfactant to decrease their tendency for aggregation. Since our $CaSO_4$ filler contains small particles, such a surface modification is assumed to be beneficial also in our case. The first choice is stearic acid for this purpose, since similarly to $CaCO_3$, it may react chemically with the surface offering efficient coating [26]. Optimum surface coverage depends on the specific surface area of the filler, as well as on the surface need and orientation of the molecules on the surface of the particles. The optimum amount of surfactant proved to be close to monolayer coverage [26, 28]. A simple way to determine the adsorption of the surfactant on the filler is offered by the dissolution method [26, 31]. The filler is coated with increasing amounts of surfactant, the coated filler is washed with a solvent and the irreversibly bonded surfactant is determined by an appropriate analytical technique (IR, UV, etc.). The method principally results in an adsorption isotherm (for further details see Ref. [31]). The adsorption of stearic acid on the surface of our $CaSO_4$ is shown in

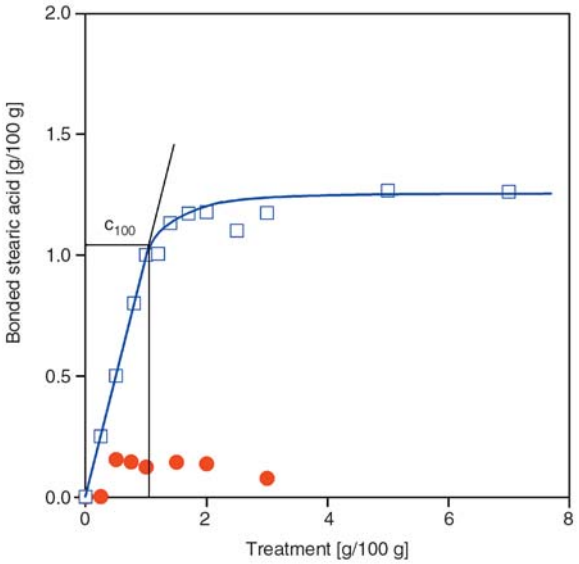

Figure 3. Adsorption of stearic acid on the surface of $CaSO_4$ (●) and on $CaCO_3$ (□) shown as reference. The dissolution curves were determined in $CHCl_3$

Figure 3. A dissolution curve recorded on $CaCO_3$ is included as comparison. The latter presents a typical example, adsorption goes to saturation and monolayer coverage is very close to the amount where the isotherm deviates from linearity (indicated in the figure by c_{100}). Contrary to the very nice adsorption isotherm obtained for $CaCO_3$, the one determined for $CaSO_4$ is very difficult to interpret. Almost no stearic acid is bonded onto the surface, which contradicts our expectations, but does not agree with the relatively large specific surface area of the filler either. Small particles indicated by model calculations and also by the SEM micrograph of Figure 2 do not settle in the suspension and bias the determination of the concentration of stearic acid by FTIR spectroscopy.

The fillers coated with different amounts of stearic acid were studied also by DSC. Free stearic acid crystallizes on the surface of the filler and the melting peak of the surfactant can be detected on the traces [29]. According to this method monolayer coverage is around 1.0–1.5 g stearic acid/100 g filler. Monolayer coating can be determined also from the change of surface tension with coverage. Surface tension decreases quite steeply with increasing coverage to a minimum, than slightly increases as a double layer of surfactant forms on the surface of the filler [29, 32]. The dispersion component of the surface tension of the filler is

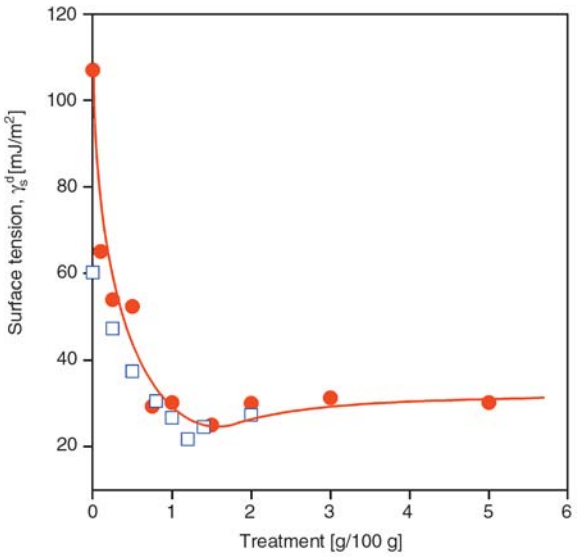

Figure 4. Change of the dispersion component of surface tension (γ_s^d) with the amount of stearic acid used for treatment; (●) $CaSO_4$, (□) $CaCO_3$

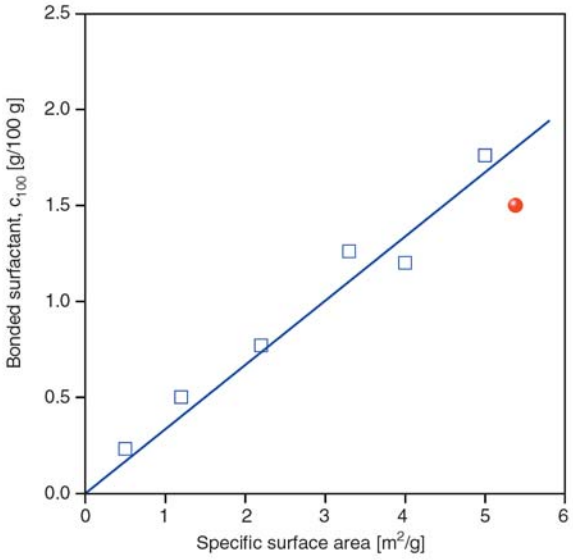

Figure 5. Correlation between the amount of stearic acid needed for monolayer coverage and the specific surface area of the filler; (●) $CaSO_4$, (□) $CaCO_3$

plotted against surface coverage in Figure 4. A $CaCO_3$ filler is used for comparison again. The dependence of surface tension on coverage is very similar for the two fillers. Moreover, the final value of surface tension is practically the same in both cases. Even the location of the minimum corresponds to the prediction, the $CaCO_3$ filler used had a specific surface area of 4.0 m^2/g, i.e. the minimum should be located at slightly smaller stearic acid content than for the $CaSO_4$ studied. According to these measurements, optimum coating is in the range of 1.0–1.5 g stearic acid/100 g $CaSO_4$ filler.

A further check of the amount of optimum coating is offered by the relationship between the specific surface area of the filler and monolayer coverage. Using previous data obtained on $CaCO_3$ fillers with different specific surface area offers us the possibility to check the results of DSC and IGC measurements presented in the previous paragraph. The relationship is plotted in Figure 5. A perfectly linear correlation was obtained in previous studies; data for all the fillers fit the line reasonably. The 1.5 g stearic acid/100 g $CaSO_4$ coverage determined by two methods also fits the correlation reasonably well. The figure and the other results presented in this section allow us to draw several conclusions. The specific surface area determined by BET adsorption is correct and the filler contains a large number of small particles as indicated by SEM micrographs. $CaSO_4$ can be covered with stearic acid, which decreases its surface tension considerably. Accordingly, some aggregation may be expected in composites containing the uncoated filler, but less in those prepared with the surface modified $CaSO_4$.

3.3. Mechanical properties, failure

The modulus of particulate filled composites does not offer much information about structure and interactions. Modulus depends on the orientation of anisotropic particles, but it is influenced by specific surface area or the strength of interaction only slightly, and by aggregation practically not at all [33, 34]. Properties measured at larger deformations, i.e. tensile yield stress and tensile strength, as well as the corresponding deformations depend strongly on structure and interaction. This is demonstrated by Figure 6, in which the tensile strength of PLA/$CaSO_4$ composites is plotted as a function of filler content both for uncoated and coated gypsum. Strength decreases with increasing filler content in both cases, but the rate of decrease differs considerably. The decrease for the uncoated filler is moderate in accordance with previous results [18]. This indicates reasonable interaction of the filler with the matrix polymer. However, the dominating deformation process is the separation of the phases at the interface, i.e. debonding, which occurs in most particulate filled composites. Surface coating leads to a significant decrease in strength. The difference in the effect of the coated

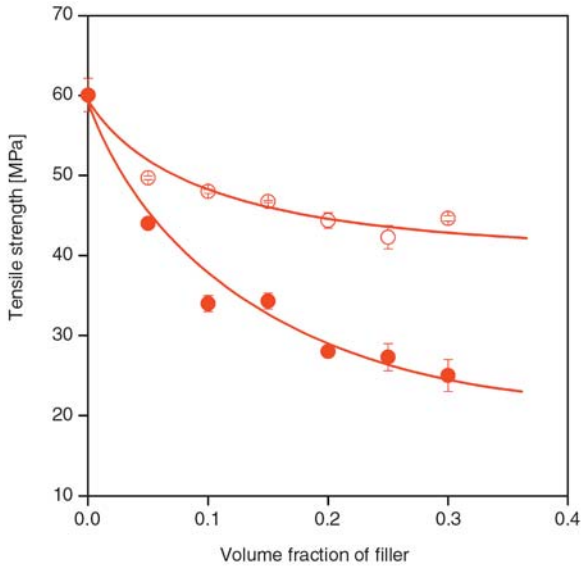

Figure 6. Composition dependence of the tensile strength of PLA/$CaSO_4$ composites. Effect of surface coating; (O) uncoated, (●) coated filler

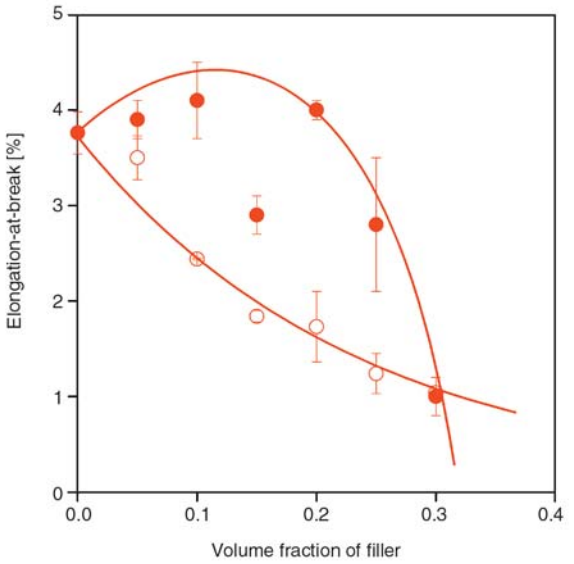

Figure 7. Effect of filler content and coating on the ultimate deformation of PLA/$CaSO_4$ composites; (O) uncoated, (●) coated filler

and uncoated filler on strength indicates that surface coating was effective and all interactions decreased in the composites. As a consequence, we may expect better dispersion in composites containing the coated filler.

The composition dependence of the corresponding deformation is presented in Figure 7. Elongation-at-break is very small for the composites prepared with the uncoated filler; the composites fail by brittle fracture. The increase of filler content results in the continuous decrease of ultimate deformation. On the other hand, surface coating increases deformability somewhat, although the elongation-at-break values remain quite small. Nevertheless, we can see the effect of decreased interaction. We may assume that debonding becomes easier as an effect of surface coating, even small particles debond and ultimate deformation increases somewhat.

The effect of coating is reflected also in the failure of the composites. Figure 8a presents the fracture surface generated by the tensile testing of a PLA composite containing 25 vol% uncoated filler. Brittle failure is clearly shown by the micrograph and the adhesion of the phases seems to be moderate, the clean surface of a large number of particles is seen. The micrograph also indicates that stress concentration around the particles initiates debonding, the separation of the phases changes stress distribution and leads to the failure of the specimen. On the

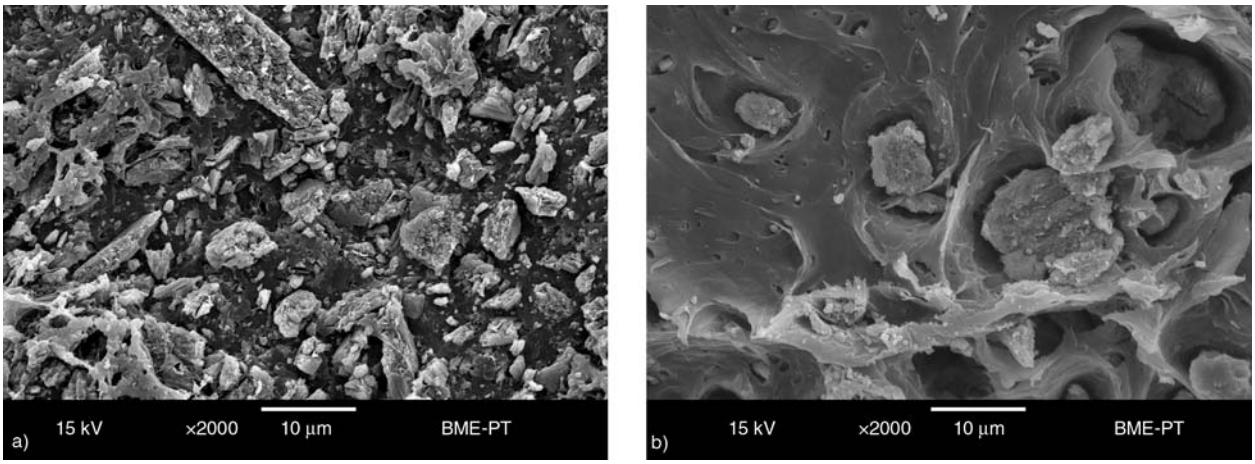

Figure 8. SEM micrographs taken from the broken surfaces of PLA/$CaSO_4$ composites containing 25 vol% filler. Fracture surfaces were created during tensile testing. a) uncoated, b) coated. See considerable plastic flow in the latter case.

other hand, the fracture surface of the composite containing the coated filler is quite surprising (Figure 8b). Large holes can be observed around larger particles showing not only debonding, but also considerable plastic flow as well. Obviously this latter causes the increase in deformability observed in Figure 7. Surface coating alone does not justify such a drastic change in the deformation behavior of the composite. The micrograph indicates a change in matrix properties, which might be caused by the stearic acid treatment. However, SEM micrographs cannot supply any proof for such a hypothesis thus we refrain from further speculation here.

3.4. Structure

The morphology of PLA/$CaSO_4$ composites is relatively complicated. The polymer can crystallize, but the rate of crystallization is rather slow thus under the conditions of normal processing operations it remains mostly amorphous; its crystalline content is very small. Besides crystalline structure, the distribution of the filler in the matrix, i.e. the possible formation of aggregates is also an important issue. The filler might influence also interphase formation and the mobility of the polymer molecules. In order to obtain a better insight into these questions, DSC measurements and microscopy were carried on the composites.

The DSC traces recorded during the second heating of PLA and some composites are presented in Figure 9. The traces are rather complicated showing several transitions. The glass transition temperature of the amorphous phase of PLA is clearly detected at around 60°C. This is followed by the peak of cold crystallization and then the melting of the crystalline polymer. Melting occurs in two steps, which indicates the recrystallization of PLA, the perfection of the crystals during heating. The crystallization and melting behavior of PLA is known; the possible effect of the filler and surface coating is more interesting for us. Based on the figure two observations can be made. The T_g of the polymer shifts to lower temperatures both in the presence of the uncoated and the coated filler. The double peak of melting also changes and transforms to a single process with increasing filler content. The temperature of the peak shifts towards lower temperatures.

The composition dependence of T_g is plotted in Figure 10. The significant shift in the glass transition temperature is rather surprising especially for the uncoated filler. Usually no change can be observed in the T_g of particulate filled polymers, or some increase is expected at very large specific surface areas due to the formation of a hard interphase. Weak interaction may lead to an increase in the mobility of the segments, but not in the extent

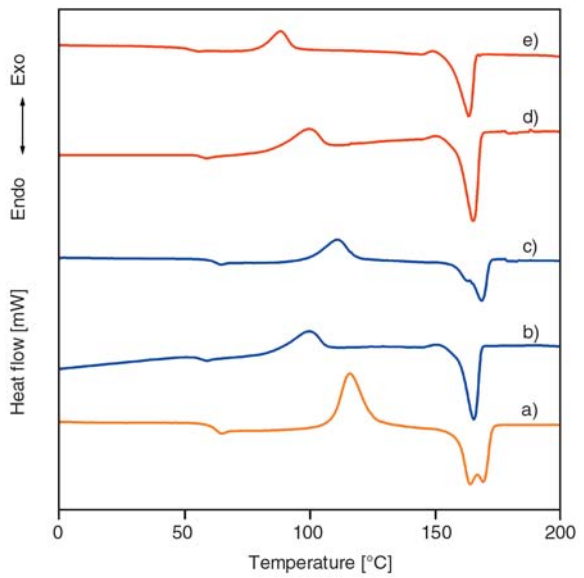

Figure 9. DSC traces recorded in the second melting run on PLA and PLA/$CaSO_4$ composites with various filler content; a) PLA, b) 10 vol%, uncoated, c) 25 vol% uncoated, d) 10 vol%, coated, e) 25 vol%, coated filler

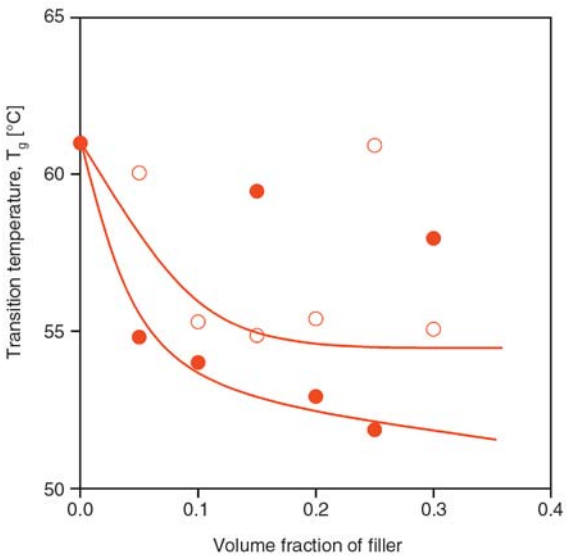

Figure 10. Decrease in the glass transition temperature of PLA with increasing filler content in PLA/$CaSO_4$ composites; (○) uncoated,(●) coated filler

observed in the figure. This increase in mobility is very difficult to explain and needs further study. On the other hand, the change in the melting behavior might be explained with the increased mobility. Cold crystallization proceeds easier if the chains are more mobile and recrystallization does not occur during melting. It is also worth to note, that several points deviate from the general tendency in the figure. This is observed in most properties (see also Figure 7) and also needs further investigation and explanation.

The dispersion of the filler particles was studied by microscopic techniques and by rheology. Rather surprisingly significant aggregation was not observed by any method. The SEM micrographs in Figure 8 indicate the homogeneous distribution of the particles. The same result was obtained by polarization optical microscopy. Large particles were clearly visible in the micrographs, but aggregates of 50–100 micron large often observed in composites prepared from $CaCO_3$ [35] could not be detected in any of them. Oscillatory rheometry is a very sensitive tool to detect aggregation. The Cole-Cole representation of the components of dynamic viscosity clearly shows the presence of a relaxation process with a different, longer relaxation time assigned to the formation of aggregates [34]. Cole-Cole plots and the calculation of average relaxation time indicated a very small degree of aggregation only at 30 vol% filler content. In view of the large specific surface area and the large number of small particles (see Figure 2) the lack of aggregation is rather surprising. Since the surface energy of $CaSO_4$ is rather large (see Figure 4), the only reasonable explanation is that small particles remain attached to the surface of larger ones even after processing, on the one hand, and they are easily dispersed after coating, on the other.

3.5. Interfacial adhesion

The effect of interactions can be estimated from properties determined at large deformations, like tensile yield stress or tensile strength, with the use of appropriate models. A simple model developed earlier [36–38] takes into account the influence of the decreasing load-bearing cross-section of the polymer due to filling, while the effect of interaction is expressed by an exponential term, i.e. (Equation (1)):

$$\sigma_T = \sigma_{T_0} \lambda^n \frac{1-\varphi}{1+2.5\varphi} \exp(B\varphi) \tag{1}$$

where σ_T and σ_{T_0} are the true tensile strength ($\sigma_T = \sigma\lambda$ and $\lambda = L/L_0$) of the composite and the matrix, respectively, n is a parameter expressing the strain hardening tendency of the matrix, φ is the volume fraction of the filler and B is related to its relative load-bearing capacity, i.e. to the extent of reinforcement, which depends on interfacial interaction. The relationship of B to the size of the interface and the properties of the interphase are expressed by Equation (2):

$$B = (1 + A_f \rho_f \ell) \ln \frac{\sigma_{T_i}}{\sigma_{T_0}} \tag{2}$$

where A_f and ρ_f are the specific surface area and density of the filler, while ℓ and σ_{T_i} the thickness and strength of the interphase. We can write Equation (1) in linear form (Equation (3)):

$$\ln \sigma_{T_{red}} = \ln \frac{\sigma_T (1+2.5\varphi)}{\lambda^n (1-\varphi)} = \ln \sigma_{T_0} + B\varphi \tag{3}$$

and plotting the natural logarithm of the reduced tensile strength of the composite against filler content should result in a linear correlation, the slope of which is proportional to the reinforcing effect of the filler.

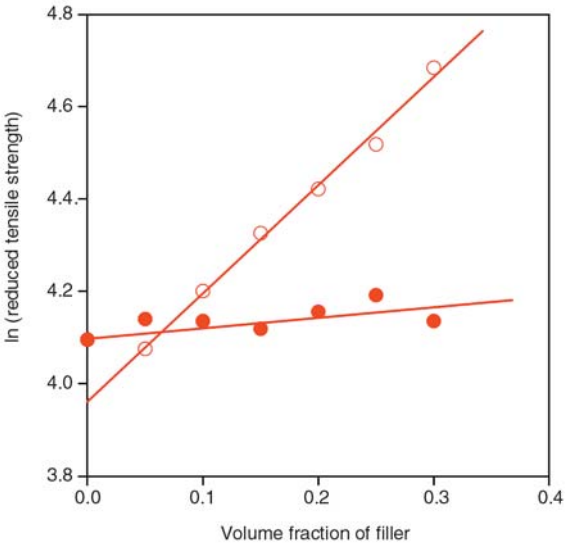

Figure 11. Quantitative determination of matrix/filler interaction in PLA/$CaSO_4$ composites. The tensile strength of the composites is plotted against composition in the representation of Equation (3); (O) uncoated, (•) coated filler

The reduced tensile strength of the studied composites is plotted in Figure 11 in the form indicated by Equation (3). We obtain straight lines in both cases indicating good dispersion and the absence of structural effects. This confirms our conclusions about structure drawn in the previous section. The intersection of the line obtained for the composites containing the uncoated filler differs slightly from the value determined for the matrix polymer. This can be the result of erroneous measurement or the effect of changing polymer properties in the presence of the filler. This latter seems to cause the difference in our case since the line obtained with the coated filler intersects the axis at the value of the matrix. The slope of the line is 2.33 for the uncoated filler indicating relatively strong interaction. According to Equation (2), the reinforcing effect, i.e. parameter *B*, depends also on the strength of the matrix, which is quite high for PLA. On the other hand, the load-bearing capacity of the coated filler is close to zero, we obtained 0.17 for parameter *B*. This again proves the drastic decrease of interaction (see Figure 4) and justifies the change in deformation mechanism (see Figure 8b).

We can clearly see the difference in reinforcing effect and interaction in the two composites containing the uncoated and coated filler, respectively, but do not know how these values relate to other polymer/filler pairs. *B* parameters obtained for PP/$CaCO_3$ composites are plotted against the specific surface area of the filler in Figure 12 for comparison. Equation (2) indicates that if the thickness and properties of the interphase are the same for all composites prepared from the same matrix, *B* should depend linearly on specific surface area, i.e. (Equation (4)):

$$B = k_1 + k_2 A_f \tag{4}$$

where $k_1 = \ln(\sigma_{T_i}/\sigma_{T_0})$ and $k_2 = k_1 \rho_f \ell$. The first part of the correlation, below 6 m^2/g surface area, corresponds to the prediction of Equation (4), but deviates at larger A_f values. The deviation is caused by the aggregation of the filler, which results in smaller interfacial area than calculated from the specific surface area and the amount of filler. The *B* value obtained for the PLA/$CaSO_4$ composite fits the correlation perfectly, which is rather surprising, since matrix properties are different from those of PP, but the surface tension of the filler is also larger which should lead to dissimilar interphase characteristics [39, 40]. Nevertheless, we can conclude from these results that the strength of interaction in the PLA/$CaSO_4$ composites is in the same range usual for particulate filled composites containing uncoated mineral fillers. Surface modification results in a drastic decrease of interaction, which is much stronger than expected and very difficult to explain. To develop some idea about the magnitude of this decrease, the *B* value of 1.98 obtained for coated $CaCO_3$ with 5.0 m^2/g specific surface area (A_f) in PMMA matrix with tensile strength (σ_m) of 54.9 MPa must be compared to the $B = 0.17$ at $A_f = 5.38$ and $\sigma_m = 60$ MPa for the PLA/$CaSO_4$ composite.

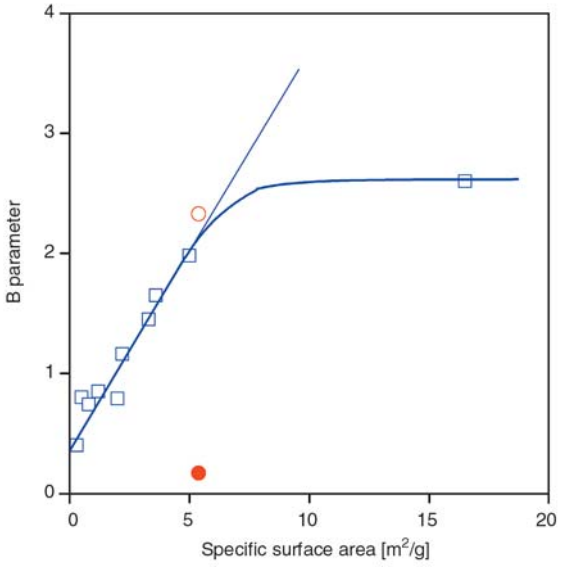

Figure 12. Dependence of parameter B on the specific surface area of the filler; (O) uncoated $CaSO_4$, (●) coated $CaSO_4$, (□) $CaCO_3$ used as reference

Rheology supplies a further proof for the extraordinary effect of the coated filler on composite properties. The relative complex viscosity of the composites measured at 220°C and 10 s^{-1} frequency is plotted against filler content in Figure 13. The viscosity of the melt increases with filler content in the presence of the uncoated filler, but it decreases continuously with increasing amount of the coated filler. This is rather surprising and against the prediction of all models even if the interaction is decreased considerably due to coating with stearic acid.

In order to shed more light onto the phenomenon and clarify the role of stearic acid, PLA blends were prepared with various amounts of the surfactant. The point indicated by (★) was obtained for a

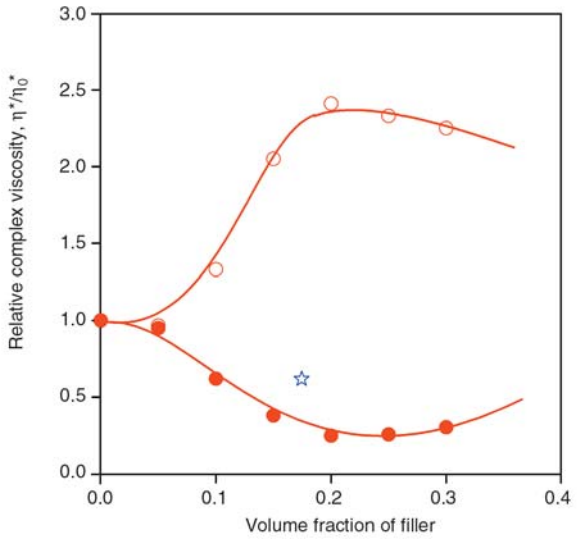

Figure 13. Composition dependence of the complex viscosity of PLA/$CaSO_4$ composites determined at 10 s^{-1} frequency and 220°C; (O) uncoated, (●) coated filler, (★) 0.5 wt% stearic acid

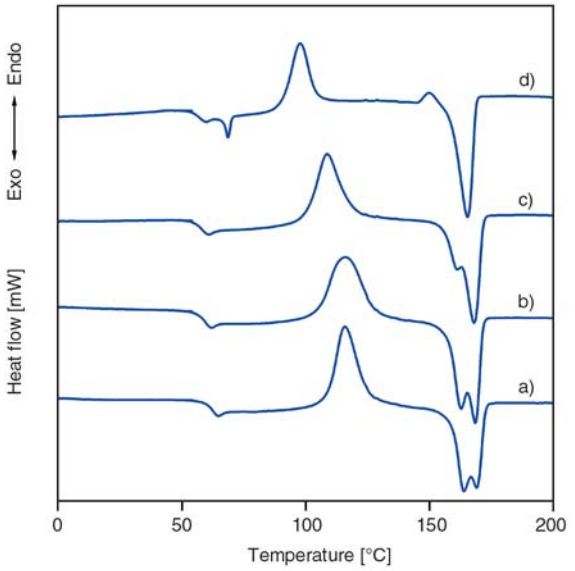

Figure 14. DSC traces recorded on PLA/stearic acid blends in the second heating run; a) PLA, b) 0.5 g, c) 1.0 g, d) 2.0 g stearic acid

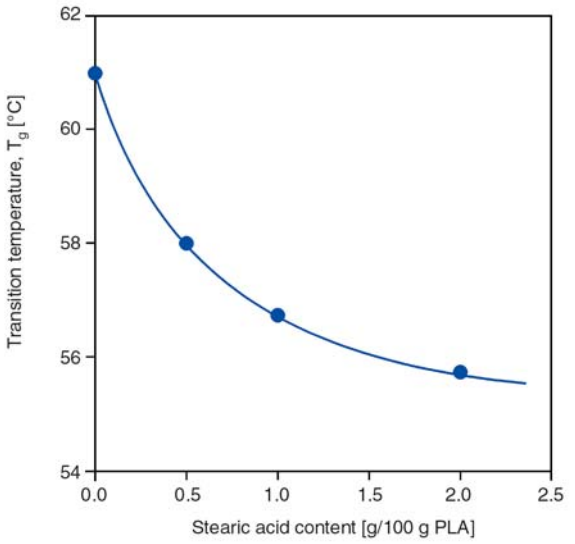

Figure 15. Effect of the amount of stearic acid on the glass transition temperature of PLA

blend, which contains the same amount of stearic acid (0.5 wt%) as on the surface of the coated filler at 17.5 vol% filler content. The point fits perfectly the general correlation indicating a lubricating or plasticizing effect of the stearic acid in PLA. We may assume that the active hydrogen atom of the acid forms strong H-bridges with the carbonyl oxygen of the polymer. The measurement of the transparency of plates compression molded from the blends indicates a solubility of about 1 wt% of stearic acid in PLA. Only the question remains whether the PLA/stearic acid interaction is strong enough to dissolve also the surfactant adsorbed on the surface of the filler or only surplus surfactant plasticizes PLA.

To check the hypothesis of lubrication or plasticization further we carried out also the thermal analysis of the blends. DSC traces recorded during the second heating of the samples are presented in Figure 14. Practically all transitions shift towards lower temperatures including glass transition, cold crystallization and melting. The very pronounced double melting peak caused by crystal perfection disappears and the polymer melts in one step probably due to the larger mobility of the chains. The very strong plasticizing effect of stearic acid is clearly shown by the change of T_g with composition (Figure 15). The decrease of the glass transition temperature by 5°C upon the addition of only 2 wt% stearic acid is very drastic indeed. From these experiments we may conclude that stearic acid must be used with care for the surface modification of fillers added to PLA, since it interacts strongly with the polymer. The presence of large amounts of excess stearic acid may result in decreased tensile strength, but also in a decrease of molecular weight due to acid catalyzed hydrolytic cleavage [18].

4. Conclusions

The $CaSO_4$ filler used for the preparation of PLA composites was characterized very thoroughly by

several techniques and the results indicated that the filler contains a considerable amount of small particles. In spite of the expectations, the presence of these small particles did not result in inhomogeneity, considerable extent of aggregation was not observed in the composites. The filler was coated with stearic acid to modify interactions and optimum coverage corresponded to the amount estimated from the specific surface area of the filler. Mechanical properties changed only slightly with increasing amounts of the uncoated filler, but coating resulted in a drastic change of properties and deformation behavior. Considerable plastic flow was observed around filler particles on the fracture surface of broken specimens. The quantitative estimation of interfacial interactions and their comparison to existing data proved that the interaction of PLA and $CaSO_4$ corresponds to values observed in other mineral filled polymers. On the other hand, the reinforcing effect of the coated filler is extremely poor indicating almost zero interaction. Supplementary experiments proved that considerable amount of stearic acid dissolves in PLA and plasticizes the polymer. Stearic acid seems to desorb also from the surface of the filler and dissolve in the polymer. Further study is needed to explain certain phenomena (large deviations in measured values, the decrease of T_g in the presence of the uncoated filler, cold crystallization and melting, etc.) and to find the best surface coating agent for the application.

Acknowledgements

The authors are indebted to Szilvia Klébert, Károly Renner and Alfréd Menyhárd for their help in the determination of particle characteristics, in the preparation of SEM micrographs and in thermal analysis. The authors also thank the assistance of János Kovács in the rheological measurements. TVK, US Gypsum Co. and NatureWorks are acknowledged for the donation of raw materials. The research on heterogeneous polymer systems was partly financed by the National Scientific Research Fund of Hungary (OTKA Grant No. K 68748 and F 68579), we appreciate the support very much. One of the authors is indebted also to the János Bolyai Research Scholarship of the Hungarian Academy of Sciences. CIRMAP thanks the Belgian Federal Government Office Policy of Science (SSTC) for general support in the frame of PAI-6/27.

References

[1] Auras R., Harte B., Selke S.: An overview of polylactides as packaging materials. Macromolecular Bioscience, **4**, 835–864 (2004).
DOI: 10.1002/mabi.200400043

[2] Li B., Chen S-C., Qiu Z-C., Yang K-K., Tang S-P., Yu W-J., Wang Y-Z.: Synthesis of poly(lactic acid-b-p-dioxanone) block copolymers from ring opening polymerization of p-dioxanone by poly(L-lactic acid) macroinitiators. Polymer Bulletin, **61**, 139–146 (2008).
DOI: 10.1007/s00289-008-0939-1

[3] Masayuki H., Yoshiharu K.: Thermomechanical properties of stereoblock poly(lactic acid)s with different PLLA/PDLA block compositions. Polymer, **49**, 2656–2661 (2008).
DOI: 10.1016/j.polymer.2008.04.014

[4] Ho C. H., Wang C. H., Lin C. I., Lee Y. D.: Synthesis and characterization of TPO-PLA copolymer and its behavior as compatibilizer for PLA/TPO blends. Polymer, **49**, 3902–3910 (2008).
DOI: 10.1016/j.polymer.2008.06.054

[5] Mert O., Doganci E., Erbil H. Y., Demir A. S.: Surface characterization of poly(L-lactic acid)-methoxy poly(ethylene glycol) diblock copolymers by static and dynamic contact angle measurements, FTIR, and ATR-FTIR. Langmuir, **24**, 749–757 (2008).
DOI: 10.1021/la701966d

[6] Södergard A., Stolt M.: Properties of lactic acid based polymers and their correlation with composition. Progress in Polymer Science, **27**, 1123–1163 (2002).
DOI: 10.1016/S0079-6700(02)00012-6

[7] Koji N., Yoshihiro N., Yuichi O., Tatsuro O.: Impacts of stereoregularity and stereocomplex formation on physicochemical, protein adsorption and cell adhesion behaviors of star-shaped 8-arms poly(ethylene glycol)-poly(lactide) block copolymer films. Polymer, **48**, 2649–2658 (2007).
DOI: 10.1016/j.polymer.2007.03.017

[8] Gua S-Y., Zhang K., Ren J., Zhan H.: Melt rheology of polylactide/poly(butylene adipate-co-terephthalate) blends. Carbohydrate Polymers, **74**, 79–85 (2008).
DOI: 10.1016/j.carbpol.2008.01.017

[9] Rohman G., Laupretre F., Boileau S., Guérin P., Grande D.: Poly(D,L-lactide)/poly(methyl methacrylate) interpenetrating polymer networks: Synthesis, characterization, and use as precursors to porous polymeric materials. Polymer, **48**, 7017–7028 (2007).
DOI: 10.1016/j.polymer.2007.09.044

[10] Wang N., Zhang X., Ma X., Fang J.: Influence of carbon black on the properties of plasticized poly(lactic acid) composites. Polymer Degradation and Stability, **93**, 1044–1052 (2008).
DOI: 10.1016/j.polymdegradstab.2008.03.023

[11] Paul M-A., Alexandre M., Degée P., Henrist C., Rulmont A., Dubois P.: New nanocomposite materials based on plasticized poly(L-lactide) and organo-modified montmorillonites: Thermal and morphological study. Polymer, **44**, 443–450 (2003).
DOI: 10.1016/S0032-3861(02)00778-4

[12] Bhat G. S., Gulgunje P., Desai K.: Development of structure and properties during thermal calendering of polylactic acid (PLA) fiber webs. Express Polymer Letters, **2**, 49–56 (2008).
DOI: 10.3144/expresspolymlett.2008.7

[13] Pluta M., Jeszka J. K., Boiteux G.: Polylactide/montmorillonite nanocomposites: Structure, dielectric, viscoelastic and thermal properties. European Polymer Journal, **43**, 2819–2835 (2007).
DOI: 10.1016/j.eurpolymj.2007.04.009

[14] Gorna K., Hund M., Vucak M., Gröhn F., Wegner G.: Amorphous calcium carbonate in form of spherical nanosized particles and its application as fillers for polymers. Materials Science and Engineering A, **477**, 217–225 (2008).
DOI: 10.1016/j.msea.2007.05.045

[15] Bleach N. C., Nazhat S. N., Tanner K. E., Kellomäki M., Törmälä P.: Effect of filler content on mechanical and dynamic mechanical properties of particulate biphasic calcium phosphate-polylactide composites. Biomaterials, **23**, 1579–1585 (2002).
DOI: 10.1016/S0142-9612(01)00283-6

[16] Bax B., Müssig J.: Impact and tensile properties of PLA/cordenka and PLA/flax composites. Composites Science and Technology, **68**, 1601–1607 (2008).
DOI: 10.1016/j.compscitech.2008.01.004

[17] Kuan C. F., Kuan H. C., Ma C. M., Chen C. H.: Mechanical and electrical properties of multi-wall carbon nanotube/poly(lactic acid) composites. Journal of Physics and Chemistry of Solids, **69**, 1395–1398 (2008).
DOI: 10.1016/j.jpcs.2007.10.060

[18] Murariu M., Ferreira A. D., Degee P., Alexandre M., Dubois P.: Polylactide compositions. Part 1: Effect of filler content and size on mechanical properties of PLA/calcium sulfate composites. Polymer, **48**, 2613–2618 (2007).
DOI: 10.1016/j.polymer.2007.02.067

[19] Pluta M., Murariu M., Ferreira A. D., Alexandre M., Galeski A., Dubois P.: Polylactide compositions. II. Correlation between morphology and main properties of PLA/calcium sulfate composites. Journal of Polymer Science Part B: Polymer Physics, **45**, 2770–2780 (2007).
DOI: 10.1002/polb.21277

[20] Sobkowicz M. J., Feaver J. L., Dorgan J. R.: Clean and green bioplastic composites: Comparison of calcium sulfate and carbon nanospheres in polylactide composites. Clean- Soil, Air, Water, **36**, 706–713 (2008).
DOI: 10.1002/clen.200800076

[21] Murariu M., Ferreira A. D., Pluta M., Bonnaud L., Alexandre M., Dubois P.: Polylactide (PLA)-$CaSO_4$ composites toughened with low molecular weight and polymeric ester-like plasticizers and related performances. European Polymer Journal, **44**, 3842–3852 (2008).
DOI: 10.1016/j.eurpolymj.2008.07.055

[22] Mishra S., Shimpi N. G.: Effect of the variation in the weight percentage of the loading and the reduction in the nanosizes of $CaSO_4$ on the mechanical and thermal properties of styrene-butadiene rubber. Journal of Applied Polymer Science, **104**, 2018–2026 (2007).
DOI: 10.1002/app.25910

[23] Vollenberg P. H. T.: The mechanical behaviour of particle filled thermoplastics. PhD Thesis, Eindhoven University of Technology, Eindhoven (1987).

[24] Nicolais L. Narkis M.: Stress-strain behavior of styrene-acrylonitrile/glass bead composites in the glassy region. Polymer Engineering and Science, **11**, 194–199 (1971).
DOI: 10.1002/pen.760110305

[25] Demjén Z., Pukánszky B., Nagy J.: Evaluation of interfacial interaction in polypropylene/surface treated $CaCO_3$ composites. Composites Part A: Applied Science and Manufacturing, **29**, 323–329 (1998).
DOI: 10.1016/S1359-835X(97)00032-8

[26] Fekete E., Pukánszky B., Tóth A., Bertóti I.: Surface modification and characterization of particulate mineral fillers. Journal of Colloid Interface Science, **135**, 200–208 (1990).
DOI: 10.1016/0021-9797(90)90300-D

[27] Pukánszky B., Fekete E.: Adhesion and surface modification. in 'Advances in Polymer Science, Mineral Fillers in Thermoplastics I' (ed.: Jancar J.) Springer, Berlin, Vol. 139, 109–153 (1999).
DOI: 10.1007/3-540-69220-7

[28] Papirer E., Schultz J., Turchi C.: Surface properties of a calcium carbonate filler treated with stearic acid. European Polymer Journal, **20**, 1155-1158 (1984).
DOI: 10.1016/0014-3057(84)90181-2

[29] Móczó J., Fekete E., Pukánszky B.: Adsorption of surfactants on $CaCO_3$ and its effect on surface free energy. Progress in Colloid and Polymer Science, **125**, 134–141 (2004).
DOI: 10.1007/b13435

[30] Renner K., Yang M. S., Móczó J., Choi H. J., Pukánszky B.: Analysis of the debonding process in polypropylene model composites. European Polymer Journal, **41**, 2520–2529 (2005).
DOI: 10.1016/j.eurpolymj.2005.05.025

[31] Fekete E., Pukánszky B.: Surface coverage and its determination: Role of acid-base interactions in the surface treatment of mineral fillers. Journal of Colloid and Interface Science, **194**, 269–275 (1997).
DOI: 10.1006/jcis.1997.5118

[32] Fekete E., Móczó J., Pukánszky B.: Determination of the surface characteristics of particulate fillers by linear IGC: A critical approach. Journal of Colloid and Interface Science, **269**, 143–152 (2004).
DOI: 10.1016/S0021-9797(03)00719-7

[33] Pukánszky B., Fekete E.: Aggregation tendency of particulate fillers: Determination and consequences. Polymer and Polymer Composites, **6**, 313–322 (1998).

[34] Kiss A., Fekete E., Pukánszky B.: Aggregation of $CaCO_3$ particles in PP composites: Effect of surface coating. Composite Science and Technology, **67**, 1574–1583 (2007).
DOI: 10.1016/j.compscitech.2006.07.010

[35] Móczó J., Fekete E., László K., Pukánszky B.: Aggregation of particulate fillers: Factors, determination, properties. Macromolecular Symposia, **194**, 111–124 (2003).
DOI: 10.1002/masy.200390071

[36] Pukánszky B., Turcsányi B., Tüdős F.: Effect of interfacial interaction on the tensile yield stress of polymer composites. in 'Interfaces in Polymer, Ceramic, and Metal Matrix Composites' (ed.: Ishida H.) Elsevier, New York, 467–477 (1988).

[37] Pukánszky B.: Influence of interface interaction on the ultimate tensile properties of polymer composites. Composites, **21**, 255–262 (1990).
DOI: 10.1016/0010-4361(90)90240-W

[38] Dányádi L., Renner K., Móczó J., Pukánszky B.: Wood flour filled PP composites: Interfacial adhesion and micromechanical deformations. Polymer Engineering and Science, **47**, 1246–1255 (2007).
DOI: 10.1002/pen.20768

[39] Vörös G., Fekete E., Pukánszky B.: An interphase with changing properties and the mechanism of deformation in particulate filled polymers. Journal of Adhesion, **64**, 229–250 (1997).
DOI: 10.1080/00218469708010541

[40] Móczó J., Fekete E., Pukánszky B.: Acid-base interactions and interphase formation in particulate filled polymers. Journal of Adhesion, **78**, 861–875 (2002).
DOI: 10.1080/00218460214099